

Annual Report 2018-2019: Ecosystem dynamics in the White Zone: history, drivers and, restoration implications

Authors: M. Ross, S. Stoffella, J. Meeder, L. Scinto, R. Vidales, H. Biswas, S. Charles, A. Wachnicka, and J. Sah,

Table of Contents

Introduction: Progress during 2018-2019	2
Section 1. <i>Concurrent vegetation change in marsh and embedded tree islands in a transgressive coastal landscape</i>	5
Section 2. <i>Salt water encroachment and the paleoecology of coastal sediments</i>	21
Section 3. <i>Soil organic carbon stocks decrease with saltwater intrusion despite mangrove encroachment in the Florida Coastal Everglades</i>	71

Introduction

A re-survey of our 1995-96 White Zone study was initiated in 2016. During 2016-17 and 2017-18, we focused on field data collection, including soils and vegetation. In the last year (2018-19), we concentrated on sample processing and analysis, collected some field data critical to several of those analyses, and began to summarize and interpret the information we had gleaned from our most recent work. As we enter the fourth and final year of this agreement, we are laser-focused on making progress on the seven papers described below.

We expect to have four or possibly five of the manuscripts submitted for publication during the next year, and the others in advanced draft form, to be completed shortly thereafter. Rough drafts of the first three titles will be included as Sections 1-3 of this report, and the status and plans for completion of all seven are discussed briefly in the following paragraphs.

1. *Vegetation dynamics (Ross, Stoffella et al.)*. This is a keystone paper, and one that's well along in development. In its current form, the paper contrasts the response of marsh and tree island vegetation to a presumptive increase in salinity brought on by sea-level rise during last two decades. Because environmental data from the earlier period are unavailable for our sites, our interpretation depends entirely on change in marsh vegetation and relative stasis in tree island composition, set against the apparent tolerance of the plant species to salinity, a transparently important factor. In other words, we use vegetation as an indicator of change in this single driver. At present, the draft is complete through the Results, but we have temporarily recessed in anticipation of expanding the paper's scope. To that end, we have initiated a collaboration with ENP scientists (Joseph Park, Kiren Bohm, Jed Redwine and their team) to use estimates of water stage and perhaps limit of tidal signal for both the 1991-1994 and 2012-2015 (pre-survey) periods. This modeled data will provide a richer summary of environmental conditions across our plot network, and by incorporating these data into our analysis, we will be able address the process of vegetation response to saltwater encroachment more ambitiously. The current draft of the developing paper is presented below as Section 1.
2. *Saltwater encroachment and the paleoecology of coastal sediments (Meeder et al.)*. Jack Meeder has produced a comprehensive picture of saltwater encroachment and organic matter enrichment in coastal wetlands from southern Biscayne Bay to western Florida Bay. The variability across the region is effectively defined by his approach, which uses mollusk composition and "fence diagrams" to track the progress of saltwater encroachment (SWE) along a well-distributed series of transects. In the Biscayne Bay watersheds, SWE has already run its course as far as the encircling canal system. However, SWE has been more variable in ENP due to the presumed impacts of fresh water delivery. In the C-111

basin it progressed rapidly throughout the early-to-mid 20th Century, only to reverse itself during recent decades in several transects most subject to canal runoff. Further west, several transects exhibited rapid SWE similar to those in the Biscayne Bay watershed, but west of Taylor Slough, sediments bore no sign of SWE. In FY2020, Jack and his team expect to shape this rich data set into an important paper. In Section 2, Meeder's results are summarized, with initial interpretations.

3. *Mangroves and soil carbon stocks in the coastal Everglades (Charles et al.)*. Sean Charles' manuscript expands on his dissertation work on mangrove effects on coastal sediments. As in the Meeder et al. study, Sean's research in the Southeast Saline Everglades concerned the dynamics of soil organic carbon with respect to coastal proximity, but his work focused more directly on present-day processes rather than changes over time. The associations of decomposition rate, root production, soil nutrient content, and mangrove cover with soil organic carbon stores are explored in depth in the draft presented in Section 3, which is well along in development toward journal submission.
4. *An algorithm for quantifying woody plant invasion into lower Everglades marshes from serial aerial photographs (Biswas et al.)*. Terrestrial and wetland ecosystems across the globe are experiencing increases in woody plant encroachment/cover due to global climatic changes (e.g. temperature, rainfall), anthropogenic effects, and sea-level rise. Himadri Biswas, whose dissertation work has been an important part of FIU's research in the C-111 Basin, has developed a novel image segmentation method to automatically detect and delineate woody vegetation from a matrix of marsh vegetation background. The method, which uses a marker-based watershed segmentation in which markers are detected from a vegetation index and Otsu's automatic thresholding, can be applied to very high resolution true color aerial photographs. We plan to use this method to analyze temporal change in mangrove encroachment in the lower Southern Everglades, both at the level of individual trees and forest patches. A paper is in development and should be completed in FY20.
5. *Effects of variable coastal environments on red mangrove leaf functional traits (Vidales et al.)*. Rosario Vidales' manuscript is based on her thesis work to quantify intraspecific variation in leaves of red mangrove of the Southeast Saline Everglades, specifically dwarf red mangrove within marshes, and "hammock" red mangrove found in the tree islands embedded throughout the landscape. Using traits including specific leaf area, stomatal size, stomatal density, and leaf carbon, nitrogen, and phosphorus ratios, the effects of putative coastal gradients of pore water salinity and available phosphorus on leaf functional traits is considered at large (from interior to coast) and small (from scrub marsh to tree island) scales. This work is expected to elucidate how leaf trait plasticity allows this plant to

navigate multiple stressors, and improve understanding of the repercussions of changing environments within the Everglades.

6. *Soil-plant relationships in two ecogeomorphic settings in the Southeast Saline Everglades (Ross, Scinto et al.).* In the south Florida coastal wetlands, tree islands in which mangroves play an important role are embedded in more extensive basin or scrub mangrove types. While several accounts of the vegetation or hydrology of these hammocks have been published, no comprehensive treatment of their physiography, soils, and nutrient relationships has yet been undertaken. In a paper we have begun to draft and expect to complete during the next year, we ask what geomorphologic factors distinguish mangrove hammocks from the smaller-statured shrublands that surround them? More specifically, we test the hypothesis that the availability of phosphorus, the limiting nutrient in most of the Everglades, is greater in mangrove hammocks than adjacent wetlands, based on a sampling design that includes paired analyses of soil and leaf tissue from hammock and basin/scrub environments at 34 lower Everglades locations.

7. *Diatoms as indicators of hydro-edaphic conditions in the coastal Everglades (Wachnicka et al.).* Surface sediments and periphyton mats in South Florida coastal zone are composed of diverse algal communities, which are dominated by diatoms. These communities are sensitive indicators of changing hydrology and water quality. They have been used in several water quality assessment studies in the freshwater Everglades wetlands and in designation of ecotonal boundaries in the adjacent coastal wetlands. However, their relationship to pore water quality, vegetation cover and hydrology and hydroperiods in the coastal zone have not been well studied yet. The manuscript that is currently being developed will investigate these relationships.

Section 1

Concurrent vegetation change in marsh and embedded tree islands in a transgressive coastal landscape

Introduction

As the world prepares for an era of increasing coastal change induced by sea-level rise, the health and movement patterns of the vegetated landscapes - which anchor the biological activity of coastal areas - becomes relevant to land managers. Predictions of the future structure and composition of coastal wetlands may emerge from the view that these attributes are largely determined by the balance between sea level and freshwater discharge (Brinson 1995), superimposed on and conducted through soils and hypsographic eccentricities formed over thousands of years. The resultant landscape is likely to remain a complex shore-normal vegetation gradient, though much changed from the patterns evident today. The effects of sea-level rise on coastal wetlands are thus analogous to what one might see on the slopes of a temperate or tropical mountain undergoing monotonic changes in a complex of climatic factors, where aspect, geological substrate, or landform modify the dynamics of vegetation zonation. When a fundamental driver shifts – when temperature increases or sea-level rises on a long-term basis – environmental models predict that zones within these gradients will move upward in mountainous terrain, or toward the interior in coastal landscapes where slope or human infrastructure allow it (Kana et al. 1988). At the shorter, e.g., decadal time scales addressed by most ecological research, however, the resistance of existing ecosystems, especially forests, to change emerges as a major force that obscures long-term trajectories, and surprising results sometimes ensue (REFs).

Mangroves are the dominant growth form in coastal wetlands of tropical and sub-tropical regions, and several global change processes have led to local expansions of these woody plant assemblages. One is the extension of mangrove ranges at their poleward limits, which has been attributed to the reduced incidence of killing freezes (e.g., Saintilan et al. 2014). More pertinent here, however, is the transgression of mangroves into interior marshes within their existing latitudinal range, where moderated temperatures are probably not as important as rising sea level (e.g., Doughty et al. 2016; Rodriguez et al. 2016; Meeder and Parkinson 2018). One way to view changes in the composition of these zones and landforms is through the lens of the subsidy-stress concept described by Odum and others (1979). Ecosystems arranged at various distances from the coast respond to subsidies or stresses associated with tidal flooding on the one hand and freshwater delivery on the other. By increasing tidal influx, sea-level rise is a complex perturbation, involving both resource subsidies (e.g., nutrient supplements) and stresses (e.g., increased salinity) that elicit variable responses among plant communities and species. Fresh water delivery acts more as a classical subsidy-stress, being beneficial at low levels and adverse at high levels to most species; on the other hand, it also serves to relieve the osmotic stress caused by tidal encroachment. Within a coastal landscape, local

vegetation changes that reflect species responses to alterations in these subsidies or stresses may be perceived as an invasion process.

A geomorphologic framework is also useful in understanding coastal ecosystem change. Moorhead and Brinson (1995) outlined the types of vegetation change they expected on three coastal landform classes: valleys, slopes, and flats. In their study area on the Albemarle-Pamlico peninsula of North Carolina, a flat landform where astronomical tides and sediment input were negligible, they expected that acceleration above the current rate of sea-level rise would lead to wetland loss due to inundation. In his paleoecological analysis of mangrove structure and dynamics, Woodroffe (1992) distinguished river-dominated, tide-dominated, wave-dominated, and carbonate sedimentary settings, which differed in their long-term trajectories in response to sea-level rise late in the Quaternary period. Within each of these settings, an assortment of mangrove functional types (Lugo and Snedaker 1974) occupy landscape positions variably influenced by rivers, tides, or neither.

In his retrospective analysis of mangrove sedimentary response to changing sea-level stage, Woodroffe (1992) looked backwards from current mangrove functional types and coastal environments to trace their development over thousands of years. But along coastlines where fresh or brackish-water wetlands are subject to transgressive processes today, mangrove invasion proceeds over some of the same landforms described by Woodroffe (1992), which may alternatively facilitate or resist mangrove encroachment over short (decadal) time frames. For instance, in some coastal wetland interiors, landscape positions destined to eventually become supratidal scrub mangrove basins or non-tidal hammock mangrove forests are currently occupied by glycophytic species in a coastal landscape of substantial geomorphologic complexity.

Prominent examples are found in Florida's Southeast Saline Everglades (SESE), where zonal patterns characterized the mangrove-to-fresh water marsh transition in the mid-20th Century (Egler 1952). In his monograph on the region, Egler noted the ubiquity of small, teardrop-shaped "hammocks", i.e., forested patches embedded in adjacent marsh or shrub communities, and made detailed observations about the species composition of those he visited. He predicted that mangroves would become increasingly dominant throughout the region as sea-level rose, fire regimes changed, and diversion of fresh water for agricultural and residential uses increased, but he did not speculate on the different trajectories that marsh and hammock might follow during this transition. While Egler's usage of the term "hammock" has since been superseded in the Everglades literature by the more general "tree island" (Loveless 1959; van der Valk and Sklar 2002), the fate of these forest ecosystems in the face of encroaching seas has not been directly addressed.

Studies of tree islands in the Everglades have revealed them to be landscape modulators *sensu* Shachak et al. (2008). That is, the habitat conditions brought on by the forest's capacity to alter geomorphology and resource availability deviate sharply from the marshes and prairies in which they form. Their landscape modulation function is evidenced by three notable characteristics: (1) Tree islands in the interior Everglades

peatlands concentrate nutrients, especially phosphorus, in a landscape in which P is limiting; (2) Tree islands in many Everglades settings build a peat surface substantially above the level of the surrounding marshes, thereby reducing flood depth and duration, and allowing less flood-tolerant species to persist; and (3) As a consequence of their relatively well-drained conditions, tree islands serve as refuges and concentrators of plant and animal diversity in the vast Everglades wetland (Robertson and Frederick 1994). However, unlike the dynamic populations of woody patches envisioned by Shachak and co-authors, tree islands in many Everglades settings nucleate on bedrock outcrops or depressions that favor the buildup of rich soils (REFs). Due to their geologic underpinnings, one might expect these landforms to persist for some time despite rising seas, and their tree assemblages to resist encroachment by mangroves that dominate the zones nearer to the coast.

Building on earlier studies that described vegetation dynamics in the Southeast Saline Everglades during the late 20th Century (Ross et al. 2000; Ross et al. 2014), we assessed concurrent changes in plant species composition in tree islands and adjacent marshes during the last two decades (1996-2016). Considering the transitioning, two-phase coastal landscape, we asked whether vegetation change in marsh and tree island both exhibited a pattern consistent with the subsidies and stresses associated with rising sea-level in adjoining estuarine waters, and what role landscape modulation played in ecosystem response. By comparing the rates and trajectories of change across these neighboring landforms, we also expected to learn more about the potential for increases in freshwater delivery to moderate or reverse these tendencies. We expected that (1) vegetation changes consistent with higher salinity and deeper water levels would be evident in both landscape phases, but (2) compared to the adjacent marsh ecosystems, mangrove invasion into the landscape-modulating tree islands would be slow, due to the superior drainage conditions and the competitive abilities of the diverse community of tropical hardwoods already present.

Methods

Study Area. Bathed by warm sub-tropical waters, the intertidal zone of the lower Everglades is mangrove-dominated. However, since at least the middle of the 20th century, red mangrove (*Rhizophora mangle*) has extended well beyond the intertidal zone into areas reached only by storm tides, where it has effectively replaced dominant graminoids such as sawgrass (*Cladium jamaicense*) in freshwater marsh and black needlerush (*Juncus roemerianus*) in salt marsh (Egler 1952; Ross et al. 2000). Our study focused on these supratidal and non-tidal wetlands, extending from drainages bordering Biscayne Bay on the east to wetlands discharging into Florida Bay on the west (**Figure 1**). The modal soils of the wetland matrix in this region are biologically produced marls (Fluvaquents of the Perrine or Pennsuco series) formed under relatively sparse graminoid cover through the metabolic activities of a periphytic algal community (REF). Soils of the small tree islands scattered throughout the landscape are organic-rich Medisaprists of the Terra Ceia or Pahokee series (USDA 1996). The slope of land is negligible, with

elevation typically rising by only 10 cm over distances of 1 km or more (e.g., Ross et al. 2002; Meeder et al. 2017). Thus, small changes in water stage in the adjacent estuaries can produce flooding across many hectares.

In 1995-96, our research group assessed ecosystem change in the coastal wetlands of the Southeast Saline Everglades since Egler's (1952) landmark study (Ross et al. 2000; Ross et al. 2014). In that survey, herein referred to as the 1995 study, we sampled vegetation in the marsh matrix and adjacent tree islands at 54 locations between Taylor Slough and Biscayne Bay. In 2016-2018, referred to as the 2016 study, we used similar sampling methods to assess vegetation in a coastal network that overlapped considerably with the earlier study, but (1) extended further to the north and west, and (2) focused more narrowly on ecotonal areas inland from the intertidal mangrove swamp. We sampled 48 locations in low matrix vegetation (hereafter, "marsh"), including 28 that were sampled in the earlier study. In 34 of these sites, we also sampled in the nearest tree island; these included 22 forests also visited in 1995-96 (**Figure 1**).

Sampling methods. Surveys of vegetation and soils were done during the 2016-18 dry seasons (November through April), a six-month period during which only ~25% of south Florida's annual precipitation normally falls (Duever et al. 1994). Sample locations were distributed along eleven transects, each comprising 1-4 sites (**Figure 1**). In the easternmost portion of the study area, three transects drain into sub-basins of Biscayne Bay, where semi-diurnal tides of 0.3 m amplitude are typical and salinity is usually in the range 15-35 psu (Wang et al. 2003). Sites further west are connected to Florida Bay, where tides are often minimal, especially in the northeast. Water levels in Florida Bay are weather-driven, and mean annual salinities increase from 30 psu in the east to 36 psu in the center or west. The next 4 transects comprise the headwaters of Northeast Florida Bay, where salinity averages only 18 psu in the coastal embayments below our sites (Lee et al. 2008; Marshall 2017). An eighth transect consists of a single site in Taylor Slough, an eastern conduit for Everglades fresh water supplying Central Florida Bay. Finally, the westernmost transects are south and southwest of Long Pine Key, an E-W trending upland that divides the Taylor Slough drainage from the much larger Shark Slough drainage on the west. These wetlands are separated from Florida Bay by a broad mangrove forest and drain into the Bay through a set of lakes in which salinities are brackish at most times.

To characterize vegetation in the marsh, we estimated shoot cover of vascular plant species in 30 1m² subplots distributed evenly along a 360⁰ arc at 50 m distance from the plot center. Water depth was measured to the nearest 1 cm at each subplot, and soil depth was determined by probing to bedrock. A single soil core was extracted at plot center with a 5.5-cm diameter plastic tube and returned immediately to the lab, where the profile was described and subsamples of each stratum prepared for complete soil analysis. Along with mean soil depth from the 30 vegetation subplots, soils data presented in this paper are limited to the weighted means for organic matter content (OM, determined by loss on ignition at 500⁰C) and bioavailable (water-extracted + sodium bicarbonate-extracted)

phosphorus (P) in the top 30 cm of the core. Values for OM and bioavailable P at each location were calculated by weighting values for each stratum by its relative length and field bulk density. OM was expressed as $\text{g}\cdot\text{g}^{-1}$ and bioavailable P as $\text{ug}\cdot\text{cm}^2$ surface area to 30 cm depth.

The abundance of tree species in the tree islands was estimated using the same method as in the 1995 study: the same observer (MSR) explored the forest thoroughly for ~30 minutes, then ranked the tree species present in terms of canopy coverage. At the same time, a team stretched a tape perpendicular to the long axis of the tree island at its widest point, beginning in the marsh 10 m outside the island and ending 10 m beyond its edge on the opposite side, comprising a transect that ranged in length from 50 to 150 m. Soil depth was determined by probing to bedrock at 5 m intervals. The location of the water table relative to the soil surface was also determined; when water was below the tree island surface, we used a soil auger to create a hole, and waited 5 minutes before measuring the depth of the water table below the soil surface. At the midpoint of the transect a soil core (4.5 cm diameter) was extracted and processed as described above for the marsh.

Due to the wide seasonal variation in salinity in south Florida coastal wetlands, we determined pore water salinity at all sites during a 10-day period in mid-April 2018, when dry season conditions (low water stage, high evapotranspiration) were near their peak. Pore water samples were collected at the marsh plot centers and the centers of the tree islands by pushing a 10-cm diameter PVC tube into the sediment to wall off surface water from entering, then extracting soil core from within with a 5 cm diameter x 30-cm deep soil corer. The core hole was then pumped free of water and allowed to refill from the sides. A pore water sample of approximately 30 ml was drawn and returned to the lab, where salinity was determined with a YSI 30 salinity-conductivity meter.

Data analysis.

Marsh matrix vegetation: To facilitate comparison of marsh vegetation in the 1995 and 2016 surveys, we based vegetation analyses on species frequencies (proportion of the 30 subplots in which each species was present), as sampling in the former period included only the identity of species in each sub-plot, not their abundance. We first classified and characterized sites through application of an agglomerative hierarchical cluster method with flexible beta (-0.25) linkage (McCune and Mefford 2011).

We examined vegetation:environment relationships and characterized shifts in species composition with time by locating sites and their temporal trajectories within non-metric multidimensional scaling (NMDS) ordination space in which environmental vectors (pore water salinity, soil depth, organic matter content, and bioavailable P), were also expressed (Oksanen et al 2019). The ordinations were applied to Site x Time combinations for the 28 sites sampled in both 1995 and 2016, plus the 20 sites sampled only in 2016 (**Figure 1**). Species frequencies were relativized to the total observed at each site. Species present in less than 5% of sites were excluded from the analysis. Relationships between species composition and environmental vectors representing hydro-edaphic characteristics recorded only during the 2016 survey were examined using

a vector-fitting procedure incorporated in the computer program VEGAN (Oksanen et al 2019). Vector fitting is a form of multiple linear regression that finds the direction along which sample coordinates have maximum correlation with the fitted vector within the ordination space. Ordination axes were rotated so that Axis 1 was aligned with pore water salinity measurements from the 2016 survey. Change across the 28 plots common to the two surveys, all of which were in the eastern portion of the study area (**Figure 1**), was first examined by Analysis of Similarity (ANOSIM) (Clarke and Warwick 2001), in which the difference in position in ordination space of centroids representing the two sampling periods were tested. This was followed by a paired t-test, which assessed whether matching site scores on Axis 1 differed between surveys, i.e., whether there was movement along an axis of increasing salinity.

To identify the species that drove compositional shifts between 1995 and 2016, we applied Indicator Species Analysis (ISA, Dufrene & Legendre 1997) to sites that were sampled in both periods, with separate analyses for groups representing each vegetation class, based on site status in 1995. Good indicator species are typically concentrated in a single group or type, and are present in most of the sites belonging to that group (Dufrene & Legendre 1997). The analysis was performed with software PCORD v.6, and indicator values were tested for statistical significance based on a Monte Carlo randomization of 4999 permutations. Significant indicator values were those with a p-value <0.1.

Tree island vegetation: Species cover ranks from the two surveys were transformed for data analysis as in Ross et al. (2014). Species ranked 1 through 4 were assigned an abundance of 10, those ranked 5 through 8 had an abundance of 5, those ranked 9 through 12 an abundance of 2, and those ranked 13 or more an abundance of 1. Ordination, vector fitting, and analyses of temporal change were implemented as described above for the marsh vegetation. Compositional data were species abundances relativized by site totals.

Results

Plant assemblages. The cluster analysis defined four marsh types, based on a cut-off level of 25% information explained (**Table 1**). *R. mangle* was the dominant species in the Mangrove Tidal Swamp, while two other mangroves (*Avicennia germinans* and *Laguncularia racemosa*) were also common. *R. mangle* was also widespread in Spikerush Mangrove Scrub - a type in which the sedge *Eleocharis cellulosa* was present in nearly all plots – but surprisingly reached even higher frequencies in Transitioning Sawgrass Marsh, where *E. cellulosa* and *Cladium jamaicense* (sawgrass) were subdominant graminoid species. *C. jamaicense* was the leading species in Sawgrass Marsh, though *R. mangle* and *E. cellulosa* remained important components of a more diverse community that includes several herbs typical of the freshwater Everglades.

Classification of the 34 tree island assemblages yielded three forest types; as in the marsh, the cut-off level for information explained by the three-group tree island classification was 25% (**Table 2**). Mangrove Forest was a relatively species-poor assemblage in which *R. mangle*, *Conocarpus erectus*, and *Laguncularia racemosa* were dominant species in nearly all stands. Mixed Hammock Forest was a heterogeneous group that included trees usually associated with saltwater or freshwater wetland

environments, but was most notable for the prominence of tropical hardwood species usually associated with well-drained substrates. Among the mesic species common in this forest type were *Metopium toxiferum*, *Eugenia* spp, *Calypttranthes pallens*, *Myrsine floridana*, *Swietenia mahogani*, and *Coccoloba* spp. In the third group, Mixed Bayhead Forest, tropical hardwoods were present but were less abundant than freshwater swamp (bayhead) species such as *Chrysobalanus icaco*, *Morella cerifera*, and *Persea borbonia*; among the halophytes, only *R. mangle* and *C. erectus* were well-represented in the group.

Both marsh and tree island types are distributed in a zonal pattern relative to the south Florida coast (**Figures 2a and 2b**). Among the marsh types, Spikerush Mangrove Scrub seems to coincide with the White Zone, a conspicuous feature on large-scale imagery in which low vegetation cover combines with a light-colored marl surface (Egler 1952; Ross et al. 2000, 2002). Also notable is the continuity of the band of Mixed Hardwood tree islands midway in the wetlands of the Southeast Saline Everglades.

Environmental characteristics. The zonal patterns evident in the vegetation of the coastal Everglades were paralleled by some of the environmental variables documented in the 2016 survey. Most prominent was marsh pore water salinity (**Figures 3 and 4a**), which decreased monotonically with distance from the coast; notably, this decrease was steeper on the east (Biscayne Bay watershed) than south (Florida Bay watershed). The spatial pattern for tree islands (not shown) was similar, and data from the 34 sites in which marsh and tree island were both sampled indicates that mean pore water salinity did not differ between these two habitats (**Table 3 and Figure 4a**). Despite several differences among individual marsh or tree island types, edaphic variables (bioavailable P, organic matter content and soil depth) did not exhibit the same monotonic patterns with respect to the coast as observed for salinity (**Figure 4b – 4d**). Also notable in **Figure 4** and **Table 3** is the higher organic matter and bioavailable P content in tree island than marsh. While bioavailable P content was also more variable in tree island soils, the high values in the Mixed Hardwood tree island type stand out (**Figure 4c**). Unlike the other physical variables, soil depth in tree island and marsh did not differ significantly (**Table 3**).

Compositional dynamics during 1996-2016. Current spatial patterns in south Florida coastal wetland plant composition and environment set the stage for analysis of vegetation change in the area between our 1995 and 2016 survey. In marshes, vectors for pore water salinity, bioavailable P and soil depth bore significant relationships to the site ordination (**Figures 5a**) while in tree islands only pore water salinity and bioavailable P fit strongly with vegetation composition (**Figure 5b**). Organic matter content did not exhibit a significant association with either the marsh or tree island site ordinations.

In the marsh, the two most coastal communities, Mangrove Tidal Swamp and Spikerush Mangrove Swamp, occupied the upper right and center right positions in the ordination, respectively, while Transitioning Sawgrass Marsh and Sawgrass Marsh occupied the upper and lower left quadrants (**Figure 5a**). With the salinity vector affixed along Axis 1, the soil depth and bioavailable P vectors find a position nearly perpendicular to it, increasing along the positive and the negative side of Axis 2 respectively. The opposite

orientations of these two vectors is supported by **Figures 4c** and **4d**, which display a coastward decrease (albeit non-significant) in marsh bioavailable P accompanied by a coastward increase in marsh soil depth. The strong relationship of this environmental axis with the marsh ordination deserves study, beginning with further exploration through spatial analyses.

Analysis of similarity (ANOSIM) revealed substantial marsh plant community change between 1995 and 2016 (Global $R=0.11$, $p\text{-value}<0.05$), particularly in the Spikerush Mangrove Scrub. Notable species changes include reductions in the abundance of *Utricularia purpurea*, a floating-leaved bladderwort, in Sawgrass Marsh and increases in the abundance of *R. mangle* in Sawgrass Marsh and Spikerush Mangrove Scrub (**Table 4**).

The trajectories for individual sites in **Figure 5a** illustrate a marsh vegetation dynamic one would expect to see at sites experiencing increased salinity stress due to sea-level rise. Plant composition at sites surveyed in both years moved significantly to the right ($t=-1.91$, $p=0.06$), i.e., in the direction of higher pore water salinity. Significant movement ($t=-2.9$, $p<0.01$) along Axis 2 suggested a trend toward marsh communities characterized by deeper soils. This change may reflect the increase in red mangrove abundance over time in a landscape in which the species is associated with deeper, peatier soils than in adjacent coastal prairies. Supporting this view is the vector for organic matter content, which despite not being significantly related to the ordination as a whole, closely paralleled the soil depth vector.

Whereas marsh vegetation dynamics trended toward more salt-tolerant species, tree islands followed a different trajectory (**Figure 5b**), or rather one with no consistent direction among sites. ANOSIM indicated no significant difference in the centroids of sites sampled in the two surveys (Global $R=-0.013$, $p\text{-value}=0.63$). Likewise, while the salinity, bioavailable P and organic matter vectors were significantly related to the site ordination, the shift in composition between matching stands was not significant along Axis 1 ($t=0.71$, $p=0.43$), representing pore water salinity, or along Axis 2 ($t=-0.85$, $p=0.41$). As in the marsh, the opposite orientations depicted by the bioavailable P and organic matter vectors along Axis 2 is supported by **Figures 4b** and **4c** which show significantly higher bioavailable P and organic matter in the Hammock and Bayhead Mix types respectively. The Indicator Species Analysis did suggest several changes in species composition in the Mixed Hardwood type, including a decline in the abundance of *Annona glabra*, a quintessential swamp forest tree, as well as the invasive non-native *Schinus terebinthifolius*, while the valuable fruit-bearing poisonwood (*Metopium toxiferum*) increased in abundance (**Table 4**).

Table 1: Relative abundance of major marsh species in four vegetation types in 2016.

Species	Sawgrass Marsh	Transitional Sawgrass Marsh	Spikerush Mangrove Scrub	Mangrove Tidal Swamp
CLAJAM	45	33	6	
ELECEL	20	19	49	5
RHIMAN	7	39	22	48
UTRPUR	7	3	9	7
RUPMAR			3	7
JUNCOE				5
DISSPI				7
AVIGER				10
LAGRAC				13

Table 2. Relative abundance of major woody species in three tree island types in 2016.

Species	Bayhead Mix	Hammock Mix	Mangrove Forest
CHRICA	16	3	
MORCER	14	8	
PERBOR	10	1	
MYRFLO	6	5	
ILECAS	6	1	
CONERE	11	14	18
RHIMAN	11	15	25
METTOX	13	12	1
EUGFOE		6	
LAGRAC		4	24
AVIGER			13
JACKEY			5

Table 3: Mean±SD soil variables in marsh and tree islands.

Variables	Marsh			Tree Island			F	p-value
	N	Mean	SD	N	Mean	SD		
PWSal (psu)	34	11.40	11.95	34	9.20	9.99	1.43	NS
Bioavailable P (ug g ⁻¹ dw)	33	55.92	25.07	32	97.85	117.73	0.05	<0.01
OM (g g ⁻¹ dw)	34	0.14	0.14	33	0.66	0.20	0.47	<0.05
SD (cm)	34	85.19	32.27	34	117.82	33.27	0.94	NS

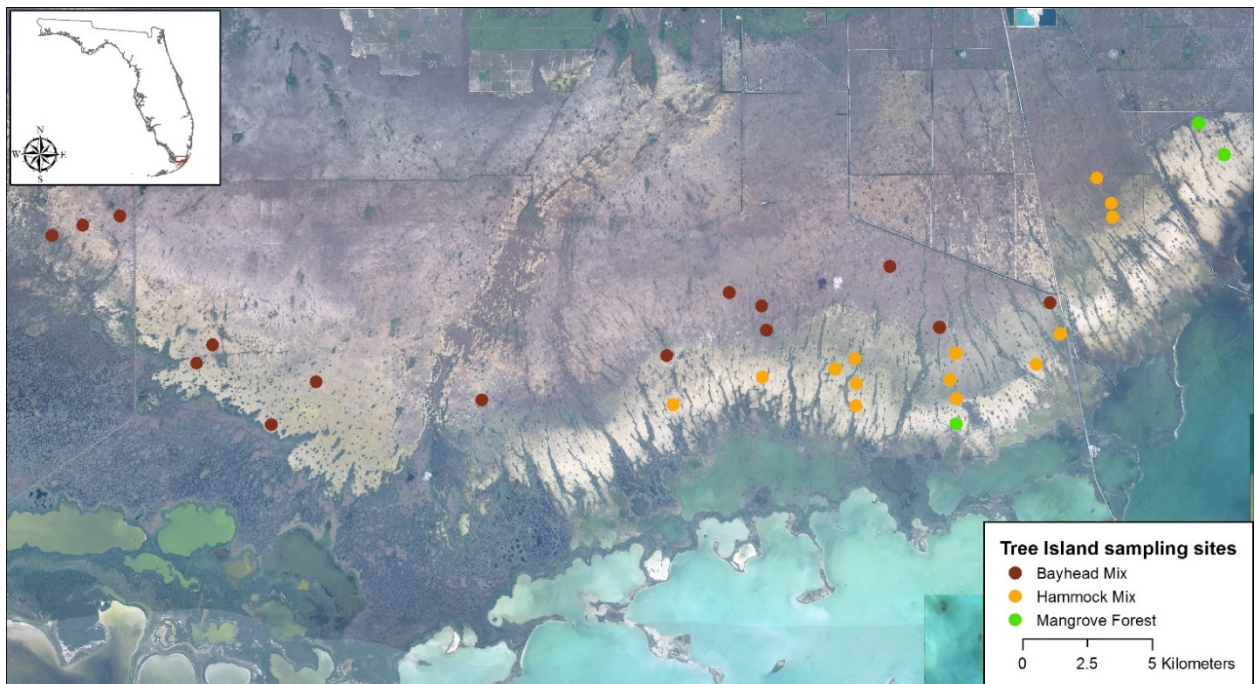
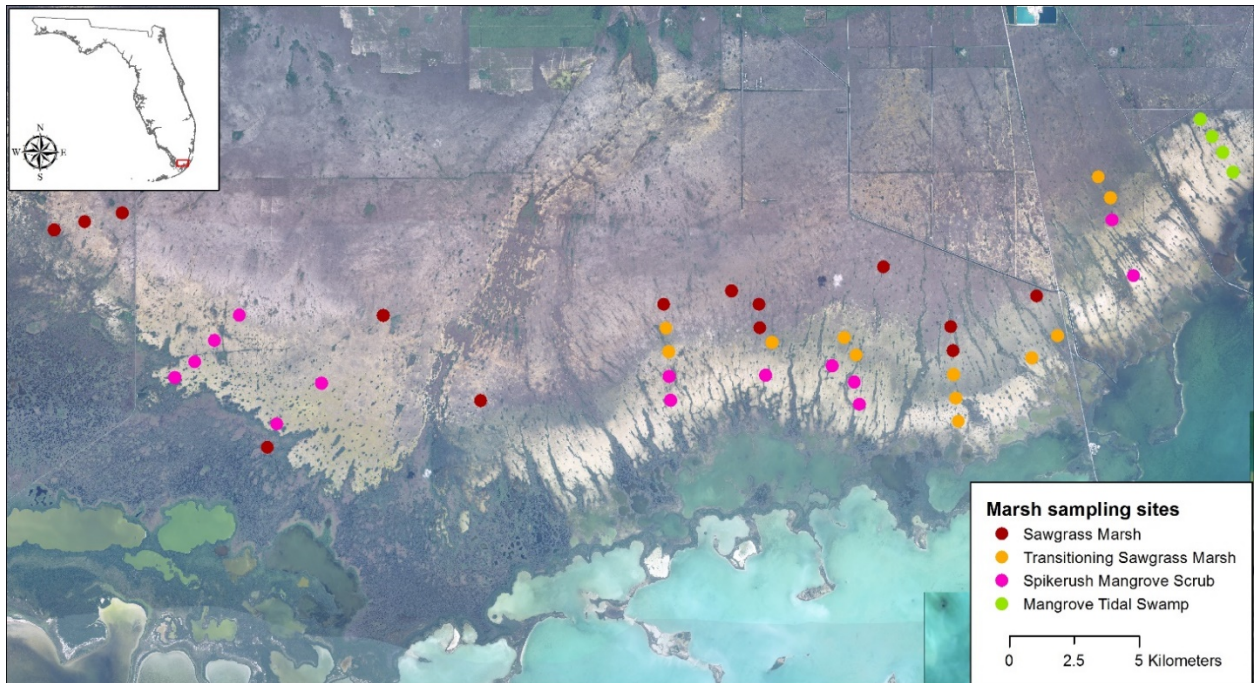
Table 4: Indicator species for differences ($p < 0.1$) in relative abundance between 1996 and 2016 for several marsh and tree island types. Only types with three or more resampled sites were analyzed.

Marsh Vegetation Types	1996	2016
Sawgrass Marsh	UTRPUR	RHIMAN
Transitional Sawgrass Marsh*		
Spikerush Mangrove Scrub		RHIMAN
Mangrove Tidal Swamp*		
Tree Island Types	1996	2016
Bayhead Mix		
Hammock Mix	ANNGLA	METTOX
	FICAUR	
	SCHTER	
Mangrove Forest*		

*3 or fewer common sites sampled in 1996 & 2016



Figure 1: Marsh and tree islands sites location sampled in 1995 and 2016.



Figures 2a and 2b: Distribution of marsh (a) and tree island (b) types in the coastal Everglades.

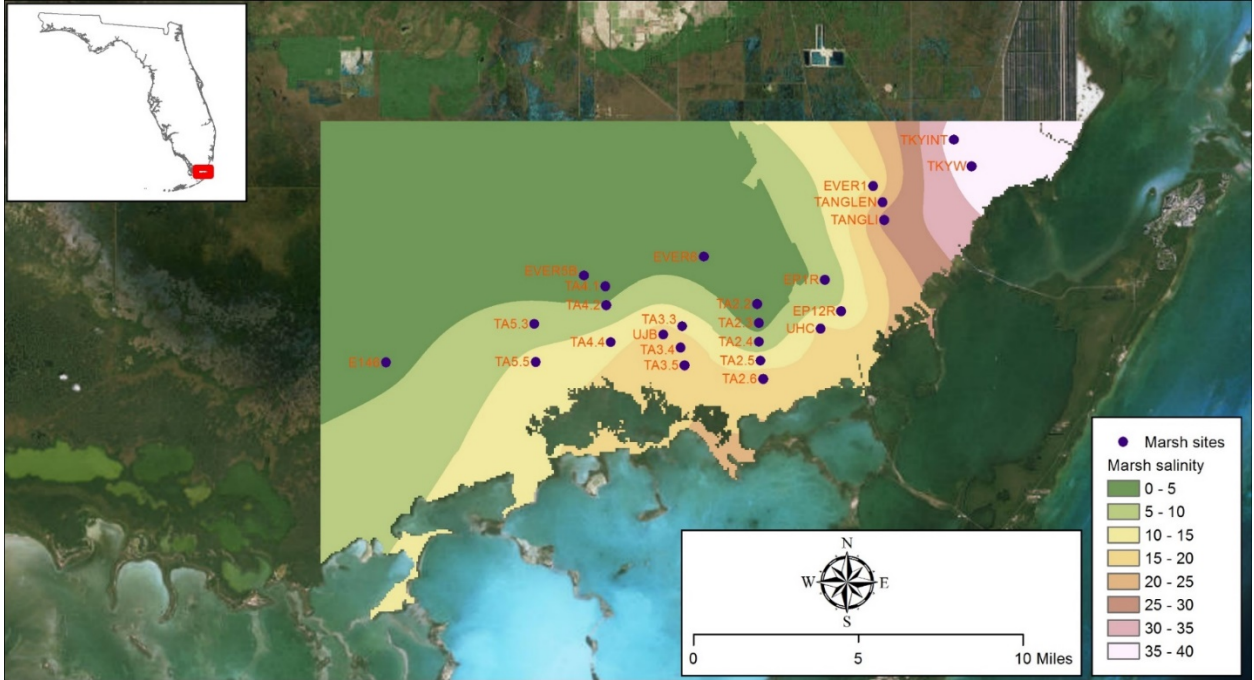


Figure 3: Marsh pore water salinity in April 2018.

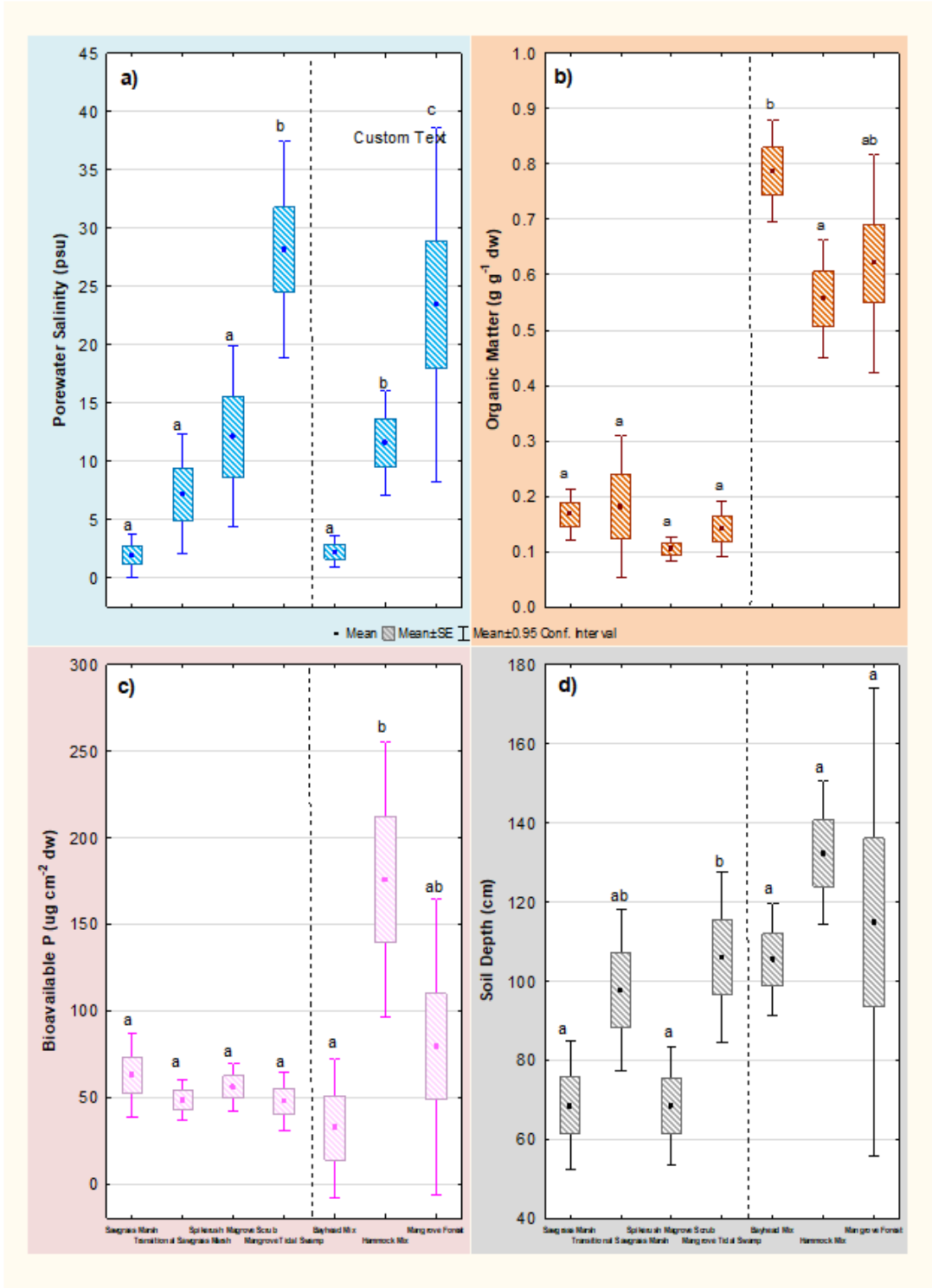


Figure 4a-d: Hydro-edaphic characteristics of marsh and tree island ecosystems in the coastal Everglades. Within marsh or tree island, vegetation type means superscripted by the same letter do not differ (p-value < 0.05).

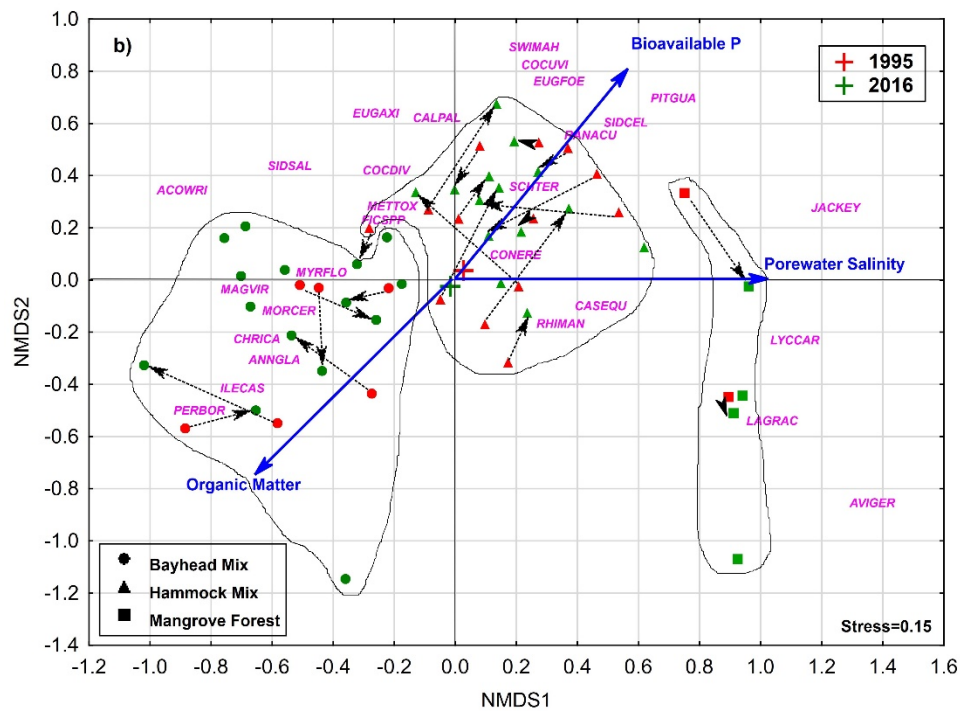
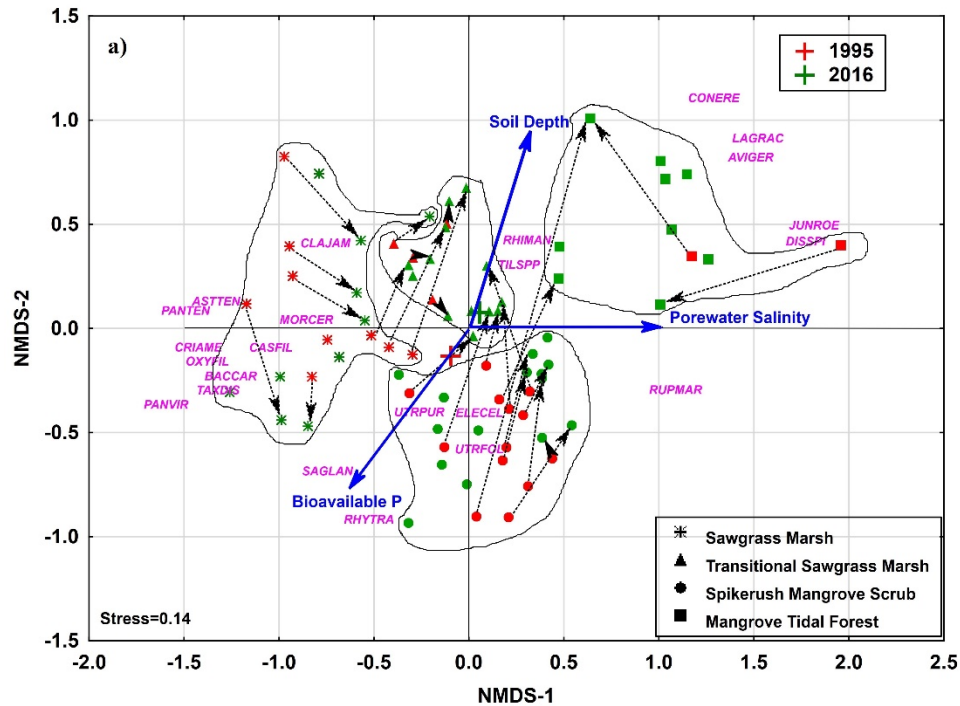


Figure 5: Movement of (a) marsh and (b) tree island communities in 2-dimensional NMDS ordination space, 1996-2016. The ordinations are based on data for site x species abundance matrices collected in 2016, and solid arrows indicate strength and direction of best linear fit to the ordination for environmental variables determined at the same time. Dashed arrows indicate 1996-2016 compositional change at individual sites sampled in both years.

Literature Cited

- Brinson, M. M., R. R. Christian, and L. K. Blum. 1995. Multiple states in the sea-level induced transition from terrestrial forest to estuary. *Estuaries* 18(4): 648-659.
- Doughty, C. L., J. A. Langley, W. S. Walker, I. C. Feller, R. Schaub, and S. K. Chapman. 2016. Mangrove range expansion rapidly increases carbon storage. *Estuaries and Coasts* 39:385-396.
- Duever, M. J., J. F. Meeder, L. C. Meeder, and J. M. McCollom. 1994. The climate of South Florida and its role in shaping the Everglades ecosystem. In: S. M. Davis and J. C. Ogden, eds. *Everglades: the ecosystem and its restoration*. St. Lucie Press, Delray Beach. 826 pp.
- Egler, F. E. 1952. Southeast saline Everglades vegetation, Florida, and its management. *Vegetatio* 3: 213-265.
- Kana, T. W., G. J. Baca, and M. L. Williams. 1988. Charleston case study. Pages 37-59 in J. G. Titus, ed. 1988. *Greenhouse effect, sea level rise and coastal wetlands*. EPA-230-05-86-013. United States Environmental Protection Agency, Washington, D. C.
- Malanson, G. P., D. R. Butler, D. B. Fagre, S. J. Walsh, D. F. Tomback, L. D. Daniels, L. M. Resler, W. K. Smith, D. J. Weiss, D. L. Peterson, A. G. Bunn, C. A. Hiemstra, D. Liptzin, P. S. Bourgeron, Z. Shen, and C. I. Millar. 2007. Alpine treeline of western North America: linking organism-to-landscape dynamics. *Physical Geography* 28(5): 378-396.
- Meeder, J. F., R. W. Parkinson, P. L. Ruiz, and M. S. Ross. 2017. Saltwater encroachment and prediction of future ecosystem response to the Anthropocene Marine Transgression, Southeast Saline Everglades, Florida. *Hydrobiologia* 803(1): 29-48.
- Meeder, J. F. and R. W. Parkinson. 2018. Southeast Saline Everglades transgressive sedimentation in response to historic acceleration in sea-level rise: a viable marker for the base of the Anthropocene? *Journal of Coastal Research* 34(2): 490-497.
- Odum, E. P., J. T. Finn, and E. H. Franz. 1979. Perturbation theory and the subsidy-stress gradient. *BioScience* 29(6): 349-353.
- Ogurcak, D. E., J. P. Sah, R. Price, and M. S. Ross. In press. The interaction of press and pulse disturbances: evidence of the effects of sea level rise on coastal forests of the lower Florida Keys. *Forest Ecology & Management*
- Parker, E. R. and R. L. Sanford. 1999. The effects of mobile tree islands on soil phosphorus concentrations and distribution in an alpine tundra ecosystem on Niwot Ridge, Colorado Front Range, USA. *Arctic, Antarctic, and Alpine Research* 31(1): 16-20.

- Raabe, E. A. and R. P. Stumpf. 2016. Expansion of tidal marsh in response to sea-level rise: Gulf Coast of Florida, USA. *Estuaries and Coasts* 39: 145-157.
- Rodriguez, W., I. C. Feller, and K. C. Cavanaugh. 2016. Spatio-temporal changes of a mangrove-saltmarsh ecotone in the northeastern coast of Florida, USA. *Global Ecology and Conservation* 7: 245-261.
- Ross, M. S., J. F. Meeder, J. P. Sah, P. L. Ruiz, and G. J. Telesnicki. 2000. The Southeast Saline Everglades revisited: 50 years of coastal vegetation change. *Journal of Vegetation Science* 11: 101-112.
- Ross, M. S., J. P. Sah, J. F. Meeder, P. L. Ruiz, and G. Telesnicki. 2014. Compositional effects of sea-level rise in a patchy landscape: the dynamics of tree islands in the southeastern coastal Everglades. *Wetlands* 34(Suppl 1): S91-S-100.
- Saintilan, N., N. Wilson, K. Rogers, A. Rajkaran, and K. W. Krauss. 2014. Mangrove expansion and salt marsh decline at mangrove poleward limits. *Global Change Biology* 20(1): 147-157.
- Schlesinger, W. H. and A. M. Pilmanis. 1998. Plant-soil interactions in deserts. *Biogeochemistry* 42: 169-187.
- Shachak, M., B. Boeken, E. Groner, R. Kadmon, Y. Lubin, E. Meron, G. Ne'Eman, A. Perevolotsky, Y. Shkedy, and E. D. Ungar. 2008. Woody species as landscape modulators and their effect on biodiversity patterns. *BioScience* 58(3): 209-221.
- Smith, J. A. M. 2013. The role of *Phragmites australis* in mediating inland salt marsh migration in a mid-Atlantic estuary. *PLOS One* 8 (5): e605091.
- Telis, P. A., X. Zhixiao, L. Zhongwei, L. Yingru, and P. Conrads. 2015. The Everglades Depth Estimation Network (EDEN) Surface-Water Model, Version 2: U. S. Geological Survey Scientific Investigations Report 2014-5209.
- Troxler, T. G., D. L. Childers, and C. J. Madden. 2014. Drivers of decadal-scale change in southern Everglades wetland macrophyte communities of the coastal ecotone. *Wetlands* 34(Suppl1): S81-S90.
- USDA-NRCS. 1996. Soil survey of Dade County area, Florida. 116 pp.
- Williams, K., K. C. Ewel, R. P. Stumpf, F. E. Putz, and T. W. Workman. 1999. Sea-level rise and coastal forest retreat on the west coast of Florida, USA. *Ecology* 80(6): 2045-2063.

Section 2

Salt water encroachment and the paleoecology of coastal sediments

John Meeder, Santiago Castaneda, Susana Stoffella, and Mike Ross

Abstract.

Salt water encroachment has already reached the L-31E levee along the Biscayne Bay coastal basins, where inundation ponding has been observed (Meeder et al. 2017; Meeder and Parkinson 2018). In contrast, coastal basins along Florida Bay experienced diverse responses to the Anthropocene Marine Transgression (Meeder and Parkinson 2018). Salt water encroachment has been continuous along Biscayne Bay despite increased fresh water delivery (Meeder et al. 2018). Major differences between Biscayne and Florida Bay coastal wetlands are their width (much less along Biscayne Bay), coastal slope (twice as great along Biscayne Bay), and means of fresh water delivery (most reaching Biscayne Bay from point sources). In this report, we examine six coastal basins. In two, salt water encroachment has not decreased since first observed in 1995 (Meeder et al. 1996; Ross et al. 2000; Ross et al. 2002; Meeder et al. 2017). In two other basins, marine-influenced sediments were replaced by freshwater sediments, and in two basins no changes were observed. Differences among Florida Bay coastal basins result from variable fresh water examined delivery, micro-topography and connection to tide waters (tidal efficiency).

Whereas salt water encroachment along Biscayne Bay resulted in increased organic carbon storage (Meeder et al. MS), a decrease in stored organic carbon was observed in Florida Bay coastal basins. Along Florida Bay differences in organic carbon content between fresh water and marine-influenced sediments are minor. Cores demonstrate a general decrease in organic carbon content during the last century and most transects document an increase in organic content with increased distance from the coast, as sawgrass-derived soils (carbon rich) is replaced by marl sediments (carbon poor) associated with salt water encroachment. One reason for the difference between Biscayne and Florida Bays is that the study focused on the leading front of salt water encroachment along Florida Bay, in contrast to Biscayne Bay, where our research has focused on mangrove expansion along a narrow zone adjacent to Biscayne Bay, where salt water encroachment reached the L31E storm protection levee decades earlier.

Introduction.

This report continues the paleosalinity analysis of cores collected in 2016-17, and processed in 2018-2019. In contrast to previous reports that addressed watersheds associated with Biscayne Bay, all cores discussed here are from coastal watersheds exchanging water with Card Sound or Florida Bay.

The core purpose of this work is to identify and assess changes that have occurred since the 1995 study of vegetation, sediments and salt water encroachment (SWE) (Meeder et al 1996; Ross et al. 2000; Ross et al. 2002; Meeder et al. 2017). Therefore our sampling

strategy emphasized the interior of the C111 coastal basins rather than coastal fringe, where SWE had already been demonstrated. Fresh water delivery increased since the 1995 study and quantification of the effects of this management change is a prime objective. In this section, we focus on the distance and rate of SWE and associated changes in organic carbon (OC) storage.

In the coastal Everglades, marine influenced sediments have lower bulk densities and higher OC content than fresh water sediments (Meeder et al. in review). An increase in OC storage has been observed in the marine transgressive stratigraphic package along Biscayne Bay. However, along Florida Bay the mangrove fringe is not as well developed and the majority of mangrove communities are not as dense as along Biscayne Bay. In this report, we describe OC distribution both horizontally and vertically in cores along Florida Bay transects.

Methods.

Ten core transects have been sampled within the Southeast Saline Everglades: three perpendicular to the Biscayne Bay shoreline, one inland from Barnes Sound, and six more at sites along the Florida Bay coast (Figure 1). Sediment cores were collected with 3-cm diameter aluminum tubes, returned to the lab, frozen, and sectioned at 1 cm intervals. All cores with more than 5% compaction were rejected. All sediment intervals were analyzed to determine bulk density, organic matter content, and a salinity index (SI). Sediment accumulation rates estimated by ^{210}Pb were used to assess the rate of organic matter burial and the timing of SWE. Data on the rate of sediment accumulation by plant-sediment association (PSA) were used from previous work (Meeder et al. 1996 and Meeder et al. 2017). Each core interval was split and aliquots used for separate analyses. Data is presented by transect, from the east to the west and from the coast to the interior.

Core descriptions. Cores were described and photographed. Among the sediment types used in this report, several have been previously described from Biscayne Bay cores (Meeder et al. 2017). However, within coastal basins along Florida Bay three types of marl were recorded based upon color and OC content. Such diversity in marl characteristics was not encountered in Biscayne Bay coastal basins.

Bulk density. Bulk density was calculated for each interval by sampling 2 cm^3 and weighing after drying at 70°C to the point of no further weight loss, usually ~24 hrs. The 2 cm^3 sediment size was utilized to incorporate the sediment variability that could be created by a single root.

Salinity index (SI). In a sample aliquot of 20.8 cm^3 (one half of the full 1 cm increment minus the 2 cm^3 that was used for bulk density and OM determination), we counted invertebrates larger than 1 mm in diameter. The large sample was necessary to recover adequate numbers of invertebrates for analysis. The sample was washed through a series of sieves, followed by identification and enumeration of specimens (nearly 100% mollusks). Based on known affinities for marine, brackish, and saltwater environments

(Thompson 1984), we applied a weighted averaging technique (Blinn 1993) to mollusk composition to determine a Salinity Index for each increment in each core (Meeder et al. 1996; 2017). The resultant SI profiles allowed us to infer historical salinity conditions during sediment deposition. Core intervals with $SI \leq 1.5$ were considered to represent a fresh water environment. Characterization of the modern salinity environment was determined by averaging the data for the upper 3 cm of core data. Within each core, strata representing different PSA's (Table 1) were identified, and SI's from all 1-cm increments within each stratum were averaged.

Rate of salt water encroachment (SWE). By examining the SI profiles in each core, we assumed SWE, i.e., the time of initiation of marine-influenced conditions, to have taken place when consecutive SI values >1.5 were found above sections in which SI values were consistently <1.5 . Then, by comparing SWE estimates among core locations along transects, we determined a rate of SWE based on the difference in the estimated year SWE was reached at adjacent points along each transect. Sediment dates were calculated using previously calculated rates of sediment accumulation determined by Pb_{210} methodology (Table 1). Data are presented as fence diagrams that illustrate both the vertical and horizontal distribution of marine influenced sediments.

Table 1. Summary of plant community - sediment type associations (Data from Meeder et al. 2017; Meeder & Parkinson 2018).

	Landscape feature	Plant community	Sediment Type	Ac*	1 cm = yrs	SI
PSA1	Fringing mangrove	Mangrove	Mangrove peat	4.1	2.4	> 1.5
PSA2	Scrub mangrove	Mangrove	Mangrove peat marl	3.25	3.1	> 1.5
PSA3	Wet prairie	Periphyton	Marl	1.35	7.4	< 1.5
PSA4	Marsh	Sawgrass	Sawgrass Peat marl	2.1	4.8	< 1.5

* Ac = Accumulation rate ($mm\ yr^{-1}$); ^ This study

Organic carbon (OC). After weighing the dry bulk density sample, the sample was heated to $500^{\circ}\ C$ for 1 hr and reweighed to determine weight after loss on ignition (Dean 1967), thereby providing the weight of organic matter. Organic matter was converted to OC using the standard conversion factor of 0.58 (Sikora and Stott 1996). Percent OC for each sample was calculated by dividing OC weight by total dry weight of the sample. Modern OC content was determined by averaging the data for the upper 3 cm of core data. As described for SI above, average OC was determined for each PSA interval, and data were presented in fence diagrams which illustrate vertical and horizontal distributions of OC.

Organic carbon deposition rate. ^{210}Pb analysis of sediment cores determined the rate of deposition for different PSAs in $g\ OC\ cm^{-3}$ (Table 1). We determined OC deposition rate in $g\ OC\ m^{-3}\ yr^{-1}$ by dividing $g\ OC\ m^{-3}$ by the number of years required for 1 cm of

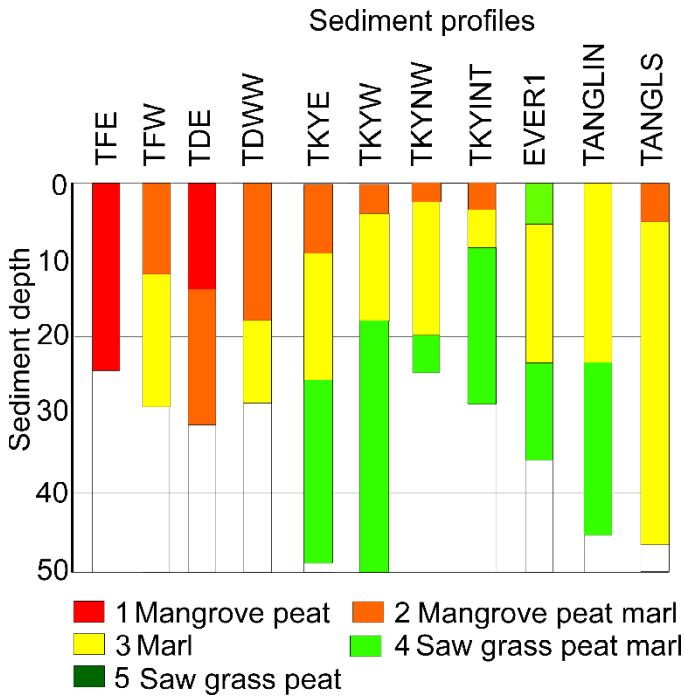


Figure 2. Core sediment descriptions from transects along Biscayne Bay and Barnes Sound coastal basins (Figure 1).

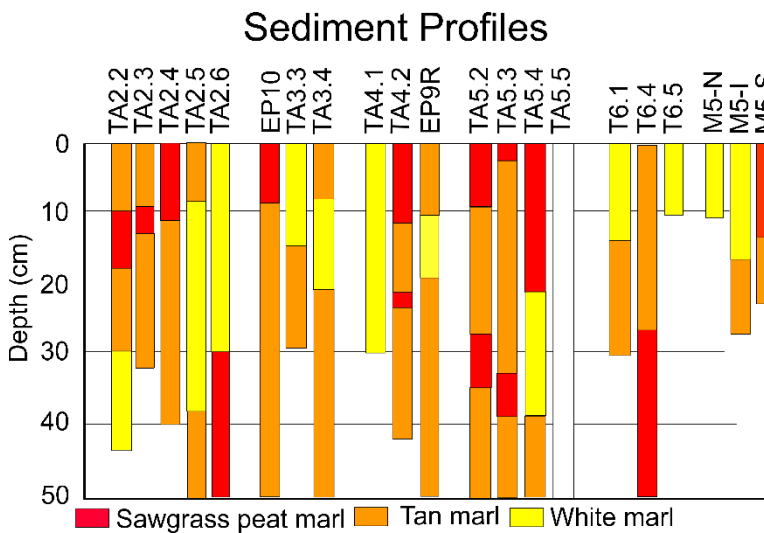


Figure 3. Core descriptions from along Florida Bay coastal basins.

Salt water encroachment

All paleosalinity data are presented in Appendix B. Red lines in fence diagrams are projected boundaries between freshwater and marine influenced sediments. Data presentation is by transect starting from the northernmost transect north of the Biscayne

National Park headquarters and finishing southeast of Shark River Slough in Everglades National Park.

Biscayne Bay: Mowry CD transect. Biscayne Bay Mowry Canal transect (CD) documents SWE to the toe of the L31E levee (Figure 4, left fence diagram).

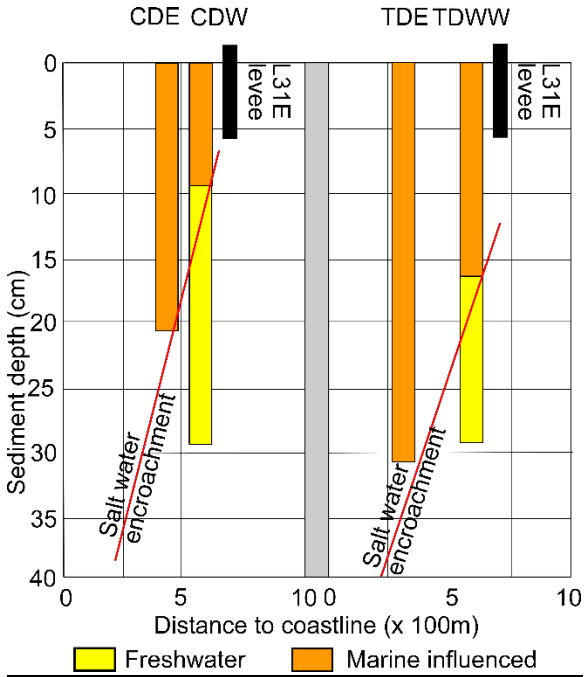


Figure 4. Fence diagram documenting SWE along the Mowry Canal transects CD and TD.

Biscayne Bay: Mowry TD transect. Biscayne Bay Mowry Canal transect (TD) documents SWE to the toe of the L31E levee (Figure 4, right fence diagram).

Biscayne Bay: Turkey Point transect. The TKY transect is 5.5 times longer than the other Biscayne Bay transects and therefore the effects of SWE are spread over greater distances. Mangrove expansion and SWE have reached the L31E levee.

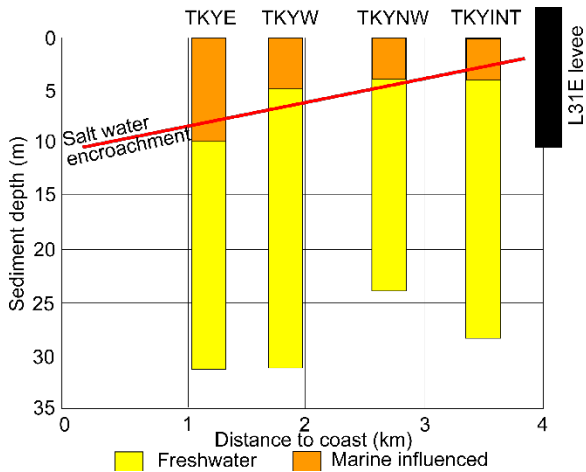


Figure 5. Fence diagram documenting SWE along the TKY transect.

Barnes Sound: Triangle Transect (TANG). The fence diagram produced from the three core profiles document that marine influenced sediments are restricted to the surface of the 2 most coastal cores (Figure 6). Based on an average marl accumulation rate of 1.35 mm yr^{-1} (Table 1), salt water encroachment (SWE) reached TANGLS, about 1.5 km from the coast, in ~1972. In 2016 SWE had penetrated beyond TANGLEN, at 4.2 km, suggesting that it reached to ~4.69 km from the coast, for an increase of 3.2 km in 44 yr, or 73 m yr^{-1} . There is no evidence of SWE slowing or reversing along this transect.

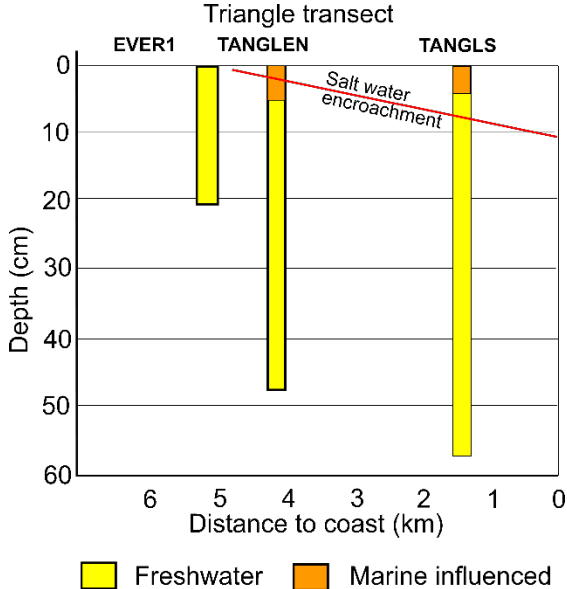


Figure 6. Fence diagram of paleosalinity of the TRIANGLE.

Transect TA2. Transect TA2 comprised five cores, TA2.2 to 2.6 (Figure 7). Marine influenced sediments were found at about 5 cm depth in 4 of the cores, extending to the most interior site, whose Distance To Coast was ~5.1 km. However, all of these marine sediment layers were shallowly buried by fresh water sediment. SWE reached TA 2.6

(1.67 km DTC) ~ 1920 (96 ybp) and reached TA2.2 (5.1 km DTC) in 1986. At the latter site, a very rapid reversal began within the time required for 1 cm of sediment to accumulate (~7 yr). Rates of SWE varied among sections of the transect: 19 m⁻¹ yr⁻¹ between TA2.6 and TA2.5 (45 yr and 0.86 km), 114 m yr⁻¹ between TA2.5 and TA2.4 (7 yr and 0.80 km), 126 m yr⁻¹ between TA2.4 and TA2.2 (14 yr and 1.77 km). TA2.3 was bypassed and did not experience SWE, perhaps because the area around TA2.3 was a local topographic high. Local highs in the study area do not have to be much elevated to affect the biota, as the difference in elevation among the study sites is only a few cm. The rate of 126 m yr⁻¹ between TA2.2 and TA2.4 is the highest we measured, and to our knowledge, rates this high have not previously been documented. Reversal of SWE was almost simultaneous along the transect and started ~ 1980.

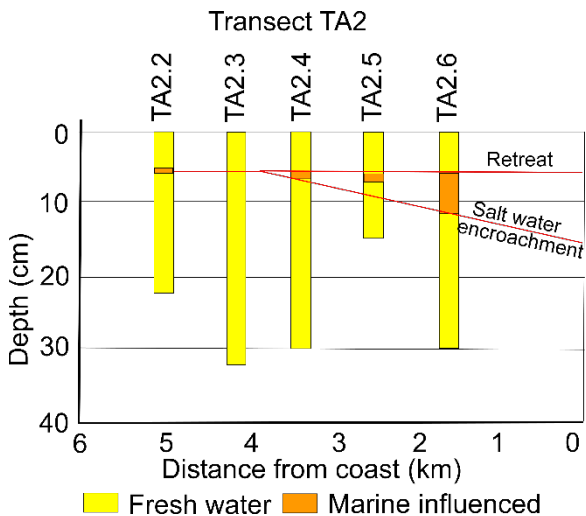


Figure 7. Fence diagram of paleosalinity along Transect TA-2.

Transect TA-3. Cores EP10, TA3.3 and TA3.4 made up Transect TA3 (Figure 8). Marine influenced sediments were found at the top of TA3.4, 3.41 km DTC. Marine influenced sediments were found in all three cores but not at the surface in EP10 or TA3.3. The upper part of TA3.3 contained no mollusks or other invertebrates, and no marine influenced horizons were found above the marine influenced interval that ended several cm from the surface. Therefore we could not use mollusk assemblages to assess the salinity conditions in the most recent intervals. An alternating sequence of fresh and marine influenced sediments were found at the top of EP10, indicating that SWE reached ~ 6 km DTC three times in the upper 10 cm. Initial SWE was rapid and bypassed local topographic highs (TA3.4). SWE between TA3.5 and EP10, a distance of 1.73 km, was so rapid that no difference in elevation between TA3.4 and EP10 was recorded for an astronomic rate of SWE <7 yr for a minimum SWE rate of 692 m⁻¹ yr⁻¹. An incomplete reversal in SWE began ~1995 but has not replaced marine influenced sediments in TA3.5. Retreat of SWE along TA3 was slow as determined by the upgrade slope towards the coast (Figure 8), which was created by continued sediment accumulation during retreat.

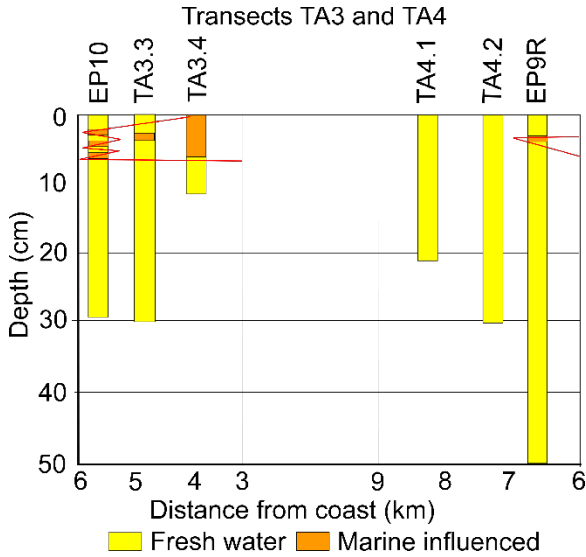


Figure 8. Fence diagram of paleosalinity of TA.3 and TA.4

Transect TA-4. Cores TA4.1, TA4.2 and EP9R make up transect TA4 (Figure 8). Based on mean accumulation rate for marl soils of 1.35 mm yr^{-1} (Table 1), SWE first reached EP9R in 1987 and reverted back to a fresh water depositional environment in 1995. SWE never reached the the two sites (TA4.2 and TA4.1) 1-2 km to the north.

Transect TA-5. Four cores, TA5.2, TA5.3, TA5.4 and TA5.5, were collected along Transect TA-5 (Figure 9). SWE reached TA5.5, 4.76 km from the coast, in 1935 and then TA5.4 (5.68 km from the coast) in 1980, moving at a calculated rate of 21 m yr^{-1} . SWE reached TA5.3 (6.6 km DTC) in ~ 2002 , displaying an encroachment rate of 42 m yr^{-1} . Though it hasn't yet reached TA5.2 (7.5 km DTC), SWE has displayed continuous movement in this coastal basin, which is located west of the C111 Canal.

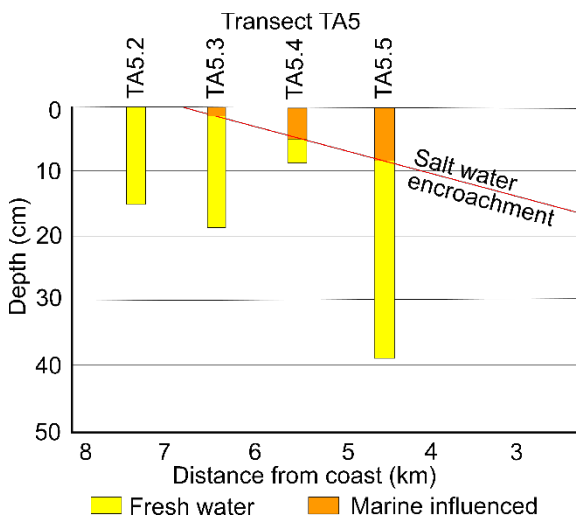


Figure 9. Fence diagram of paleosalinity along transect TA5.

Transect T6. Three cores, T6.1, T6.4 and T6.5 were analyzed along Transect T6 (Figure 10). T6.5 is located 8.59 km from the coast. No marine influenced sediments were observed.

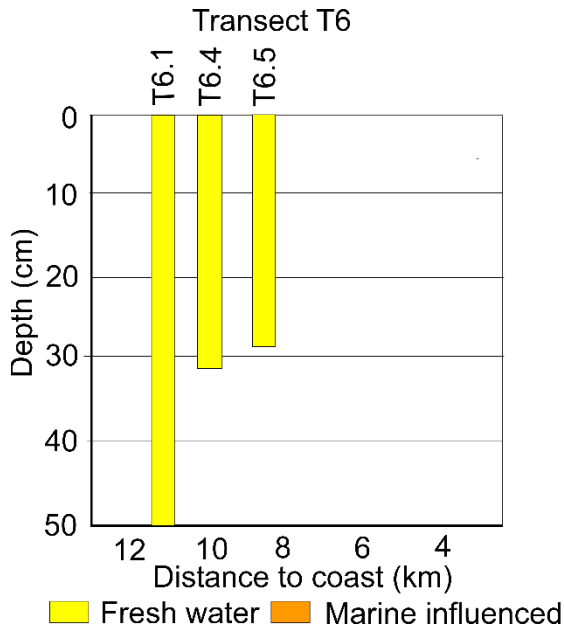


Figure 10. Fence diagram of paleosalinity along transect TA6

Transect M5. Three cores, M5-N, M5-I and M5-S were collected along transect M5 (Figure 11). No marine influenced sediments were observed at even the most coastward site, M5-S, which is 8.86 km from the coast. The absence of marine sediments at this site is notable, as mangroves are well established there.

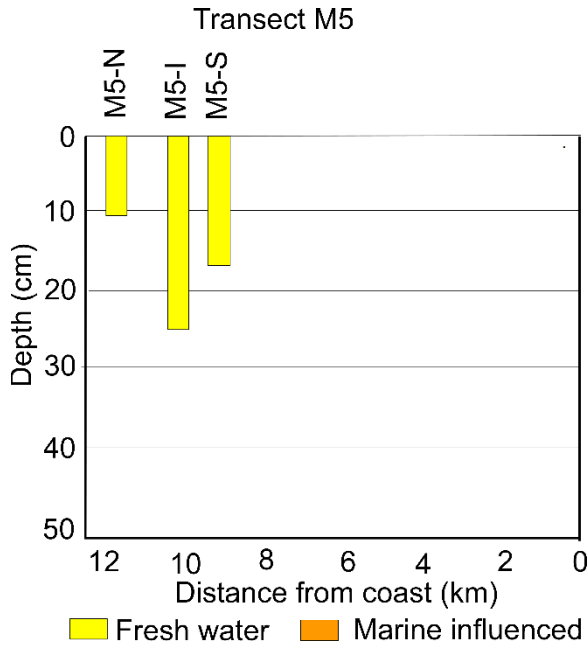


Figure 11. Fence diagram of paleoecology along transect M5.

Organic Carbon distribution

Bulk density

The relationship between bulk density and OC content is demonstrated separately for Florida and Biscayne Bay watersheds in Figure 12. As expected, decreases in percent OC yielded increasing bulk density in both watersheds. Along Florida Bay, this trend was non-linear; once % OC decreased to ~ 7%, bulk density reached ~ 0.45, but beyond that point OC content varied little with further increases in bulk density. Bulk densities > 0.6 are likely created by dewatering and reordering of calcite crystals after decomposition of plant material leaving black organic stains. In the Biscayne Bay watersheds, where the transects reach only to the L-31E levee, the relationship appears linear because the entire gradient from organic to marl soils is not sampled.

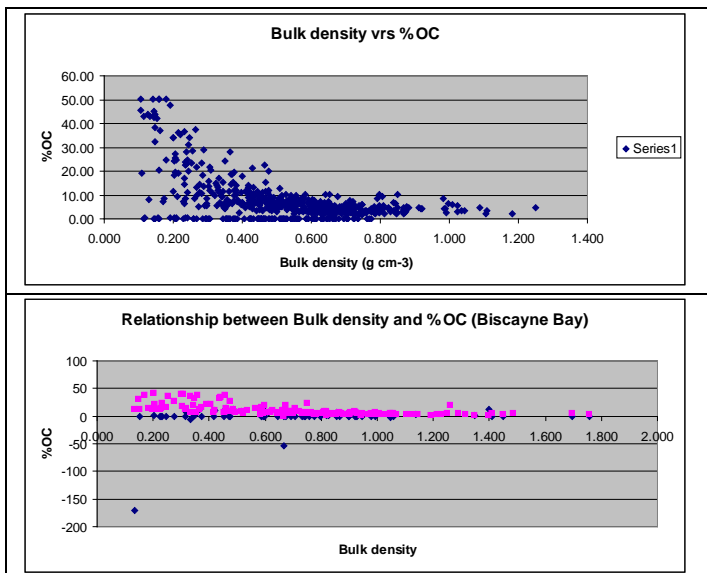


Figure 12. Upper graph. Scatter plot displaying the relationship between bulk density and OC content in Florida Bay coastal basins. Lower graph. Scatter plot displaying the relationship between bulk density and OC content in Biscayne Bay coastal basins.

In Figure 12A, data from low bulk density intervals that form the upward sloping tail are black marls (> 30% OC) with high organic content (PSA4: sawgrass peat-marl; Table 1)). Between 7 and 30% OC, the slightly heavier group are mostly tan marls (), similar to marls found along Biscayne Bay. . The heavy concentration of data points below 7% OC represent white marls. It's clear that as OC content increases, so does bulk density. However, while bulk density varies among PSA's, it doesn't increase downward within any interval of any PSA beyond the top few cm of cores. Increasing bulk density at the

top of cores is the result of compaction and decomposition of the periphyton mat, leaving primarily the mineral component, or marl, behind (Figure 13).



Figure 13. Upper interval from CoreTA3.3 shows the active surface periphyton mat (highly porous texture for the upper 2.5 cm (for scale ~ 0.5 cm of the ruler is exposed). The vacuolar texture grades downward into undulatory laminations with significant porosity between them to the depth of ~ 3 cm on the right side of the core where a marl texture begins.

The mean bulk density and OC content for each of the three types of marl was calculated (Figure 14). Black marl, the least common, is well compacted, and most often found in the subsurface strata. Two exceptions were M5-N and M5-S, where it was present at the surface. At these sites, the black marl was rich in OC but contained few identifiable materials.

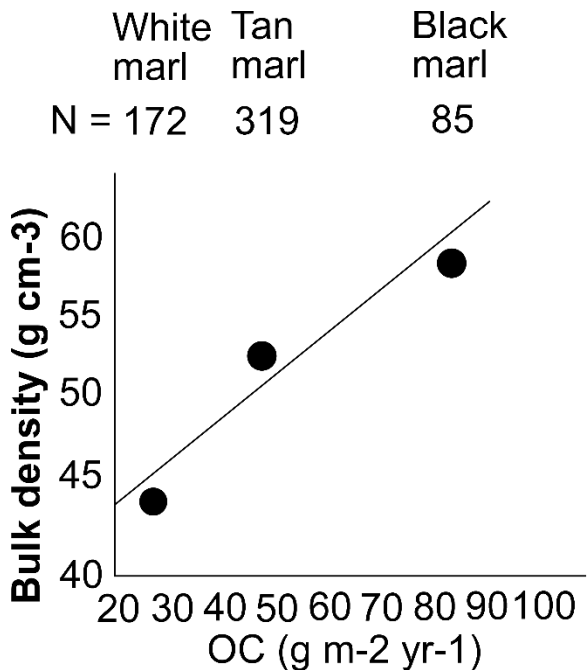


Figure 14. Bulk density compared to OC content for the three sediment types from Florida Bay coastal basins.

Paleosalinity

The relationship between depositional salinity and OC (Figure 15) was assessed on the basis of all Florida Bay and Barnes Sound transects. OC content in marine influenced sediments (SI > 1.5) was not greater than in freshwater sediments (Figure 12). These sediments were primary of PSA3 (marl) transitioning into PSA4 (sawgrass peat-marl). The tight data ball between 20 and 80 g OC are PSA3 and the upward data tail is PSA4.

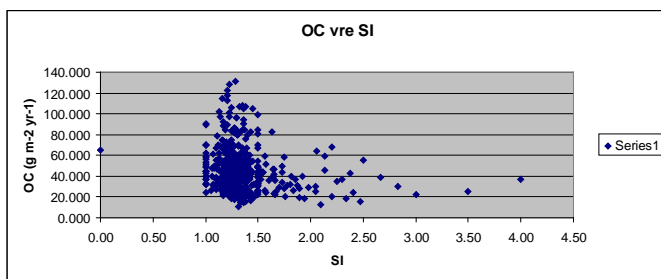


Figure 15. Scatter plot displaying the relationship between salinity index and OC content.

Florida Bay OC distribution contrasts with that in Biscayne Bay coastal basins (Figure 16). OC along Biscayne Bay are considerably higher than along Florida Bay and PSA3 data forms a tight grouping to the left of SI 1.5 (white circles). PSA4 forms a tight data grouping just above PSA3 (black circles). Mangrove sediments obviously contain much more OC than PSA3.

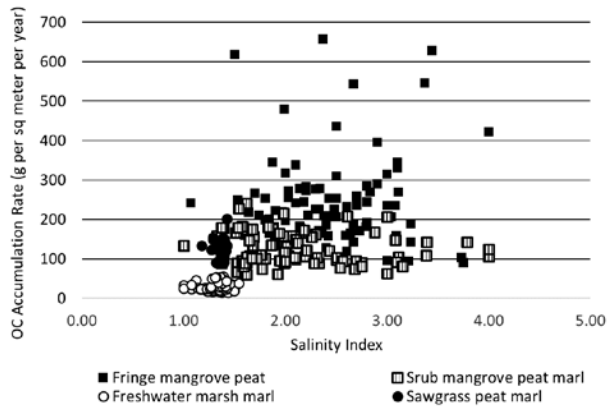


Figure 16. Relationship between SI and OC in Biscayne Bay coastal basins.

Organic Carbon

The distribution of OC along all transects was documented both horizontally and vertically over time. The data is presented one sub basin at a time starting in the east and moving west. Supplemental data [Appendix C](#) contains the OC data for all cores.

The relationship between plant community associated sediment types are established as plant sediment associations ([Table 2](#)). PSAs are recognized with confidence by color, texture and weight (which is obvious without a scale) in the field and in cores. These characters are directly related to OC content. For instance, as OC content increases bulk density decreases, color shifts from white (very low OC content) to black and then to red-brown (very high OC content and texture from a fine mud (marl) to fibrous (peat)) ([Figure 17](#)). In the interpretation of sediment cores and landscape, PSAs grade into one another naturally. In cores, gradual changes are sometimes encountered, but changes between PSAs are marked by distinct contacts. We interpret this to reflect a rapid change in watershed dynamics, related to water delivery or SWE or both; these changes are documented in graphs of profiles in sediment OC and SI ([Figures 18-27](#)).

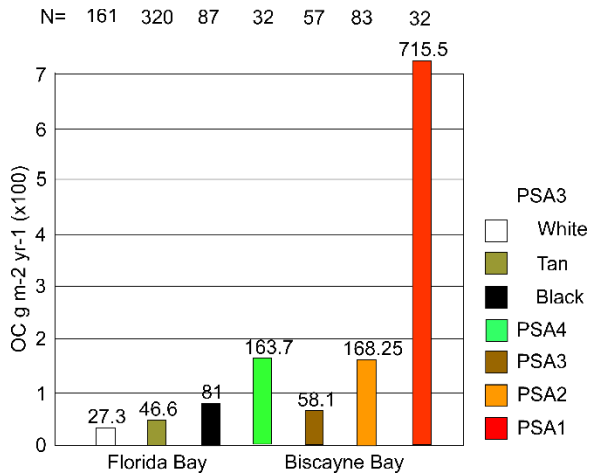


Figure 17. Average OC content by sediment type for sediments from Florida and Biscayne Bays.

Table 2. Plant community and associated sediment types (PSA).

PSA	Community	Sediment	Bulk density (g cm ⁻³)	%O C	Mean OC g m ⁻² yr=1
Biscayne Bay					
PSA1	Fringe mangrove	Peat	0.233	21.5	715.5
PSA2	Scrub mangrove-periphyton	Peat marl	0.729	7.7	168.3
PSA3	Periphyton	Marl	0.819	1.6	58.1
PSA4	Sawgrass-periphyton	Peat marl	0.749	7.1	163.7
PSA5	Sawgrass	Peat	n.r.	n.r.	n.r.
Florida Bay					
PSA1	n.r.	n.r.	n.r.	n.r.	n.r.
PSA2	n.r.	n.r.	n.r.	n.r.	n.r.
PSA3	Periphyton	White marl	0.583	3.505	27.3
	Periphyton-spike rush	Tan marl	0.525	6.269	46.6
	Periphyton-saw grass	Black marl	0.437	20.37	81.0
PSA4	n.r.	n.r.	n.r.	n.r.	n.r.
PSA5	n.r.	n.r.	n.r.	n.r.	n.r.

n.r. = not recovered in cores

Biscayne Bay Transect TD. The Biscayne Bay transects are all shorter than those in Florida Bay coastal basins, Core TDE was taken 0.281 km and TDWW 0.591 km from the coast. The coastline is dominated by a well developed mangrove fringe forest whose origins date back 3,165 yr (Meeder and Parkinson 2018). The mangrove peat is 2.1 m thick along the coast. In TDE there is a major increase in OC storage beginning ~ 1913, associated with a change from PSA2 to PSA1 (Figure 18). Core TDWW also exhibits a large increase in OC storage upwards starting in ~ 1891 as PSA3 (low OC marl) is overlain by PSA2. There is a large increase in OC content towards the top of the cores as DTC increases. This is a typical transgressive stratigraphic sequence.

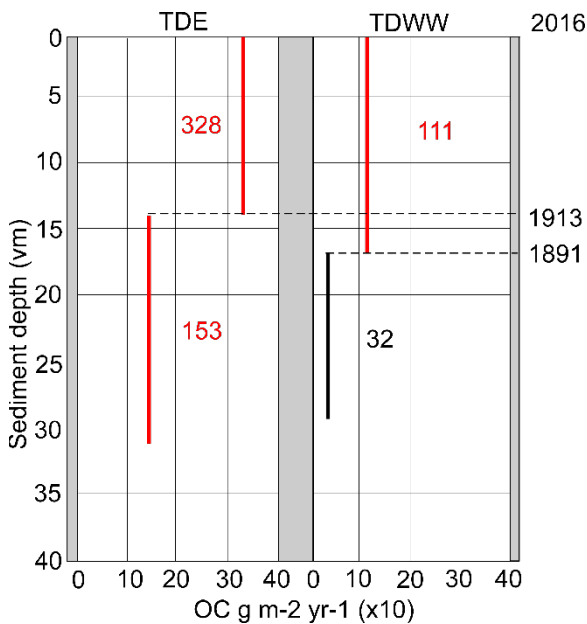


Figure 18. OC distribution along Biscayne Bay transect TD. Red line denotes marine influenced sediments.

Biscayne Bay transect CD. OC was high throughout the core at CDE, located 0.472 km from the coast (Figure 19). The profile at CDW exhibited a large increase in OC beginning in ~ 1949. Marine influenced sediments had much higher OC than fresh water derived sediments here and elsewhere in the Biscayne Bay watersheds. OC content decreased with with increased DTC in this transgressive stratigraphic sequence. However, OC content greatly increased upwards beginning in 1949, when PSA3 was replaced by PSA2.

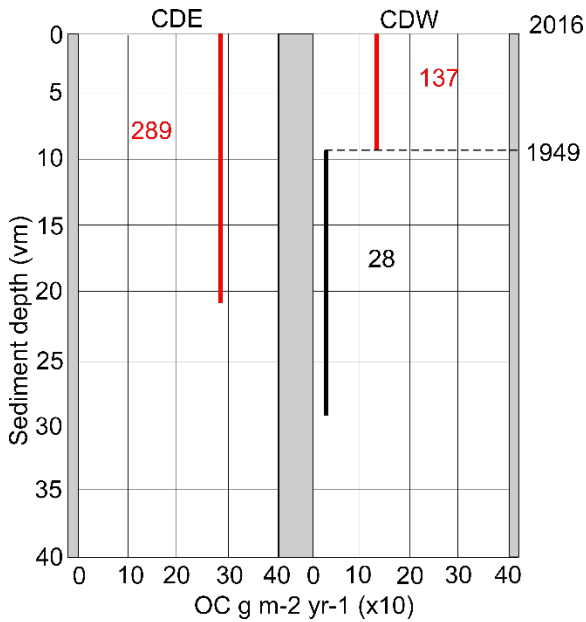


Figure 19. OC distribution along Biscayne Bay transect CDC. Red line denotes marine influenced sediments.

Biscayne Bay TKY transect. The TKY transect is 3.5 km in length beginning at the coastline. TKYE, the first core, is 1.09 km from the coastline and exhibits a large increase in OC starting ~ 1949 as the sediments change from fresh to marine influenced (Figure 19). Marine influenced sediments have much higher OC content than fresh water sediments in the core. The sediment at TKYNW exhibits a large decrease in OC content beginning ~ 1920, when site characteristics changed from PSA4 (green line) to PSA3. TKYINT also exhibits a decrease in OC content beginning ~ 1949 with a change from PSA4 to PSA3. Beginning in 1994 OC increased as marine influenced sediments replaced freshwater sediments.

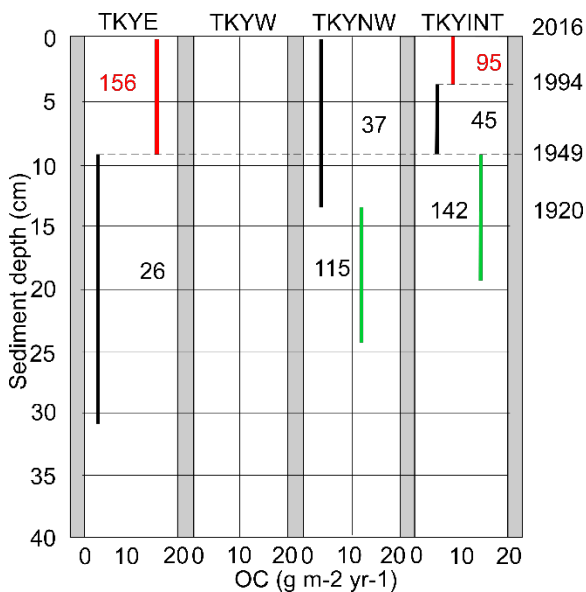


Figure 20. OC distribution along Biscayne Bay transect TKY. Red line denotes marine influenced sediments. Green lines indicate PSA4, sawgrass peat marl.

Triangle transect. The results of the sediment analysis of the three Triangle transect cores document spatial patterns with variation in DTC, and parallel vertical change in individual cores during the last century (**Figure 21**). A long term decrease in OC storage is documented in all three cores with the exceptions of an increase observed in TANGLEN and EVER1 since ~ 1972, and the period 1913 to 1943 at TANGLS. This long term trend started prior to anthropogenic perturbation to the Everglades ecosystem. Presently and for the last 38 yr, there has been an increase in sediment OC with increasing distance to the coast. Moreover, unlike the Florida Bay transects, OC varied little between marine influenced (red lines) and fresh water sediments along the Triangle transect.

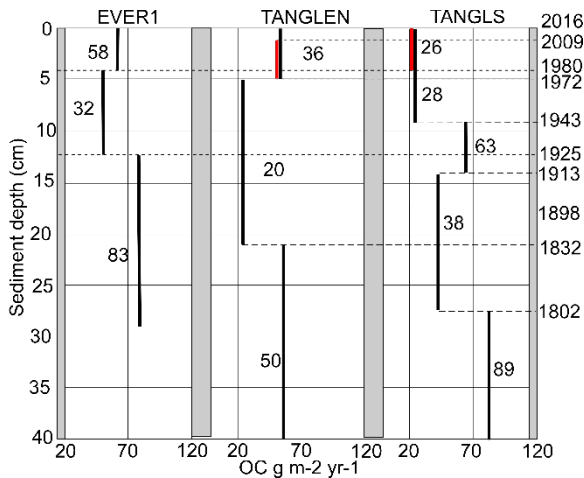


Figure 21. Distribution of OC in Triangle transect cores. Heavy vertical lines are the average values for the depth profiles indicated. The heavy red lines are the average values for marine influenced sediments.

Transect 2. TA2 is composed of five cores (**Figure 22**). Here, the difference in OC content between fresh water and marine influenced sediments is minimal. Very little change in OC storage has occurred since 1938 in the southern three cores. There's a slight increase in OC with increased distance to the coast in both the fresh and marine influenced sediments. The southern three cores all exhibit a long term decrease in OC content. TA2.3 exhibits a decrease in OC storage since 1898 and the most interior core, TA2.2, exhibited no change in since 1890. A marine interval at 24 cm (~1818) in TA2.5 predates anthropogenic perturbation of the Everglades watershed and may represent a rare storm deposit.

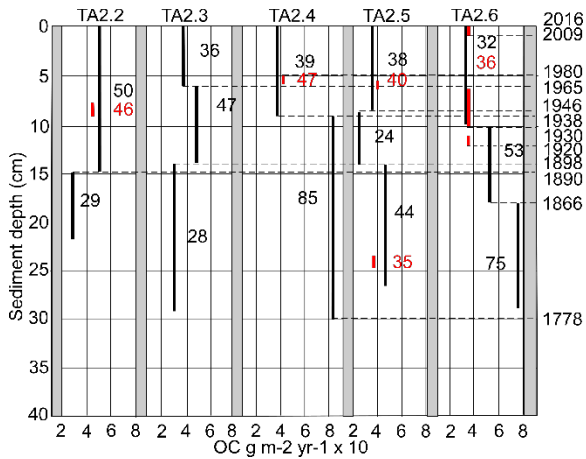


Figure 22. Distribution of OC along TA2. Red line denotes marine influenced sediments.

Transect 3. OC content doesn't vary between fresh water and marine influenced sediments on these four cores (Figure 23). OC deposition varied little after 1920 in all cores and after 1883 in TA3.5, the site closest to the coast. OC storage exhibits a minor increase with increased distance to the coast.

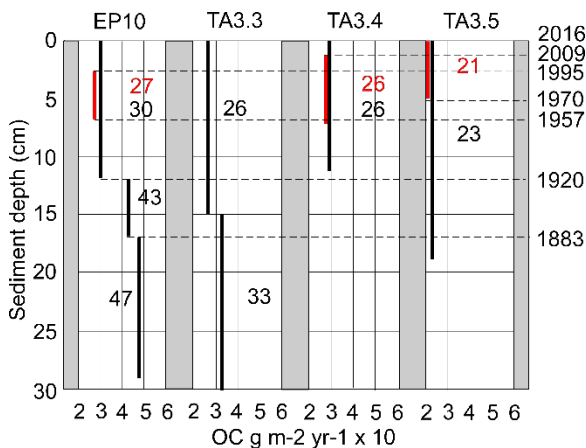


Figure 23. Distribution of OC along TA3. Red line denotes marine influenced sediments.

Transect 4. There was very little difference in OC content along the transect since 1972 (Figure 24). There was an increase in average OC content in the southernmost core, EP9R in 1928 in contrast to no change in TA4.2 prior to 1962 and very minor change TA4.1. No distinguishable trend of increasing OC with increased distance to the coast was observed.

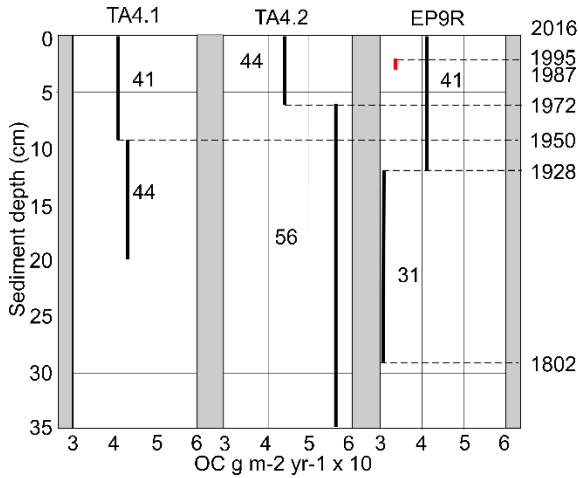


Figure 24. Distribution of OC along Transect 4. Red line denotes marine influenced sediments.

Transect 5. The 3 southern cores of TA5 experienced SWE but very little associated change in OC content (Figure 25). The lack of evidence of SWE at the top of TA5.5 is suspicious. The site is likely marine influenced but lacks marine restricted mollusks. Instead, *monroensis*, a species characteristic of fresh to brackish conditions, was the only mollusk found. OC content generally increased with increased distance to the coast. TA5.5 exhibited an upwards decrease in OC starting ~ 1891. Little difference in OC content was recorded in TA5.5, T5.4 or TA5.2 during the last century.

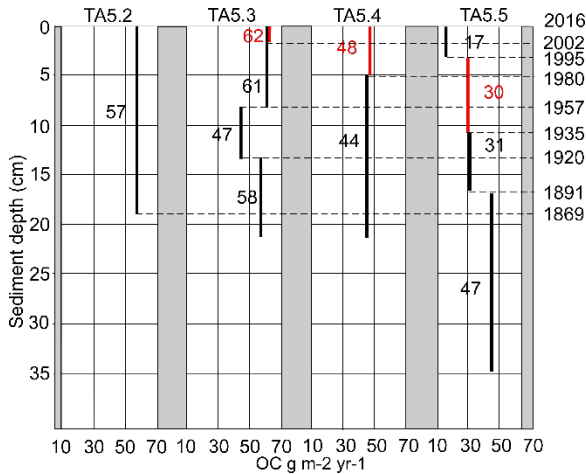


Figure 25. Distribution of OC along TA5. Red line denotes marine influenced sediments.

Transect 6. TA6 consisted of three cores, but the northernmost core, T6.1 was not analyzed (Figure 26). Comparing T4.4 and T6.5, only a small increase in OC was observed with increasing distance to the coast. An increase in OC content was observed in both TA6.5 in 1928 and in TA6.4 in 1913. No evidence of SWE was found in sediments and no change in OC related to SWE was detected.

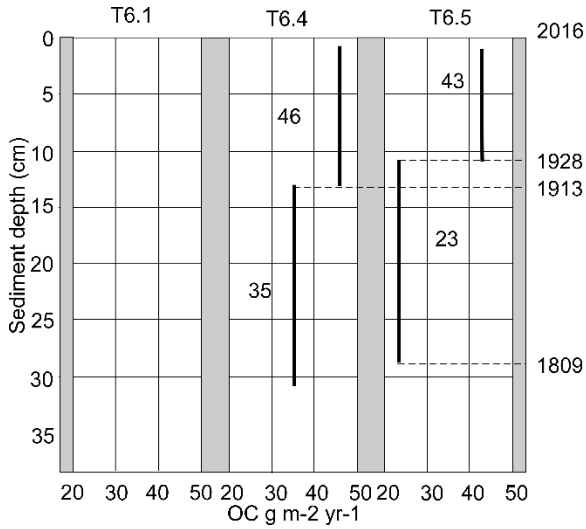


Figure 26. Distribution of OC along TA6.

Transect M5. Transect M5 exhibited a change in OC storage in 1943 resulting in increased OC content in M5-I and M5-S and decrease OC content in M5-N (Figure 27). Since that time OC remained constant in M5-I and M5-S, whereas there was a decrease in 1972 in OC content in M5-N; this site had the highest OC content of all cores in Florida Bay coastal basins, a pattern that is currently unexplained. There was no evidence of SWE along this transect.

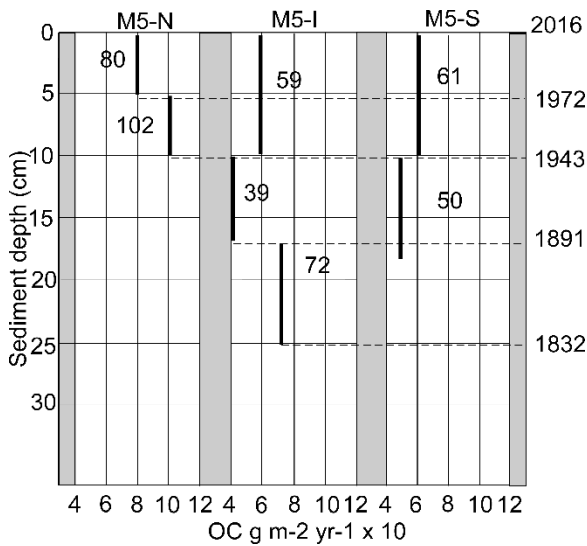


Figure 27. OC storage along Transect M5.

Comparison between mangrove cover and sediment OC

Mangrove are highly productive and mangrove-derived sediments contain high levels of OC. Since mangrove propagules are transported by tides, their distribution expands with tidal ingress. Therefore mangroves should represent good markers of salt water

encroachment. We compare mangrove cover, sediment OC content and DTC ([Table 3](#)). Because of large differences between Biscayne and Florida Bay, OC content data are presented separately for the two basins ([Figure 28 and 29](#)).

Based on transect end members across the 10 transects, five exhibited an increase in OC, two showed little or no change, and three exhibited a decrease with increasing DTC. The three in which OC decreased with increased DTC were located along Biscayne Bay and also exhibited a decrease in mangrove % cover with increased DTC. The five transects that exhibited an increase in OC with increasing DTC were found along Florida Bay; four of them also exhibited a decrease in mangrove % cover with increased DTC; the exception was TA2, which exhibited an increase in mangrove % cover with increased DTC. Two transects, TA3 and TA4 exhibited little change in OC content; the former exhibited an increase in % mangrove cover with increasing DTC, while the latter exhibited a decrease in mangrove % cover with increased DTC.

Table 3. Mangrove cover, sediment OC content and distance to coast (DTC) by transect.

Location	Mangrove cover+	Sediment OC g m ⁻² yr ⁻¹ #	DTC* (km)	Location	Mangrove cover	Sediment OC g m ⁻² yr ⁻¹	DTC (km)
TF=TDE	63.55	568	0.28	TA 3-3	37.67	25.1	5.05
TS=TDWW	46.94	89.8	0.59	TA 3-4	22.28	27.8	4.04
CF=CDE	26.33	363.5	0.48	TA 3-5	24.38	21.4	3.15
CS=CDW	24.93	107.2	0.58	TA 4-1	19.00	42.6	8.15
TKY E	33.90	147.6	1.09	TA 4-2	15.91	42.2	7.36
TKY W	33.55	94.8	1.93	EP9R	35.26	41.3	6.64
TKY NW	9.22	26.0	2.67	TA 5-2	34.75	62.6	7.52
TKY INT	17.71	26.0	3.49	TA 5-3	27.62	63.0	6.61
EVER 1	15.59	59.7	5.12	TA 5-4	36.73	52.3	5.68
TRIANGLI	30.81	37.9	3.50	TA 5-5	61.88	21.1	4.76
TRIANGLS	28.96	25.9	1.20	TA 6-1	0		11.19
TA 2-2	29.14	48.1	5.08	TA 6-4	4.50	45.0	10.06
TA 2-3	29.42	38.0	4.21	TA 6-5	21.00	39.9	8.57
TA 2-4	25.67	40.0	3.41	M5N	0	84.3	11.6
TA 2-5	38.32	37.2	2.53	M5I	0.8	52.3	10.08
TA 2-6	23.26	30.1	1.67	M5S	44.21	62.2	8.87
EP10R	33.89	24.8					

OC data from [Supplemental data Appendix C](#).

+ Mangrove cover data from [Supplemental data Appendix D](#).

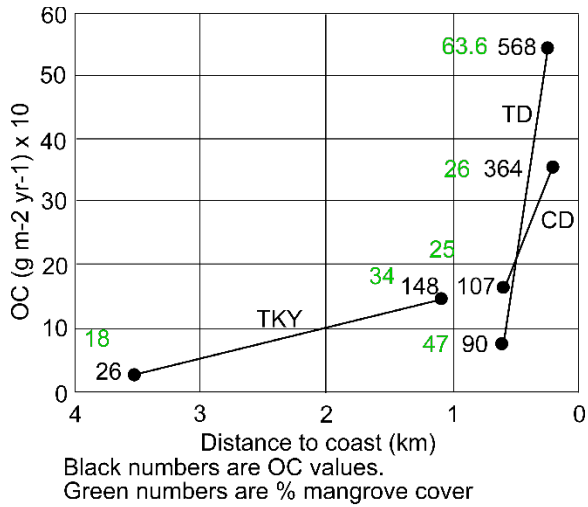


Figure 28. Relationship between OC content and distance to the coast along Biscayne Bay. Mangrove % cover for each location is in green.

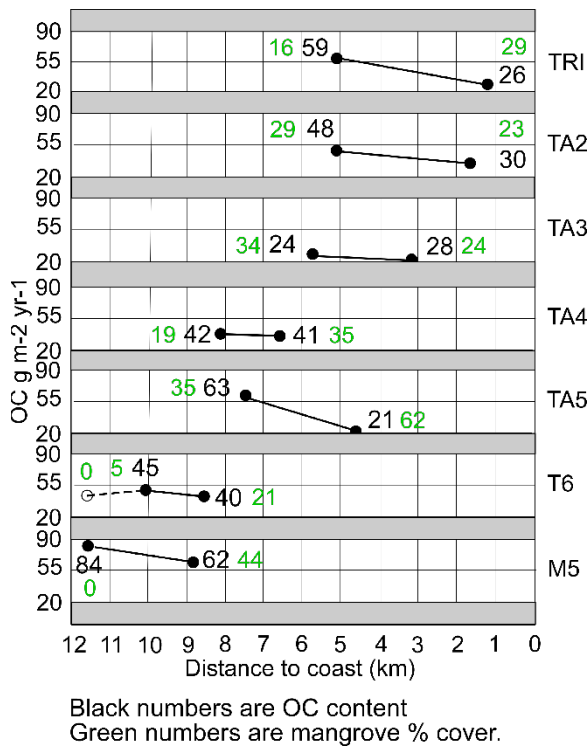


Figure 29. Relationship between OC content and distance to the coast along Florida Bay.

Figure 30 illustrates that as mangrove percent cover increases, so does the variation in its cover. Particularly in Florida Bay watersheds, even in locations where mangrove cover is high, it is patchily distributed.

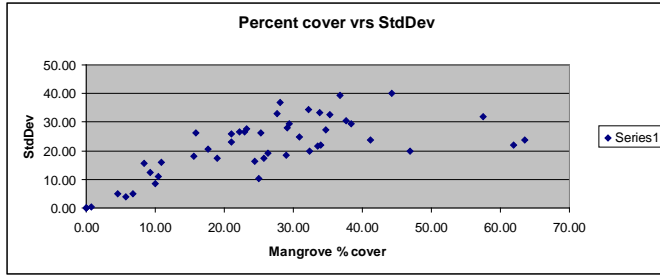


Figure 30. Relationship between percent mangrove cover and standard deviation. N =20 1 m⁻² plots at each core site.

In Figure 31, current mangrove cover is plotted against soil OC production rates. While the figure confirms that organic carbon production increases as mangroves become more abundant, the relationship is weak. Nevertheless, no sites with mangrove cover less than 25% had productivity rates that exceeded 100 g OC per m² per year. Vegetation at all these sites was Mangrove Tidal Swamp (Figure 31), and sediment type in all was PSA 1.

Discussion

Depositional environments

Five depositional environments were recognized in the SESE (Table 4): (PSA1) mangrove peat, associated with *Rhizophora mangle*, sometimes mixed with *Avicennia germinans*, and/or *Laguncularia racemosa*; (PSA2) mangrove peat-marl, associated with *Rhizophora mangle*, *Eleocharis cellulosa* and periphyton; (PSA3) marl associated with periphyton, *Eleocharis cellulosa* and a few mangrove; (PSA4) sawgrass peat-marl associated with *Cladium jamaicensis*, *Eleocharis cellulosa*, and periphyton; and (PSA5) sawgrass peat, associated with *Cladium jamaicensis*. The relationship between described plant communities and PSAs is shown in Table 4. PSA's 2 and 3 are very similar sedimentologically, but the broad spike rush-mangrove scrub as defined in the vegetation section varies along the gradient sufficiently to produce separate PSAs that grade into one another. The prime difference between the two is in the amount of organic matter, which is directly related to the period and abundance of mangroves; the longer mangroves are present and the greater their % cover, the greater the sediment OC content. Therefore, there's usually a gradient associated with SWE and sea level rise that determines mangrove ingress. Similar gradients are found on the fresh water end of transects where PSA 3 is moving into areas previously PS4 and PSA4 into areas of PSA5.

Table 4. Relationships between sediment types and plant communities.

		Sediment type	Dominant plants	Plant communities*
1	PSA1	Mangrove peat	Rhizophora mangle occasionally with Avicennia germinans and Laguncularia racemosa	Mangrove Tidal Swamp
2	PSA2	Mangrove peat marl	Rhizophora mangle, Eleocharis cellulosa and periphyton	Spike rush-mangrove scrub^
3	PSA3	Marl	Periphyton and Eleocharis cellulosa	Spike rush-mangrove scrub^
4	PSA4	Saw grass peat marl	Cladium jamaicensis, Eleocharis cellulosa, and periphyton	Transitioning Sawgrass Marsh
5	PSA 5	Saw grass peat	<i>Cladium jamaicensis</i>	Sawgrass Marsh

* Plant communities based upon plant species assemblages (this study).

^ The plant community spike rush-mangrove scrub is divided into two PSAs based upon sediment type

Found within the "White Zone" or PSA3 are three different types of marl based upon OC content; black, tan and white. These marls are associated with the gradient discussed above and are characterized by high, medium and low OC content, respectively (Figure 14). The origin of the white marl, with its very low OC content, is speculative at best because of the small number of cores in which it was present. However, the very low OC content suggests deposition in an area of very low productivity and sparse exploitation by plant roots. The topographic lows within coastal basins in the "White Zone" are likely candidates. The basins are depositional features developed by differential sediment accumulation rates (Meeder et al. 2017). These sediments contrast sharply with the black marls, which contain organic residue from saw grass but very little identifiable OM. these sediments are only reported from northernmost cores. The tan marls are abundant and also are the only type marl observed in the Biscayne Bay watersheds.

Mangrove presence.

Mangroves are important because of their high OC content and higher sediment accumulation rates. Mangrove presence has expanded greatly in the recent past but mangrove organic material is rarely found in cores in transects in the Florida Bay coastal basins. This signifies that mangrove expansion has been very recent, and that there is a considerable lag time between successful propagule settlement and mangrove sediment deposition. Mangrove expansion has not been evenly distributed in the area of SWE along Florida Bay (Figure 29), as documented in the Vegetation section of this Report. This uneven colonization pattern contrasts sharply with the mangrove distribution in the Biscayne Bay coastal basins, which generally displays a uniform decrease in mangrove cover with increasing DTC.

In general, mangrove % cover in Florida Bay coastal basins generally decreases with increased distance to the coast (Figure 31). However, there are many outliers and the trend is not tight, with considerable variation exhibited at most DTC increments. There are only three sites with no mangroves, all at least 8 km DTC. This broad variable distribution of mangrove % cover is likely a response to micro-topography, differences in fresh water delivery, tidal access, and presence or absence of suitable propagule settlement substrate. This is significant if mangroves are expected to increase OC storage or increase resilience. If mangroves do not increase the sediment accumulation rate soon, they will become inundated and submerged by not keeping up with SLR and associated SWE. The time lag between mangrove settlement and associated plant community change and the resultant change in sediment type is paramount in determining the future survival of these wetlands. Observed regional rates of mangrove sediment accumulation are currently in deficit relative to the present rate of SLR.

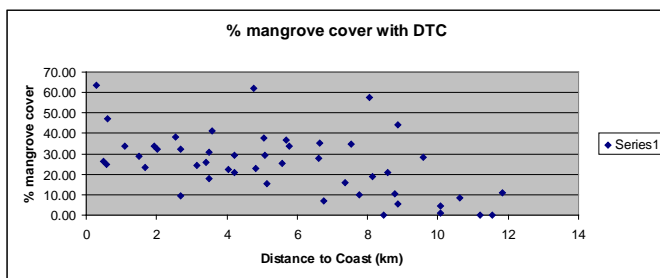


Figure 31. Percent mangrove cover in respect to distance to the coast.

The distribution of colonizing mangrove is important for the interpretation of core transects. Mangrove distribution does not decrease with DTC evenly in coastal basins or between coastal basins. Therefore, discrepancies along transects need to be addressed with this in mind. Mangrove patterns of settlement reflect micro-topography which also suggests differences in hydroperiod or inundation explaining lack of marine influenced sediments in some places. Micro-topography becomes evident in the coastal Everglades, where 10 to 30 cm variation in elevation is not uncommon along a 100 m transect (Meeder et al. 1996). This topography is a major component of hydroperiod which has a strong influence on plant communities (Duever et al. 1983). This topography likely affects settlement of mangrove propagules and may explain some distribution patterns. In addition, plant community characteristics influence successful settlement. Thick, even periphyton mats don't seem to contain many mangroves, whereas more successful settlement seems to occur in areas with higher densities of emergent vegetation. Successful settlement is very common along tidal channel margins which are often difficult to traverse because of mangrove density. SWE occurs in small increments, which means a few cm difference in elevation from surrounding areas may result in one location not experiencing SWE at the same time as surrounding areas. When SWE is not reported from one core within a sequence of cores exhibiting SWE, SWE bypass must be considered. For example along TA2 SWE was found in all cores between TA2.2 to TA2.6 with the exception of TA2.3 which exhibited no evidence of SWE. This must be interpreted that TA2.3 was a local topographic high in an area affected by SWE.

Salt water encroachment and changing OC storage.

The relationships between SWE and OC storage will be discussed by Transect. Changes in SWE will be presented first, trends in OC storage next, followed by a summary statement of the relationship between the two.

Biscayne Bay coastal basins. SWE in the coastal basins along Biscayne Bay has reached the L31E storm protection levee which has stopped further SWE and mangrove expansion by eliminating accommodation space (Figure 4). Since 1995 (Meeder et al. 1996; 2017) there has been very little increase in SWE, however the thickness of marine influenced sediment package increased and even with increased fresh water delivery there's no sign of reversal of SWE (Meeder et al. 2018). The same is true of the TKY transect, although SWE has crept further toward the interior during the last two decades, finally reaching the L31E levee in places (Figure 5). Even with removal of this anthropogenic structure impeding SWE and SLR, at least 66% of the area between the levee and the Atlantic Coastal Ridge is highly altered by anthropogenic structures (Homestead Air Force Base, Turkey Point Power Plant, one of the largest landfills found along the Atlantic coast, four north south roadways, urbanization and agriculture. In contrast, SWE along Florida Bay coastal basins takes place within much more accommodation space prior to reaching the C111 canal and remnant levee system and the last of the Atlantic Coastal Ridge just west of Taylor Slough. West of Long Pine Key, there's no constraint on accommodation space.

In all three transects along Biscayne Bay an increase in OC storage is observed as carbon rich (0.0248 g cm^{-3}) PSA2 mangroves replaced low carbon (0.0028 g cm^{-3}) PSA3. This was more pronounced in the two shorter northern cores. OC storage increased with SLR along Biscayne Bay.

Transect TRI. The Triangle transect fence diagram documents continuous SWE since 1972 to ~ half way between EVER 1 and TANGLEN a distance of about 3.2 km at the rate of 72 m yr^{-1} . This transect is located between two roadways and associated borrow canals which altered the fresh water budget to local rainfall until recently when construction of weirs and diversions along Card Sound Road were constructed in ~2000. There's seems to be no relief of SWE from the construction of weirs along the Card Sound roadway to increase freshwater delivery. Or perhaps without these diversion structures, SWE might be more pronounced than observed. Regardless, there's no evidence of a reversal of SWE.

A long term decrease in OC storage is documented in all three cores, apparently by the slow transition from saw grass peaty marl to marl since at least 1802, prior to anthropogenic alterations. There's an increase in OC content as DTC increases since 1972. Marine influenced sediments are not much different in OC content than fresh water sediments that they are replacing.

Late Holocene transgression must account for the decrease in OC storage prior to the Anthropocene Marine Transgression, starting 1938. PSA4 was replaced by PSA3 or

marls containing lower OC content (white marl) replacing tan marl. SWE is resulting in lower OC storage along the transect.

Transect TA.2. The easternmost Florida Bay coastal basin transect, TA2, along the western margin of Highway Creek, documents the beginning of SWE between 1920 and 1938. The earlier date is likely, associated with the construction of the Flagler Railroad borrow canal that permitted rapid tidal ingress at the rate of 19 m yr^{-1} . SWE rates beginning in 1965 ranged between 114 and 126 m yr^{-1} from TA2.4 inland. This was close to the time of construction of the C111 Canal. In 1996 SWE was recognized at 6.8 km DTCC on the east side of Highway Creek (Meeder et al. 1996; 2017). In ~1980 marine influenced sediments were very rapidly replaced by increased freshwater delivery, i.e., all cores responded within a 7 year time frame. This very rapid change is likely a response to increased freshwater delivery by the way of breaches in the C111 levee and increased delivery canal stage.

A general increase in OC storage is observed as DTC increases. There's no difference between freshwater and marine influenced sediment OC content. In the southern 3 cores there's a general decrease in OC storage since 1775, prior to any landscape alterations. The SWE reversal beginning in ~ 1980 did not alter OC storage significantly either. There has been very little change in OC storage since ~ 1938. This may represent the nature of SWE in the broad "White Zone", or PSA3; OC storage does not change with shifts in marl types. It requires increased emergent vascular vegetation to significantly increase OC. The little change over time may be evidence of the resilience of PSA3, unfortunately, PSA3, is very low in OC.

Transect TA3. SWE extended past EP10 (DTC ~6 km) three times in the upper 10 cm, as documented by alternating 1 cm thick strata. This idiosyncratic pattern suggests that conditions of either fresh water delivery or sea level rise have changed repetitively, and perhaps that EP10 is close to the invading front of SWE. The location being close to the leading edge of SWE may have experienced the effects of 7 yr regional climatic dry and wet season cycles (Duever et al. 1994), which matches the length of time required to accumulate 1 cm of marl sediment. A retreat in SWE that began ~ 2002 did not reach TA3.4 at 4 km DTC.

Cores along Transect TA3 exhibit very little change in OC since 1883. Although all cores record SWE, no difference between freshwater and marine influenced sediment OC was observed. A general increase in OC content is observed landward as SWE replaces higher OC content marl with lower OC marl.

Transect TA4. SWE began in 1980 along transect TA4, reaching to EP9R (6.6 km DTC) but not to TA4.2 (7.36 km DTC). SWE reversal began in ~ 1980. The present return to fresh water sediment at the surface may or may not be a result of water delivery. At least for the present, an equilibrium between fresh water delivery and SWE has established very near EP9R.

Very little change in OC content is observed since 1972, nor along the transect as DTC increases. The period of SWE between 1987 and 1995 created a decrease of ~ 22 % in OC storage in the southernmost core, EP9R. Perhaps this decrease is associated with salinity stress.

Transect TA.5. SWE began in TA5.5 ~ 1935, moving slowly north and reaching TA5.4 ~1980 a distance of 920 m in 45 yr 21 m yr^{-1} . SWE reached TA5.3 ~ 2002 for a rate of 42 m yr^{-1} , an increased rate that could correlate with increased global rate of SLR. This trend appears in three transects. No evidence of SWE reversal was observed.

There is a general increase in OC as DTC increases in both marine influenced sediments in the upper parts of the southern three cores subjected to SWE but no difference between OC in freshwater and marine influenced sediments. Little change in OC has been observed since 1869, predating anthropogenic alterations to the system.

Transect T6. No SWE was observed along TA-6. The southernmost core is located 8.6 km DTC, further north than observed SWE. T6 is also located close to Taylor Slough which delivers considerable freshwater.

A small increase in OC storage is observed between 1913 and 1928 when OC in the southern two transect increased. This increase is unrelated to SWE.

Transect M5. No salt water encroachment was observed along this transect. The southernmost core is located 8.86 km DTC. M5 is our westernmost transect, and likely receives water from the Shark River system.

OC content increased since 1891 in the southern two cores which is not related to SWE. There is also an increase in OC with increased DTC.

SWE summary. Much of the variation along Florida Bay is the result of the distance transects started from the coast, those that document SWE started between 1.5 to 6.5 km from the coast and exhibit SWE to distances between 3.75 and 7 km from the coast. Those that haven't experienced SWE begin at $> 8 \text{ km}$ from the coast. The two western most transects, T6 and M5 both start the furthest from the coast and are closest to both Shark River and Taylor Slough, which both delivery considerable freshwater, perhaps explaining why they haven't experienced SWE. Fresh water delivery seems to be a means of increasing resilience but will not work indefinitely as SLR continues because the plant community response to increased fresh water delivery is not likely to increase community sediment accumulation rates and is very likely to add additional stress to those communities by increasing hydroperiod and water depth. However, the area around the two southern cores in Transects T6 and M5 have mangrove cover ([Supplemental data D, Figure 30](#)) and propagule dispersal even though no marine mollusks have been found at these sites. The lack of marine tolerant mollusks is likely because transported mollusk larvae did not find sustained preferred habitat; either the area didn't remain saline very long, dry conditions prevailed for a while soon after ingress, or there wasn't sufficient current or suspended food for the filter feeders. With continued SWE and increasing

water depth and tidal exchange salt tolerant mollusks should arrive. The key here is that marine conditions for sustained mollusk presence is not available in contrast to successful mangrove settlement as mangrove propagules can survive fresh water without difficulty for an indefinite period.

Organic Carbon storage summary

Accompanying SWE in the Biscayne Bay coastal basins is an increase in OC storage as PSA1 and PSA2 (high OC content) replace freshwater PSA3 and PSA4 (low OC content). Biscayne Bay transects ran from the coast with well developed mangrove fringe landward across PSA2 that has been expanding since 1938 (Ross et al. 2018; Meeder and Parkinson 2018). Florida Bay transects begin well within PSA3 and extend into fresh water environments (Figure 32).

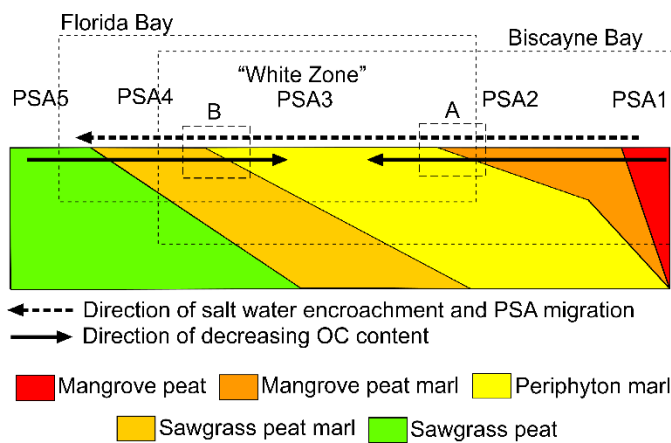


Figure 32. Schematic illustration comparing Biscayne and Florida Bay coastal basin transects. Biscayne Bay coastal basin transects (large and small dashed line boxes) range from the coast (PSA1) to the interior (PSA4) with the focus on the transition between PSA2 and PSA3 (small long dashed line box). Florida Bay coastal basin transects range from PSA2 to PSA5 with a focus on the transition between PSA3 and PSA4.

Whereas changing OC content with SWE is straight forward relationship along Biscayne Bay the relationship is much more complicated along Florida Bay because of the differences in fresh water delivery, micro-topography, tidal water exchange and lower salinities because of much longer water renewal times in Florida Bay than along Biscayne Bay. This means that tidal ingress along Biscayne Bay is not impeded by shallow banks and islands as in Florida Bay, and that Biscayne Bay waters are more saline than those along inner Florida Bay. Other differences are the: greater slope along Biscayne Bay coastal plain than along Florida Bay, narrower coastal plain along Biscayne Bay, and much less fresh water delivery to the wetlands. The abundant mangrove along Biscayne Bay is replaced by a very narrow band of mangroves along the Florida Bay coastline, with a buttonwood-dominated ridge immediately behind the mangrove lined coastline. This buttonwood ridge and the erosional nature of the coastline have prevented a mangrove fringe development similar to Biscayne Bay and further west in the Ten Thousand Islands.

Three general trends in OC storage along Florida Bay are reported: (1) general decrease in OC upwards, especially in the southern cores along the transects, (2) increase in OC landward as PSA3 (low OC content) replaces PSA4 and PSA 5 (higher OC content) and (3) little difference in OC content between marine and fresh water sediments.

Although our transect data are applied reliably to individual coastal basinsreliably, the data from the sediment cores are best applied on a large scale, i.e., for the Southeast Saline Everglades as a whole, rather than to local coastal basins because of the variability we have documented, especially when looking at the effects of regional processes such as SLR.

Summary

Several differences exist between coastal basins along Biscayne and Florida Bays that result in different responses to SLR. They include: 1. salinity of ingressing tidal water, 2. more efficient tidal exchange along Biscayne Bay, 3. greater slope and a shorter coastal plain along Biscayne Bay, 4. freshwater delivery is different (among most coastal basins) and 5. nutrient availability along Biscayne Bay is greater (Meeder and Boyer, 1999), though not addressed in this study. These differences resulted in different rates of SWE and changes in OC storage. We assume the SLR is the same for both Biscayne and Florida Bays based upon (Wdowinski et al. 2016) and unpublished data (Jerry Lorenz, National Audubon Society).

The greater coastal slope along BB would make one think it would be less vulnerable to SLR but SWE was more effective along BB than FB. Perhaps the greater wetland width more than compensated for the increased slope along BB. The biggest factors are that ingressing tidal waters along BB are often at normal marine salinities and average > 25 ppt, in contrast to much lower salinities along Florida Bay, and theabsence of restrictions to tidal ingress such as the Florida banks provide in Florida Bay.

Sediment distribution sequence. The core transects document a transgressive stratigraphic sequence driven by SLR (Meeder and Parkinson 2017). This transgression is the result of plant communities aligned along the fresh to marine environment shifting landward with SWE. In this biogenic system, as plant communities change, so do sediment type and OC content. PSAs from the coast inland are arranged from PSA1, PSA2, PSA 3, PSA4 and PSA5. In a "perfect" core with representation of the entire wetland system, one would find PSA5 at the base followed by PSA4, PSA3, PSA2 and PSA1. Along Florida Bay PSA1 is often replaced by the Buttonwood Ridge. Each PSA has a characteristic OC content. And within PSA3 we document three types of marl, all with low, but different OC content which can be described as black, tan and white marl. In some areas overstep is being observed as the "White Zone", essentially PSA3, is diminishing or has disappeared along transects such as along Biscayne Bay and areas to the west along Florida Bay. Inundation is already underway in places where PSAs can not keep up with SLR.

SWE. SWE in all three Biscayne Bay coastal basins (CD, TD and TKY) is terminated because SWE has reached an anthropogenic barrier, the L31E storm protection levee. There has been no reversal since increases in fresh water delivery were instituted. Along Florida Bay the coastal basins exhibit variability in response to SLR. SWE has been continuous along the Triangle and TA5 transects, no SWE is documented along T6 or M5 transects, transects TA4 and TA2 document reversals in SWE and along the TA3 transect SWE has been reversed along the northern portion of the transect but remains incomplete.

SWE along TA2 began soon after the construction of the Flagler Railroad borrow pit and reversed after the construction of the C111 canal that moved water eastward. The eastward movement of water is likely the explanation of the reversals in SWE documented along TA3 and TA4. This eastward movement of water may have decreased delivery to TA5, causing continuous SWE. T6 and M5 are located between Taylor Slough and Shark River, which both deliver considerable water preventing permanent SWE but not occasional tidal ingress transporting mangroves. This balance is expected to change with continued sea level rise.

OC storage. Changes in OC storage is related to SWE. In general, an increase in OC storage is observed with SWE along Biscayne Bay coastal basins, as PSA2 (high OC content) replaces PSA3 (low OC content). In contrast, Barnes Sound and Florida Bay coastal basins have remained the same in terms of OC storage or are decreasing in OC storage as PSA3 (low OC content) replaces PSA4 and 5 (high OC content). There's been a general decrease in OC upwards in the eastern Florida Bay coastal basins for more than the last century, prior to watershed alterations. Near surface sediment along Florida Bay transects increase in OC with increased DTC, contrasting with those along Biscayne Bay. Most significantly marine influenced sediments are not significantly different from precursor sediments in terms of OC content.

SWE reached the L31E levee in all three transects along Biscayne Bay but does not imply an increase to marine salinities. This will occur when the majority of the area is inundated at which time it is submerged and a subtidal environment. At the present rate of sea level rise this is likely to occur within 50 yr, regardless of fresh water delivery. The coastal basins along Florida Bay have experienced continuous SWE (Triangle and TA5), a reversal of SWE (TA2, TA3 and TA4) and the two westernmost transects with beginnings at ~ 7 km from the coast have experienced no SWE (T6 and M5). At the two southern core locations along both of these western transects, mangrove cover (Table 3) documents tidal ingress but not a salt water environment stable enough for marine mollusk colonization.

The future. An increase in OC storage is documented along the three Biscayne Bay transects. This increase is the result of expanding mangrove (with high OC content) distribution at the expense of periphyton prairie (with low OC content) in response to SWE. However, this increase may already be on the decline because of loss of PSA1 area by Hurricane Andrew and inundation of PSA2. The threshold of resilience of mangroves along Biscayne Bay has been reached or nearly reached. With no accommodation room for further expansion the area east of L31E is very likely to convert

to subtidal mudflats within the next 50 yr at the present rate of sediment accumulate rate deficit in respect to the rate of SLR.

The expansion of mangrove in Florida Bay coastal basins is incredibly fast, documenting that mangroves can keep pace with sea level rise in terms of maintaining their presence, although they are not displaying any tendency to produce peat sediment. This bodes poorly for their long term survival at precursor sites. The sediment accumulation rates in the "White Zone" area average 1.35 mm yr^{-1} and with the lag time required for mangrove to produce faster accumulating PSA3 it is likely that the present White Zone or at least the southern portion will convert to open water lake environments, like Madera Bay, Joe Bay and Long Sound within the next 50 yr, with increased fresh water delivery or not. The Buttonwood Ridge will remain an emerged landform analogous to the elongate banks in Florida Bay. Within the next century this landform will become a submerged bank like its predecessors that also formed under conditions of SLR (Wanless and Tagett, 1989). The major question facing managers is: can additional fresh water delivery save the SESE? The answer is "not likely", because adding fresh water may prevent SWE to a degree by physical displacement but how will additional freshwater affect sediment accumulation rate? If sediment accumulation rate is not enhanced than SLR will inundate the area regardless of fresh water delivery. Additionally, an increase in freshwater delivery may have detrimental affects on plant communities by increasing hydroperiod and water depth.

References

Blinn, D.W. 1993. Diatom Community Structure Along Physicochemical Gradients in Saline Lakes. *Ecology* 74:1246-1263. <https://doi.org/10.2307/1940494>

Dean, W.E. 1974. Determination of carbonate and organic matter in calcareous sediments and sedimentary rocks by loss on ignition; comparison with other methods. *Journal of Sedimentary Research*, doi.org/10.1306/74D729D2-2B21-11D7-8648000102C1865D

Duever et al. 1983. Big Cypress

Duever, M.J., J.F. Meeder, L.B. Meeder and J.M. McCollom. 1994. The climate of south Florida and its role in shaping the Everglades Ecosystem. pp. 225-248, *In* Everglades, (eds. S.M. Davis and J.C. Ogden), St. Lucie Press.

Meeder, J.F. R.W Parkinson, J. Kominoski, M.S. Ross and S. Castaneda. (submitted to Nature Geoscience) Anthropocene Marine Transgression and Changing Organic Carbon Storage, Southeast Saline Everglades, Florida, USA. .

Meeder, J.F. and R.W. Parkinson. 2018. SE Saline Everglades Transgressive Sedimentation in Response to Historic Acceleration in Sea-Level Rise: A Viable Marker for the Base of the Anthropocene? *Journal of Coastal Research* 34: 490-497. (Sept 2017) doi.org/10.2112/JCOASTRES-D-17-00031.1

Meeder, J.F. M.S. Ross, R.W. Parkinson and S. Castaneda. 2018. Enhancing coastal wetland resilience to SLR: just add water? *Solutions*. www.thejournal.com/article/enhancing-coastal-wetland-resilience-slr-just-add-water/

Meeder et al. 2017 Meeder, J.F., R.W. Parkinson, P.L. Ruiz and M.S. Ross. 2017. Saltwater encroachment and prediction of future ecosystem response to the Anthropocene Marine Transgression, Southeast Saline Everglades, Florida. *Hydrobiologia* 803 (Issue 1): 29–48. [doi: 10.1007/s10750-017-3359-0](https://doi.org/10.1007/s10750-017-3359-0)

Meeder, J.F., M.S. Ross, G.T. Telesnicki, P.L. Ruiz and J.P. Sah. 1996. Vegetation analysis in the C-111-Taylor Slough Basin. Document 1. The Southeast Saline Everglades revisited a half-century of coastal vegetation change, 56p. Document 2. Marine transgression in the Southeast Saline Everglades, Florida; rates, causes and plant-sediment responses. 95p. Final report. To: Dr. Rich Alleman, SFWMD

Ross, M., J. Meeder, L. Scinto, J. Sah, S. Stoffella, Himadri Biswas and Sean Charles. 2018. Annual Report: ecosystem dynamics in the White Zone: history, drivers, and restoration implications October 4, 2016 to October 3, 2017. Task Agreement # P15AC01625. Cooperative Agreement # H5000-10-5040/ South Florida Natural Resources Center

Ross, M.S., E.E. Gaiser, J.F. Meeder and M.T. Lewin. 2002. Multi-taxon analysis of the “white zone”, a common ecotonal feature of South Florida coastal wetlands. pp. 205-238
In: The Everglades, Florida Bay and Coral Reefs of the Florida Keys.(J.W. Porter and K.G. Porter, eds.) CRC Press, Boca Raton, FL USA 1064p.

www.taylorfrancis.com/books/e/9780429123917/chapters/10.1201/9781420039412-11

Ross, M. S., J. F. Meeder, J. P. Sah, P. L. Ruiz, & G. J. Telesnicki. 2000. The Southeast Saline Everglades revisited: a half-century of coastal vegetation change. *Journal of Vegetation Science* 11:101-112. doi.org/10.2307/3236781

Sikora LJ and DE Stott. 1996. Soil Organic Carbon and Nitrogen. In: Doran JW, Jones AJ, editors. *Methods for assessing soil quality*. Madison, WI. p 157-167.

Thompson, F.G. 1968. *The aquatic snails of the Family Hydrobiidae of peninsular Florida* University of Florida Press

Thompson, F. G. 1984. *Freshwater snails of peninsular Florida*. Florida State Museum.

Wanless, H.R. and Tagett, M.G., 1989. Origin, growth and evolution of carbonate mudbanks in Florida Bay. *Bulletin of Marine Science*, 44(1), pp.454-489.

Wdowinski, S., Bray, R., Kirtman, B. P., & Wu, Z. (2016). Increasing flooding hazard in coastal communities due to rising sea level: Case study of Miami Beach, Florida. *Ocean & Coastal Management*, doi.org/10.1016/j.ocecoaman.2016.03.002.

List of Tables

Table 1. Summary of plant community - sediment type associations (Data from Meeder et al. 2017; Meeder & Parkinson 2018).

Table 2. Plant community and associated sediment types (PSA).

Table 3. Mangrove cover and sediment OC content by transect.

Table 4. Relationships between sediment types and plant communities.

List of Figures

Figure 1. Transect and core locations.

Figure 2. Core sediment descriptions from transects along Biscayne Bay and Barnes Sound coastal basins (Figure 1).

Figure 3. Core descriptions from along Florida Bay coastal basins.

Figure 4. Fence diagram documenting SWE along the TKY transect

Figure 5. Fence diagram documenting SWE along the TKY transect.

Figure 6. Fence diagram of paleosalinity of the TRIANGLE.

Figure 7. Fence diagram of paleosalinity along Transect TA-2.

Figure 8. Fence diagram of paleosalinity of TA.3 and TA.4

Figure 9. Fence diagram of paleosalinity along transect TA5.

Figure 10. Fence diagram of paleosalinity along transect TA6

Figure 11. Fence diagram of paleoecology along transect M5.

Figure 12. Upper graph. Scatter plot displaying the relationship between bulk density and OC content in Florida Bay coastal basins. Lower graph. Scatter plot displaying the relationship between bulk density and OC content in Biscayne Bay coastal basins.

Figure 13. Upper interval from Core3.3 shows the active surface periphyton mat (highly porous texture for the upper 2.5 cm (for scale ~ 0.5 cm of the ruler is exposed). The vacuolar texture grades downward into undulatory laminations with significant porosity between them to the depth of ~ 3 cm on the right side of the core were a marl texture begins.

Figure 14. Bulk density compared to OC content for the three sediment types from Florida Bay coastal basins.

Figure 15. Scatter plot displaying the relationship between salinity index and OC content.

Figure 16. Relationship between SI and OC in Biscayne Bay coastal basins.

Figure 17. Average OC content by sediment type for sediments from Florida and Biscayne Bays.

Figure 18. OC distribution along Biscayne Bay transect TD. Red line denotes marine influenced sediments.

Figure 19. OC distribution along Biscayne Bay transect CDC. Red line denotes marine influenced sediments.

Figure 20. OC distribution along Biscayne Bay transect TKY. Red line denotes marine influenced sediments.

Figure 21. Distribution of OC in Triangle transect cores. Heavy vertical lines are the average values for the depth profiles indicated. The heavy red lines are the average values for marine influenced sediments.

Figure 22. Distribution of OC along TA2. Red line denotes marine influenced sediments.

Figure 23. Distribution of OC along TA3. Red line denotes marine influenced sediments.

Figure 24. Distribution of OC along Transect 4. Red line denotes marine influenced sediments

Figure 25. Distribution of OC along TA5. Red line denotes marine influenced sediments.

Figure 26. Distribution of OC along TA6.

Figure 27. OC storage along Transect M5.

Figure 28. Relationship between OC content and distance to the coast along Biscayne Bay.

Figure 29. Relationship between OC content and distance to the coast.

Figure 30. Relationship between percent mangrove cover and standard deviation. N =20 1 m⁻² plots at each core site.

Figure 31. Percent mangrove cover in respect to distance to the coast.

Figure 32. Schematic illustration comparing Biscayne and Florida Bay coastal basin transects. Biscayne Bay coastal basin transects (large small dashed line box) range from the coast (PSA1) to the interior (PSA4) with the focus on the transition between PSA2 and PSA3 (small long dashed line box). Florida Bay coastal basin transects range from PSA2 to PSA5 with a focus on the transition between PSA3 and PSA4.

Appendices

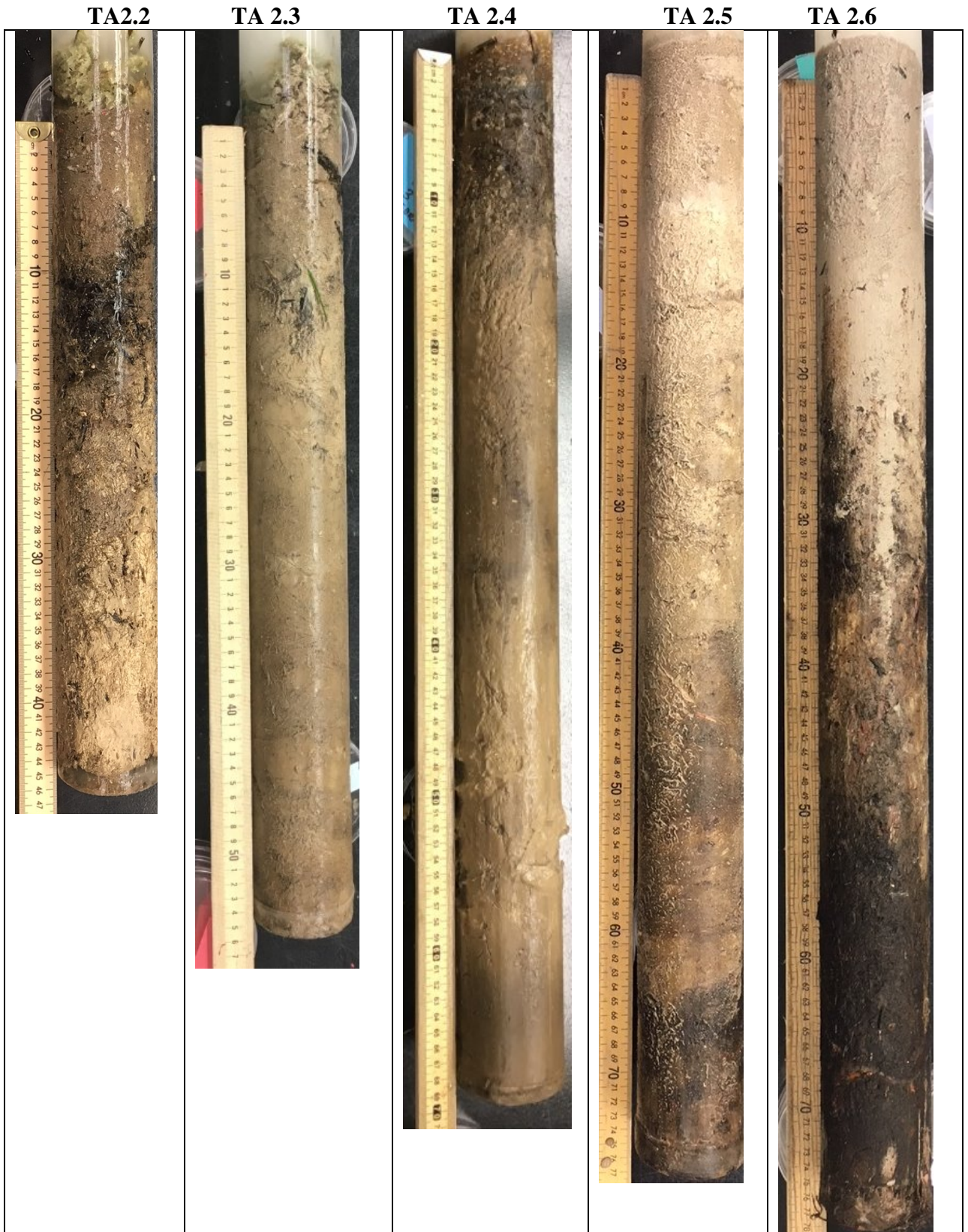
Appendix A. Core photos

Triangle Transect:

EVER 1



Transect TA -2:



Transect TA – 3:

EP10R

TA 3.4



Transect TA -4:

TA4.2

EP9R

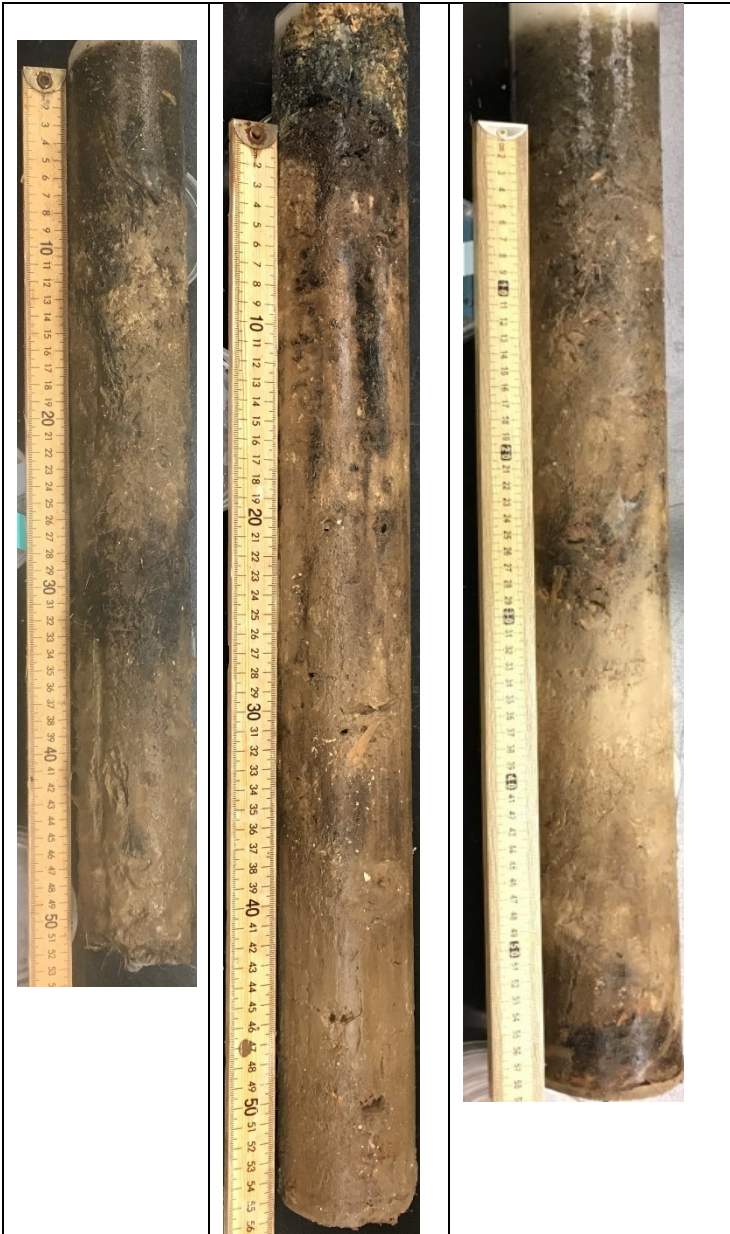


Transect TA- 5:

TA5.2

TA 5-3

TA 5-4



Transect TA - 6:

TA 6-1



Transect M5:

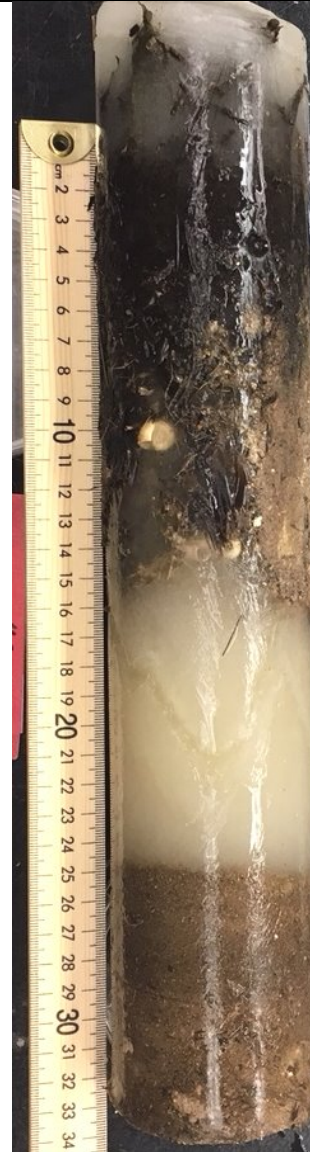
M5-N



M5-I



M5-S



Appendix B. SI data for cores arranged by transect

Depth	EVER1	TANGLIN	TANGLS	TA-2.2	TA-2.3	TA-2.4	TA-2.5	TA-2.6	EP10R	TA-3.4	TA-4.2	EP9R	TA-5.2	TA-5.3	TA-5.4	TA-5.5	TA-6.1	TA-6.4	TA-6.5	M5N	M5I	M5S
0	1.50	0	1.85	1.5	1.25	0	0	1.38	0	1.5	nd	1.00	1	2.13	3.5	nf	1.5	0	1.10	0.00	1.5	1
1	1.38	1	2.3	1	1	1.25	0	1.7	0	1.5	nd	1.50	1.25	2.06	1.35	nf	1.17	0	1.20	0.00	1	0
2	1.36	1.5	2.1	1.25	1	1.39	0	1.17	0	2.4	1	1.33	1.25	1.2	2.2	nf	1.23	0	1.17	0.00	1.33	0
3	1.33	2.13	1.89	1	1.17	1.31	0	1.25	3	0	nd	1.22	1.39	1.25	1.75	1.25	1.2	0	1.20	1.30	1.25	1.5
4	1.35	1.92	1.65	1	1.5	1.25	1.5	1.44	1.25	1.4	1	1.73	1.5	1.19	1.65	nf	1	0	1.25	1.33	1.33	1.5
5	1.34	1.17	1.5	1	1.5	1.65	1.5	1.75	1.87	2.05	1	1.47	1.1	1.25	1.64	1.33	1.1	0	1.29	1.29	1.25	1
6	1.36	1.83	1.42	0	1.5	1.53	2.38	1.17	1.33	1.56	1.1	1.06	1	1.25	1.25	1.25	1.19	0	1.27	1.23	1.41	1.33
7	1.31	1.38	1.46	0	1.29	1.13	2.67	2.83	1.75	1.66	1.21	1.18	1	1.18	1.25	1.57	1.21	1	1.36	1.35	1.3	1.17
8	1.19	1.32		2.5	1.22	1.27	1.5	2.25	1.25	1.17	1.3	1.30	1.25	1.17	1.33	1.80	1.23	0	1.31	1.19	1.31	1.5
9	1.20	1.33		4	1.25	1.27	1.38	1.6	1.13	1.35	nd	1.41	1.19	1.17	1.32	1.98	1.3	1.3	1.39	1.13	1.17	1.28
10	1.25	1.35	1.37	1	1.29	1.23	1.33	1.66	1.25	1.29	1.1	1.19	1.07	1.28	1.18	1.81	1.36	1.3	1.21	1.16	1.17	1.37
11	1.33	1.43	1.4	1.38	1.25	1.31	1.43	1.38	1.31	1.33	1.2	1.41	1.23	1.13	0	1.67	1.38	1.3	1.29		1.42	1.5
12	1.16	1.42	1.36	1.29	1.07	1.38	1.4	1.57	1.23		1.23	1.23	1.25	1.25	1.17	1.32	1.4	1.31			1.35	1.17
13	1.25	1.33	1.4	1.38	1.14	1.5	1.2	1	1.21		1.3	1.23	1.08	1.06	1.30	1.17	1.37	1.31	1.27		1.25	1.5
14	1.38	1.33	1.42	1.3	1.25	1.31	1.3	1.5	1.31		1.43	1.17	1.18	1.28	1.23	1.30	1.33	1.3	1.33		1.33	1.28
15	1.27	1.31	1.39	1.21	1.17	1.32	0	1.5	1.33		1.2	1.25	1.33	1	1.30	1.20	1.21	1.2	1.37		1.36	1.27
16	1.31	1.38	1.31	1.2	1.25	1.21		1.36	1.32		1.25	1.10	1.18	1.21	1.29	1.07	1.27	1	1.32		1.27	1.27
17	1.29	1.42	1.34	1.33	1.29	1.25		1.5	1.22		1.27	1.19	1	1.31	1.20	1.13	1.23	1.1	1.46		1.17	1.34
18	1.25	1.28	1.27	1.17	1.4	1.25		1	1.11		1.28	1.33	1.25	1.27	1.19	1.21	1.24	1.3	1.32		1.38	
19	1.5	1.44	1.46	1.17	1.29	1.13		1	1.33		1.28	1.10	1.25	1.17	1.17	1.36	1.35	1.5	1.30		1.3	
20	1	1.43	1.29	1.17	1.18	0		0	1.2		1.25	1.17	1.39	1.38	1.16	1.23	1.35	1.2	1.38		1.33	
21		1.33	1.36	1.17	1.16	1.27		1.25	1.23		1.3	1.25		1.21	1.33	1.32	1.38	1.2	1.33		1.32	
22		1.5	1.38	1.33	1.25	1.14		0	1.19		1.4	1.25			1.18	1.35	1.32	1.43			1.22	
23		1.25	1.17		1.3	1.21		1.3	1.23		1.19	1.30			1.27	1.26	1.2	1.32			1.34	
24		1.56	1.5		1.15	1		0	1.28		1.08	1.38			1.10	1.31	1.1	1.41			1.35	
25		1.42	1		1.25	0		1.5	1.31		1.25	1.30			1.31	1.24	1.35	1.39			1.33	
26		1.3	1.3		1.38	0		1.4	1.35		1.17	1.29			1.29	1.38	1.4	1.25			0	
27		1.63	1.28		1.25	1.5		1.11	1.15		1.14	1.29			1.26	1.33	1.3	1.76				
28		1.33	1.37		1.25	1.21		1.38	1.43		1.24	1.00			1.20	1.31	1.5	1.43				
29		1.29	1.35		1.05	1.25		1.16	1.33		1.33	1.17			1.17	1.19	0.00	1.36				
30		1.42	1.43		1.1	1.17		1.1			1.3				1.29		0.00					
31		1.4	1.36		1.33										1.29		0.00					
32		1.45	1.38		1.2										1.22							
33		1.73	1.5												1.25							
34		1.42	1.35												1.21							
35		1.4	1.23												1.21							
36		1.73	1.28												1.17							
37		1.64	1.22												1.23							
38		1.38	1.12												1.27							
39		1.33	1.25												1.23							
40		1.44	1.45																			
41		1.5	1.36																			
42		1.15	1.21																			
43		1.38	1.28																			
44		1.50	1.27																			
45		1.13	1.23																			
46		1.43	1.29																			

Continuation Appendix B

Depth	EVER1	TANGLIN	TANGLS	TA-2.2	TA-2.3	TA-2.4	TA-2.5	TA-2.6	EP10R	TA-3.4	TA-4.2	EP9R	TA-5.2	TA-5.3	TA-5.4	TA-5.5	TA-6.1	TA-6.4	TA-6.5	M5N	M5I	M5S
47		1.00	1.36																			
48		1.33																				
49		1.23																				
50		1.38																				
51		1.25																				
52		1.25																				
53		1.38																				
54		1.17																				
55		1.19																				
56		1.17																				
57		1.20																				

Appendix C. Bulk density (BD), OC (%), OC (g m² yr⁻¹) and SI for the Triangle transect cores.

depth	EVER1				TANGLIN				TANGLS			
	BD	%OC	OCgm2yr	SI	BD	OC%	OCgm2yr	SI	BD	OC%	OCgm2yr	SI
0	0.297	0.13	48.54	1.50	0.515	5.17	33.241	1.00	0.496	6.00	37.19	1.85
1	0.302	0.20	75.47	1.38	0.513	4.94	31.719	1.50	0.508	5.78	36.65	2.30
2	0.360	0.12	55.10	1.36	0.669	5.51	46.038	2.13	0.391	2.53	12.40	2.10
3	0.352	0.13	56.04	1.33	0.601	5.26	39.476	1.92	0.601	2.62	19.68	1.89
4	0.476	0.09	54.52	1.35	0.601	5.19	39.005	1.17	0.602	3.14	23.67	1.65
5	0.519	0.04	26.68	1.34	0.629	3.32	26.136	1.83	0.704	2.98	26.21	1.50
6	0.705	0.03	24.11	1.36	0.639	2.67	21.351	1.38	0.715	2.75	24.54	1.42
7	0.725	0.04	40.71	1.31	0.609	2.25	17.110	1.32	0.747	3.42	31.90	1.46
8	0.695	0.03	25.59	1.19	0.550	2.16	14.863	1.33	0.774	3.28	31.76	
9	0.611	0.03	26.64	1.20	0.449	3.92	22.004	1.35	0.620	5.17	40.09	
10	0.735	0.03	31.39	1.25	0.636	2.29	18.197	1.43	0.542	9.07	61.48	1.37
11	0.603	0.05	38.06	1.33	0.867	2.00	21.641	1.42	0.310	20.47	79.32	1.40
12	0.680	0.05	45.78	1.16	0.846	2.30	24.288	1.33	0.458	11.04	63.18	1.36
13	0.653	0.07	55.90	1.25	0.748	1.75	16.349	1.33	0.623	6.39	49.77	1.40
14	0.551	0.09	61.81	1.38	0.665	1.33	11.056	1.31	0.322	15.03	60.54	1.42
15	0.592	0.11	81.89	1.27	0.704	1.77	15.551	1.38	0.507	5.98	37.92	1.39
16	0.385	0.17	80.62	1.31	0.723	2.29	20.663	1.42				
17	0.241	0.32	96.10	1.29	0.721	2.46	22.149	1.28	0.232	14.53	42.12	1.34
18	0.210	0.41	106.10	1.25	0.812	2.31	23.418	1.44	0.495	4.87	30.16	1.27
19	0.202	0.33	84.10	1.50	0.612	2.74	20.989	1.43	0.548	4.63	31.76	1.46
20	0.156	0.47	90.70	1.00	0.627	2.73	21.351	1.33				
21	0.128	0.46	73.99		0.668	3.07	25.665	1.50	0.705	4.06	35.74	1.36
22	0.145	0.46	83.23		0.615	4.21	32.371	1.25	0.696	3.88	33.71	1.38
23	0.159	0.45	88.23		0.437	10.83	59.160	1.56	0.646	4.73	38.21	1.17
24	0.136	0.42	71.05		0.598	5.13	38.316	1.42	0.647	4.33	34.98	1.50
25	0.178	0.41	90.70		0.535	5.58	37.337	1.30	0.606	5.69	43.14	1.00
26	0.177	0.41	90.23		0.281	23.47	82.469	1.63	0.705	5.47	48.21	1.30
27	0.155	0.37	70.91		0.467	8.69	50.750	1.33	1.036	3.24	41.91	1.28
28	0.224	0.35	98.42		0.566	7.60	53.795	1.29	0.199	33.93	84.35	1.37
29	0.181	0.35	79.10		0.502	5.93	37.193	1.42	0.235	22.74	66.66	1.35
30					0.516	7.72	49.735	1.40	0.306	21.71	82.90	1.43
31					0.507	8.54	54.158	1.45	0.249	33.89	105.27	1.36
32					0.547	7.31	49.989	1.73	0.233	36.79	107.30	1.38

Appendix D: Mangrove and total vegetation cover by core location sorted from most southern to northern mangrove.

Sites	Easting	Northing	Mangrove Cover	Mangrove Cover StdDev	Total Cover	Total Cover StdDev
T6.6	525377	2791086	10.00	8.66	32.74	40.15
T6.5	525748	2791985	21.00	25.76	13.82	19.41
TA2.6	552032	2792084	23.26	27.74	15.20	24.40
TA3.5	548199	2792747	24.38	16.32	8.53	11.96
E146	533608	2792886	6.80	4.92	17.82	20.49
TA5.5	540925	2792908	61.88	21.96	14.83	27.33
TA2.5	551918	2792976	38.32	29.51	16.89	26.50
T6.4	527465	2793565	4.50	4.95	11.19	13.13
TA3.4	548017	2793614	22.28	26.44	11.78	20.17
T7.4	521808	2793786	10.44	11.06	11.37	15.96
TA5.4	540866	2793830	36.73	39.28	12.79	25.86
TA4.4	544586	2793873	25.33	26.11	11.39	19.50
TA2.4	551831	2793899	25.67	17.50	16.75	15.74
UJB	547160	2794242	23.00	26.77	10.24	18.48
T7.3	522577	2794386	28.08	36.94	12.16	17.96
UHC	554851	2794546	32.30	19.78	18.22	21.62
TA3.3	548093	2794642	37.67	30.54	17.72	26.16
TA5.3	540857	2794768	27.62	32.95	13.41	24.72
TA2.3	551827	2794821	29.42	29.59	14.13	23.44
EP9R	544834	2795135	35.26	32.71	27.14	31.04
T7.2	523341	2795216	8.32	15.76	24.23	28.89
EP10	547613	2795310	33.89	33.24	19.76	28.89
EP12R	555853	2795391	32.15	34.47	18.10	29.85
TA5.2	540749	2795675	34.75	27.36	21.42	24.63
TA4.2	544374	2795689	15.91	26.12	18.34	23.58
TA2.2	551533	2795730	29.14	27.90	18.78	15.58
T6.1	529846	2796180	0.00	0.00	9.18	11.12
T7.1	524302	2796185	10.91	15.88	12.61	14.00
TA5.1	540662	2796598	0.00	0.00	8.17	8.45
TA4.1	544337	2796604	19.00	17.46	24.03	27.72
EP1R	555049	2796919	41.20	23.86	17.31	22.57
EVER5B	543272	2797125	5.67	3.79	15.11	15.32
TANGLS	558781	2797711	28.96	18.39	16.66	19.07
EVER6	549130	2798041	57.50	31.82	52.35	34.30
M5-S	517157	2799478	44.21	40.02	36.54	37.30
M5-I	518334	2799788	0.80	0.27	11.49	12.88
TANGLI	557949	2799845	30.81	24.77	11.95	20.02
M5-N	519778	2800131	0.00	0.00	2.20	3.20
TANGLN	557886	2800712	21.08	22.89	10.26	17.87
EVER1	557418	2801508	15.59	18.05	11.39	12.24
TKYE	562620	2801696	33.90	21.92	33.90	21.92

Continuation Appendix D

Sites	Easting		Northing	Mangrove Cover	Mangrove Cover StdDev	Total Cover	Total Cover StdDev
TKYNW	561812		2803080	9.22	12.55	5.84	9.44
TKYINT	561353		2803751	17.71	20.66	9.51	14.91
TDWW	565715		2817355	46.94	19.90	34.15	26.74
TDE	566026		2817358	63.55	23.63	27.69	31.78
CDE	565823		2818760	26.33	19.25	14.13	14.37
CDW	565719		2818782	24.93	10.25	12.31	11.85

Section 3

Soil organic carbon stocks decrease with saltwater intrusion despite mangrove encroachment in the Florida Coastal Everglades

Sean P. Charles, John S. Kominoski, Mike S. Ross, Jay Sah, John F. Meeder, Leonard J. Scinto

ABSTRACT

Accelerated sea-level rise and freshwater management are drastically altering the structure and function of coastal ecosystems, with uncertain impacts on critical soil carbon storage. Coastal wetlands sequester more atmospheric carbon per unit area than any other ecosystem, largely by storing organic carbon (OC) in soil, providing substrate to increase their soil elevation to keep pace with sea level rise. Saltwater intrusion can affect OC storage by creating functional changes in existing wetland ecosystems, thereby altering the balance between OC gain from in situ production or OC loss from decomposition, or by driving vegetation shifts. Throughout the tropics and subtropics, saltwater intrusion often drives the inland encroachment of mangrove forests. One such are is the Southeast Saline Everglades, where the heterogeneous nature of mangrove recruitment provides an ideal template to quantify the interacting impacts of vegetation shifts and saltwater intrusion. We used short-, intermediate-, and long-term response variables to identify structural and functional attributes of ecosystems with different patterns of C storage. We measured soil nutrient chemistry (percent nitrogen, phosphorus and nutrient ratios) and vegetation dynamics (marsh and mangrove cover) and developed models to determine their impact on organic carbon stocks (root biomass and soil organic

carbon) and fluxes (root productivity, and organic matter breakdown). Despite considerable spatial variation in mangrove recruitment, cover of the primary invading species, *Rhizophora mangle*, was negatively related to distance from the coast. whereas soil nitrogen, N:P and C:N ratios increased toward the wetland interior. Soil OC stocks were highest inland, and decreased toward the coast, indicating that saltwater intrusion may decrease soil C storage. Organic matter breakdown rates were positively related to soil C:N ratios, and higher soil C:N ratios were measured in inland relative to coastal wetlands, providing indirect evidence that interior marshes are currently experiencing carbon loss as a result of saltwater intrusion. Although saltwater intrusion may be reducing soil organic carbon, mangrove vegetation enhances both root biomass stocks and inputs from root productivity, but did not impact breakdown rates, indicating that mangroves may limit soil carbon loss. Soil organic carbon develops over long time frames, and saltwater encroachment can rapidly destabilize soil organic carbon stocks, and although mangroves may enhance root carbon storage, we did not find a relationship between root processes and overall soil carbon stocks.

INTRODUCTION

Accelerated sea-level rise (SLR) is causing drastic changes to the structure and function of coastal wetlands. Saltwater intrusion is expected in many freshwater ecosystems as SLR increases (Rahmstorf 2007; Milne et al. 2009), climate change alters temperature and precipitation patterns (Smith et al. 2005; Mily et al. 2005), and anthropogenic alterations upstream continue to reduce freshwater flows to coastal wetlands (Meehl et al. 2007). Additionally, global changes are causing major shifts in

plant communities worldwide (Chen et al. 2011), and saltwater intrusion is expected to lead to the replacement of freshwater marsh communities with halophytic species (Sutter et al. 2013). In tropical and subtropical ecosystems, saltwater intrusion has caused mangroves to move inland and displace herbaceous marshes in Australia (Rogers et al. 2000, 2006; Winn et al. 2006), Mexico (Lopez-Medellin et al. 2011), and the United States (Ross et al. 2000; Krauss et al. 2011; Smith et al. 2013; Guo et al. 2017). Any shifts in coastal wetland C storage associated with these changes will have profound impacts locally on marsh resilience, and globally on the sequestration of CO₂, yet we lack a clear understanding of the impacts of shifts in hydrologic conditions and foundation plant species.

Shifts between plant communities with drastically different traits are likely to alter ecosystem function (Kominoski et al. 2013). One of the most distinct vegetation shifts across landscapes worldwide is the encroachment of woody vegetation into grasslands (Van Auken 2000; Frelich and Reich 2010; Knapp et al. 2008; Saintilan et al. 2015). Woody plant invasion may influence C cycling through effects on productivity, litter chemistry, microclimate, capture of allochthonous inputs and soil aeration (Furukawa et al. 1997; Bowman et al. 2004; Lovett et al. 2004; Wittman et al. 2004; Fagherazzi et al. 2006), and in terrestrial ecosystems woody encroachment generally leads to increased soil C storage (Elridge et al. 2011). In coastal wetlands, differences in the impact of marsh and mangrove C storage is uncertain (Kelleway et al. 2017). In sediment-poor coastal wetlands like the Southeast Saline Everglades (Figure 2), organic matter dynamics drive elevation change, particularly through the production and

accumulation of roots (Hatten et al. 1983; Nyman et al. 1993; Turner et al. 2001; Delaune and Pezeshki 2002).

The interactive effects of mangrove encroachment and saltwater intrusion on soil OC storage are uncertain. Mangrove and saltmarsh ecosystems store soil OC at similar rates globally (Chmura et al. 2013). In studies that compared adjacent mangrove and saltmarsh ecosystems, some found greater soil C storage capacity in mangroves (Bianchi et al. 2013; Yando and others 2016; Charles et al. in review), while others found no difference (Perry and Mendelsohn 2009; Henry and Twilley 2013; Doughty and others 2015; McKee et al. 2017). Independently, saltwater intrusion can drive loss of soil OC by decreasing plant productivity and biomass with salt stress (e.g., Krauss et al. 2009; Neubauer 2008), and cause major biogeochemical changes that often lead to enhanced breakdown of soil organic matter (Weston et al. 2006; Neubauer 2013; Chambers et al. 2013). However, in many coastal wetlands in the tropics and subtropics, saltwater intrusion may also drive the landward encroachment of mangroves into wetlands previously dominated by freshwater and brackish marsh species. Although mangrove encroachment into the wetland interior has happened broadly across the Everglades, fire, disturbances, propagule distribution, and underlying habitat characteristics (Smith et al. 2012) limit mangrove recruitment, thus creating a patchwork of vegetation across a landscape experiencing saltwater intrusion.

The Florida Coastal Everglades are particularly susceptible to saltwater intrusion from sea-level rise due to low elevation and slope (Titus and Richman 2001), porous limestone bedrock, and a series of 2500 km of canals and water control structures that greatly reduce natural freshwater availability (Sklar et al. 2000; McVoy et al. 2011).

Everglades, plant communities are oriented in zones according to their salinity tolerance. Glycophytic communities dominated by *Cladium jamaicense* occupy inland areas through competitive advantages in freshwater environments, mangrove species dominated by *Rhizophora mangle* prevail nearer to the coast due to salt tolerance, and the ecotone between the two is occupied by mixed graminoid-mangrove communities (Egler 1952; Koch 1996; Ross et al. 2000). Between 1940 and 1994, the mixed graminoid-mangrove community moved inland 3.3 km and was replaced by stands of *R. mangle* (Ross et al. 2000), a pattern identified elsewhere in the Everglades as well (Krauss et al. 2011; Smith et al. 2013). Saltwater intrusion along the Everglades ecotone has also increased P availability (Sandoval et al. 2016), often temporarily increasing sawgrass productivity. However, sawgrass production is reduced once salinity reaches 5 ppt (Macek and Rejmankova 2007; Wilson et al. 2015), and sawgrass mortality follows when salinity averages around 15 ppt (Troxler et al. 2014). Unless halophytes (particularly mangroves) can replace these glycophytic assemblages, root death can lead to rapid loss of root biomass and soil carbon, driving a decrease in elevation and greater inundation (Delaune et al. 1994), potentially making future plant establishment impossible. In the Southeast Everglades, an interior band of sparse vegetation – the “white zone” (Ross et al. 2000; Egler 1952) has expanded into what was previously denser-canopied freshwater marsh (Figure 2).

We selected wetlands along coastal gradients in the Southeast Saline Everglades – a region with rapid changes in vegetation cover (Ross et al. 2000) – to quantify the impacts of shifting vegetation, saltwater intrusion and underlying soil characteristics on stocks and fluxes of belowground carbon. As saltwater intrudes into the Everglades

interior, mangrove colonization of the landscape is spatially variable and heterogeneous, providing an opportunity to quantify the impacts of saltwater intrusion with and without concomitant vegetation shifts. We used short- (organic matter fluxes that manifest rapidly), intermediate- (development of root biomass that requires vegetation establishment and development), and long-term response variables (soil organic carbon that changes over decades to centuries) to identify structural and functional attributes of ecosystems with differential C storage (Figure 1). We compared OC fluxes and stocks to shifting vegetation (vegetation species, cover, height), environmental characteristics (soil depth, type, nutrient and organic matter content) and distance to the coast (a proxy for shifting marine connectivity) to quantify drivers and effect across the landscape. We predicted that proximity to the coast would alter soil nutrient characteristics due to low P availability in the Everglades interior interacting with marine P subsidies (Figure 1), and that mangrove cover would be higher closer to the coast. We predicted that increasing marine influence on soil would increase breakdown rates, causing OC storage to decrease, but this decline would be at least in part counterbalance by the establishment of mangroves, which might effect greater root biomass and productivity (Figure 1). We predicted that increasing mangrove cover would increase root productivity and biomass stocks, whereas soil characteristics associated with saltwater intrusion would drive increased breakdown and a decrease in soil OC storage (Figure 1). Overall, we predicted that OC stocks would decrease in marine influenced coastal soils in the absence of mangrove encroachment, but that mangrove cover would increase OC storage, with the ultimate fate of soil carbon in a more marine influenced coastal wetland to be determined by establishment of mangrove cover (Figure 1). Our results will help identify the

functional differences driven by vegetation dynamics from those driven by larger scale biogeochemical changes associated with saltwater intrusion, and pinpoint conditions that contribute to OC storage, vulnerability to loss of OC and inundation by rising seas

METHODS

Experimental Design

We established 19 sites along five transects in the Southeast Saline Everglades, with each transect representing a gradient across the marsh-mangrove ecotone. Included in the gradient are the lower and upper portions of the white zone, the “incipient” white zone (Ross et al. 2000; 2002) and the distal edge of the freshwater marsh for a total of 24 sites (Figure 2).

Vegetation and soil dynamics with proximity to coast

At each site we estimated the aboveground cover of vascular plant species rooted within 30 1-m² sub-plots distributed along a 50 m radius circle (Ross et al 2000). The design allowed us to identify larger vegetation patterns, as well as heterogeneity within the larger landscape. For each plot and sub-plot, we calculated total vegetation cover, total mangrove cover and total marsh (graminoid) cover.

At the center of each plot, we extracted one soil core (15 cm diameter • 30 cm deep) to determine soil nutrient content. Cores were taken to the lab and sectioned based on visually apparent horizon shifts. All samples were dried at 40°C to constant weight to determine dry mass, and then ground using an 8000-D ball mill (Spex SamplePrep, Metuchen, New Jersey, USA). Soil cores were separated into soil 0-15 and 15-30 cm deep sections. Percent total carbon (%C) and total nitrogen (%N) were determined using

a Carlo Erba NA 1500 CHN Analyzer (Carlo Erba, Milan, Italy). Percent total phosphorus (%P) was determined by the ash/acid extraction method (Allen 1974), followed by spectrophotometric analysis. We calculated total nutrient ratios (C:N, C:P, N:P), expressed on a molar weight basis.

Organic matter fluxes

We measured organic matter flux as root production and the breakdown of standardized organic matter within a subset of 12 of our 19 sites. Root productivity was measured as ingrowth into a mesh bag filled with commercial peat moss that had been inserted into holes created by belowground biomass cores (McKee et al. 2007). Root ingrowth bags were retrieved after 6-12 months in the field, based on access to sites (helicopter scheduling). On retrieval, roots were separated from the ingrowth bags, dried and weighed. Root productivity was standardized to represent kg root OC m⁻² y⁻¹.

We tested breakdown rates for labile (cellulose) and recalcitrant (wood) OM, using standard substrates on the soil surface and at two depths in the soil. Adjacent to each root ingrowth experiment, we measured the breakdown of wood and cellulose standard substrates on the soil surface, and at 10-15 cm and 15-30 cm depths in the soil. After incubation in the field for 8-16 months, we returned all OM breakdown samples to the laboratory on ice, rinsed them of sediment, and dried the samples at 40°C until their mass stabilized. We estimated breakdown rate, k , using a linear regression of the ln-transformed fraction of AFDM remaining vs. time (negative exponential model; sensu Benfield 2006). The specific model used was $M_d = M_0 \cdot e^{-kt}$, where M_0 is the initial litter

mass, M_t is the litter mass on a given sampling day, and d is number of days of incubation). In addition, we used data from a NOAA local temperature station (N 25.3903°, W -80.6803) to determine average daily temperature and degree days (days of incubation • degree C) throughout the incubation period. To examine breakdown as a function of temperature, we also calculated breakdown as $M_{dd} = M_0 \cdot e^{-kdd}$, where dd is degree days.

Organic carbon stocks

To determine organic carbon stocks at each plot, we extracted a soil core (15 cm diameter • 30 cm deep) from the center, northernmost, and southernmost vegetation sub-plots. We measured bulk density and calculated percent OC from ash-free dry mass (AFDM) as loss on ignition in a muffle furnace at 550°C for 5.5 h (Karam 1993), and converted to %OC by dividing by 2 (Pribyl et al. 2010).

At each site, we also took three root biomass cores (15 cm diameter • 30 cm deep) adjacent to soil OC cores. Root biomass cores were transported to the lab, where living roots were separated from the bulk soil, dried at 40°C. We calculated root biomass and root OC content with the same methods as soil OC.

Data analyses

We created models to determine relationships between proximity to the coast and soil (%OM, %P, %N, %C, C:P, C:N and N:P) and vegetation (cover of red mangrove, total mangrove cover, cover of marsh and total cover) characteristics. We created a

second set of models to determine how soil carbon stocks (root biomass, soil OC) and fluxes (root productivity and breakdown of organic matter standard substrates) are driven by soil and vegetation characteristics. Each response and predictor variable was normalized by the equation $variable = (x - mean(x))/stdev(x)$, to insure normality and to provide similar scales. We used hierarchical linear mixed-effects models using the R package “lme4” (Bates et al. 2015) to test for relationships between response variables and fixed effects (distance to coast and soil and vegetation characteristics), and random effects of transects nested within region. We calculated Akaike’s information criterion corrected for small sample size (AIC_c) to determine the most parsimonious model from our combination of vegetation, soil and (Hurvich and Tsai 1989). We used an alpha level of 0.05 to determine significant relationships. We used the “MuMIn” package in R (Barton 2016) to determine goodness of fit (conditional R²; Nakagawa and Schielzeth 2013) for top models.

We used piecewise structural equation models (Lefcheck 2016) to measure linkages between proximity to the coast, vegetation and soil chemical characteristics, soil carbon fluxes (root productivity and organic matter breakdown rates) and soil carbon stocks (root biomass and soil organic carbon content). Piecewise structural equation models permit the use of linear mixed effects models, which were essential for dealing with spatial correlation in our study design (Lefcheck 2016). The corresponding model list is composed of linear mixed effects models (individual statistical output described in table 1), run with the R package “lme4”. We ran the model in R with the package “piecewiseSEM.” We identified the most parsimonious overall model and removed linkages to minimize AIC_c. We show only significant correlations ($P < 0.05$) as

standardized path coefficients. All analyses were performed using R (version 3.3.2, R Core Team 2016).

RESULTS

Vegetation and soil dynamics with proximity to coast

Mangrove cover declined with increasing distance from the coast and (Figure 3a; Table 1; $P = 0.049$; $R^2 = 0.19$), but marsh cover did not change with coastal proximity ($P > 0.05$). No significant relationships were observed between distance to coast and soil characteristics in the deeper soil layer (>15 cm), but numerous associations were detected when surface sediments (0-15 cm) were considered. Distance to the coast was positively associated with surface (0-15 cm) %N (Figure 3b; Table 1; $P = 0.01$; $R^2 = 0.35$), and surface %OM ($P < 0.0001$; $R^2 = 0.65$), but relationships with %P or %C ($P > 0.05$) were non-significant. Surface C:N ratios decreased with distance to the coast (Figure 3c; Table 1; $P = 0.01$; $R^2 = 0.34$), while surface N:P ratios increased (Figure 3d; Table 1; Table 1; $P = 0.03$; $R^2 = 0.55$).

Organic matter fluxes

Root productivity was best described by a model that only included mangrove cover, which showed a positive relationship (Figure 4a; Table 1; $R^2 = 0.30$; $P = 0.001$). However, a model that included mangrove cover and soil N:P ratio created a similarly parsimonious model ($\Delta AICc < 2$; Burnham and Anderson 2002), with significant negative impact of soil N:P ($P = 0.04$), and explained more variance (Table 1; $R^2 = 0.38$).

Root productivity did not show significant relationships with any other soil characteristics ($P > 0.05$).

When incubated on the soil surface, neither cellulose nor wood standard substrate breakdown rates ($k \text{ dd}^{-1}$) were related to vegetation parameters, or soil chemical characteristics ($P > 0.05$). However, when placed belowground, breakdown rates of these materials were positively related to soil C:N ratio. Wood standard substrates were positively related to C:N ratios in the shallow soil (Figure 4b; Table 1; $P = 0.04$ $R^2 = 0.66$) and deeper (15- 30 cm) soil (Table 1; $P = 0.03$ $R^2 = 0.36$). In addition, cellulose breakdown was positively related to soil C:N ratio in deeper soil (Table 1; $P = 0.04$ $R^2 = 0.36$). Though it was not included in the most parsimonious model, wood breakdown was positively related to distance from coast in deeper soil ($P = 0.03$; $R^2 = 0.14$). Breakdown rates were not related to mangrove cover, nor were they related to any other nutrient concentrations or ratios.

Organic carbon stocks

The best predictor of root biomass (0- 30 cm) was *Rhizophora mangle* (red mangrove) cover (Figure 5a; Table 1; $R^2 = 0.58$; $P < 0.001$). In addition, root biomass was negatively related to soil N:P ratio ($R^2 = 0.34$; $P = 0.04$), though this relationship did not improve a model based on *R. mangle* cover alone.

Surface soil OC (0- 15 cm) was positively related to distance from coast (Figure 3b; Table 1; $R^2 = 0.62$; $P < 0.001$), but there was no relationship with deeper soil ($P > 0.05$). In addition, there was no relationship between vegetation cover and soil OC at the surface or in deeper soil ($P > 0.05$). Tests of the interacting effects of mangrove cover

and distance to coast on soil organic carbon stocks indicated that mangrove cover created a near-significant increase in soil OC stocks ($P = 0.06$), though model parsimony decreased ($AIC = -22.47$; $R^2 = 0.65$),.

Structural equation model

Our piecewise structural equation model illustrates the direct and indirect contributions of proximity to coast on organic carbon stocks and fluxes (Figure 6; $K = 17$; Fisher's C value = 25.78; $P = 0.004$). Path coefficients demonstrate that proximity to coast has a greater (or more consistent) impact on soil chemistry ($N:P = -0.38$; $P < 0.001$; $C:N = 0.6$; $P < 0.001$) than on mangrove cover (0.19 $P = 0.05$), demonstrating the heterogeneity of mangrove recruitment. Path coefficients show that mangrove cover explains about half the variation in root productivity (0.51 ; $P = 0.001$) and root biomass (0.56 ; $P = 0.002$). Soil $N:P$ ratio decreased root productivity (-0.3 ; $P = 0.05$), and $C:N$ ratios increased wood breakdown (0.43 ; $P < 0.001$). Finally, path coefficients show a strong negative impact on surface soil OC stock (-0.79 ; $P < 0.001$), but no impact of our measured OC fluxes or root biomass.

DISCUSSION

Saltwater intrusion and mangrove encroachment

We identified strong and consistent shifts in soil chemistry and significant, but more heterogeneous changes in mangrove cover across the study gradient, with no impact on total vegetation cover. Surface %N in the surface soil increased consistently toward

the freshwater interior (Figure 3a), and N:P ratios followed the opposite pattern (Figure 2b) ratios consistently decreased with proximity to the coast. Saltwater intrusion generally drives an increase in P availability throughout the coastal Everglades (Sandoval et al. 2016), because P is more available in seawater in this “upside-down estuary” (Childers et al. 2006). Furthermore, as saltwater intrudes into freshwater marshes, P adsorbed to sediment and limestone bedrock, is rapidly released, providing a pulse of P which becomes available for plant uptake (Price et al. 2010; Flower et al. 2016; 2017). Although N:P ratios shifted along our coastal gradient, we found no significant change in total soil P, probably due to the Southeast Everglades’ proximity to the P-limited and microtidal Florida Bay rather than the more productive Atlantic and Gulf Coasts (Childers et al. 2006).

Inland encroachment of mangroves is spatially variable and likely slow in carbonate coastal wetlands. Percent cover of *R. mangle* was negatively related to distance to coast in our study (Figure 3a), yet mangrove cover was heterogeneous and the impact of proximity to coast was weaker than that for soil nutrient change (Figure 6). Furthermore, within our study area red mangroves have increased 44% in the last twenty years while sawgrass marshes have declined 15% (Ross et al. in prep), indicating that interior wetlands are becoming increasingly influenced by saltwater through time. However, in coastal regions with low plant biomass like the Southeast Saline Everglades, saltwater intrusion continues to rapidly expand (Ross et al. 2000), and mangrove cover does not appear to be replacing the rapidly retreating freshwater vegetation. Encroachment of freshwater and brackish marsh with salt-tolerant species has been identified globally (Sutter et al. 2013; Herbert et al. 2015), and mangrove encroachment

into freshwater ecosystems has been observed in Australia (Rogers et al. 2000, 2006; Winn et al. 2006), Mexico (Lopez-Medellin et al. 2011), and the United States (Ross et al. 2000; Smith et al. 2013). On the west coast of Florida, the range of mangroves expanded inland by 35% at the expense of marsh between 1927 and 2005 (Krauss et al. 2011). However, in our study area, the encroachment of mangroves has been patchy and associated with the expansion of the low biomass “white zone.” The patchy nature of recruitment, coupled with widespread shifts in soil chemistry allows us to determine the impacts of saltwater intrusion with and without mangrove encroachment, and may have profound impacts on similar ecosystems globally.

Located at the intersection of marine and freshwater ecosystems, coastal wetlands are particularly vulnerable to shifts in hydrology. The combination of SLR and reduced freshwater availability alters the balance of fresh and marine water (Dessu et al. 2018), and creates widespread saltwater intrusion into freshwater and brackish wetlands (Ross et al. 2000; White and Kaplan 2017). With much of the Everglades less than 1.5 m above sea level (Titus and Richman 2001), projected SLR rates of 1-2 m in this century (Haigh et al. 2014) will cause widespread saltwater intrusion throughout the Everglades, altering soil and water chemistry and driving widespread shifts in vegetation communities, particularly around our study area in the Southeast Saline Everglades ecotone (Ross et al. 2000).

Saltwater intrusion effects on organic carbon stocks and fluxes

We predicted that organic matter breakdown rates would be positively related to marine influence, yet we found a positive indirect relationship between organic matter

breakdown and freshwater conditions (Figure 6). Added phosphorus frequently drives increased breakdown rates in peat soils (Davis 1991; Newman et al. 2001; Qualls and Richardson 2008). In a mesocosm experiment testing the impact of saltwater encroachment, phosphorus additions increased breakdown rates of leaf-litter (18%), and roots (11%) (Charles et al. in prep). However, across the Southeast Saline Everglades, a lack of spatial trends in phosphorus concentrations, and dominance of low organic matter marl soils, likely limits the impact. This may also be because many of these wetlands have experienced some saltwater intrusion in the past. Phosphorus adsorbed to limestone is often released immediately upon saltwater intrusion (Flower 2016; 2017). Therefore, limestone near the coast may have released their available phosphorus, and the low levels of OC in these coastal wetlands may indicate that OC breakdown from saltwater encroachment has already peaked and low OC availability may limit breakdown in coastal wetlands, limiting any potential response. Although our results indicate that saltwater intrusion is not increasing breakdown rates, it may mean that higher OC interior wetlands are undergoing changes to become similar to the low OC wetlands closer to the coast.

We found that vegetation cover did not have a relationship to breakdown rates at the surface or either depth. Other studies have found that mangroves can influence breakdown rates by priming the soil with root exudates (Kuzyakov 2010; Bernal et al. 2016) and particularly in the case of wetland plants like mangroves, by aerating soils with their roots (Gill and Tomlinson 1977). Mangroves can also decrease breakdown rates by creating shade from their canopy and reducing soil temperature (D'Odorico et al. 2013; Charles et al. in review). In our study, vegetation cover did not influence organic

matter breakdown, potentially through a balance between positive and negative impacts of mangrove vegetation on organic matter breakdown.

Priming of recalcitrant organic matter is a globally important process in driving organic matter breakdown (Guenet et al. 2018). There is debate on the influence of nutrients on priming, with two main schools of thought, 1) that nutrients increase soil OM breakdown by providing microbes with nutrients for growth, or 2) that microbes decompose OM faster in nutrient-poor conditions to “mine” for nutrients (Craine et al. 2009). However, there may be differential responses depending on OM quality, and microbial *k* strategists often mine nutrients and thus do not increase breakdown with nutrient addition (Chen et al. 2014).

Increasing mangrove cover increased root productivity and root biomass standing stocks across coastal wetlands. Roots and rhizomes are the primary sources of SOM, C storage and soil elevation change in coastal wetlands (Twilley 1999; McKee et al. 2007; Chmura 2011; Deegan et al. 2012) and in our study mangroves explained about 50% of all variance in root OC stocks and inputs (Figure 6). Because mangroves increased stocks of root OC and did not impact organic matter breakdown rates, it is likely that they will enhance OC storage over time. However, in our study OC stocks decreased with increasing marine influence. In this low-productivity region with soil C storage is a slow process (Meeder et al. 2017). However, we did find some evidence that mangroves may help to increase OC storage by identifying a near-significant interaction of mangroves with distance to coast ($P = 0.06$). We suggest that any positive impact of mangrove vegetation is partially confounded by association with marine influence on soil characteristics.

Wetlands closer to the coast had lower soil OC stocks despite higher mangrove cover. Saltwater intrusion is negatively related to sawgrass productivity and survival (Ewel et al. 2006; Macek and Rejmankova 2007; Troxler et al. 2014). The Southeast Saline Everglades have been subjected to some of the most extreme saltwater intrusion in the greater Everglades due to road and canal development, that isolated the region from freshwater flow (Sklar et al. 2005). Over the past half century, saltwater intrusion has driven the interior expansion of a zone of sparse vegetation (the “white zone,”) into what was previously denser-canopied freshwater marsh (Egler 1952; Ross et al. 2000). Similarly, along the ecotone, sawgrass marsh has been converted to a patchwork of open water ponds, through a poorly-understood process called “peat collapse”. In much of the Southeast Saline Everglades, the loss of freshwater and brackish vegetation and the white zone expansion has driven soil OC loss, for decades due to saltwater intrusion that was exacerbated.

Our results indicate that saltwater intrusion is likely to reduce soil OC stocks across the coastal wetlands Everglades, but that mangrove expansion and colonization could mitigate some OC loss. Although our study suggests mangroves may enhance carbon storage across the landscape by increasing root biomass and productivity, mangroves are becoming established in a region that has already undergone soil OC loss. Our results indicate that mangroves enhance OC inputs, but soil development and OC accretion is slow in low-productivity, severely P-limited wetlands like the Southeast Saline Everglades (Meeder et al. 2017), and the recovery of lost soil OC has not yet occurred. The storage of organic matter is a slow process governed by the balance between OC inputs and breakdown (Baustian et al. 2012). Additionally, soil elevation is

governed by accumulation of organic and inorganic materials (Morris et al. 2002, Nyman et al. 2006; McKee 2011), but in sediment-poor wetlands >1 km from the coast, like the Southeast Everglades, elevation gains are largely determined by organic matter accumulation particularly from roots (Hatton et al. 1983; Nyman et al. 1993; 2006; Turner et al. 2001; Delaune and Pezeshki 2002).

In P-limited oligotrophic estuaries, like the Florida Everglades, saltwater intrusion provides a nutrient subsidy (potentially stimulating productivity), but also increase the stress of salinity, with uncertain overall impacts on plant productivity and biomass accumulation (Childers et al. 2006). The impacts of saltwater intrusion on belowground C storage are uncertain. Salinity often decreases root productivity, and nutrient subsidies often increase aboveground biomass but have uncertain impacts on root productivity. Nutrient addition can increase above and belowground productivity in some coastal ecosystems (McKee et al. 2007), but root productivity can be high in low-nutrient peatlands (Castaneda-Moya et al. 2011) compared to carbonate-rich wetlands. Although saltwater intrusion is likely to drive OC loss from many coastal wetlands, we lack an understanding of how saltwater intrusion, vegetation shifts, soil characteristics and nutrient availability interact across coastal wetland landscapes.

Coastal wetlands store more OC per area than other ecosystems (Chmura et al. 2003; Bouillon 2011; McLeod et al. 2011), providing a globally important feedback to climate change and the storage of OC and belowground biomass in soils often drives wetland surface elevation change (Nyman et al. 1993, 2006; Turner et al. 2000; McKee et al. 2007; Neubauer 2008). Many coastal wetlands have increase their surface elevation to persevere through gradual rates of SLR for thousands of years (Woodroffe et al. 1990;

McKee et al. 2007). As SLR accelerates, there is concern that large portions of coastal wetlands may be lost to submergence in the coming century (Wanless et al. 2004; Cooper et al. 2008; Morris et al. 2016). Our data suggests that OC loss from coastal wetlands may exacerbate the submergence of wetlands. However biophysical feedbacks such as mangrove encroachment that enhance vertical elevation gain may increase resilience and preserve most wetland area (Kirwan et al. 2016). Our results suggest that soil OC loss is likely as saltwater intrudes into freshwater and brackish wetlands, but that the inland encroachment of mangroves may increase coastal wetland C storage and increase resilience to SLR. The fate of many coastal wetlands rests on the interaction of biophysical changes associated with water and soil chemistry and the survival or replacement of wetland vegetation.

ACKNOWLEDGMENTS

This research was funded in part by an Institutional Grant (####) from Everglades National Park. Sean Charles was supported by a Dissertation Year Fellowship from Florida International University. Patricia Leroy, Suzanna Stofella and Jesus Blanco provided laboratory and field assistance. This publication is contribution number XXXX for the Southeast Environmental Research Center.

LITERATURE CITED

- Bernal B, McKinley DC, Hungate BA, White PM, Mozdzer TJ, Megonigal JP. 2016. Limits to soil carbon stability; Deep, ancient soil carbon decomposition stimulated by new labile organic inputs. *Soil Biology and Biochemistry* 98:85-94.
- Bianchi TS, Allison MA, Zhao J, Li X, Comeaux RS, Feagin RA, Kulawardhana RW.

2013. Historical reconstruction of mangrove expansion in the Gulf of Mexico: Linking climate change with carbon sequestration. *Estuarine, Coastal and Shelf Science* 119:7-16.
- Cahoon, D. R., P. Hensel, J. Rybczyk, K. L. McKee, C. E. Proffitt, and B. C. Perez. 2003. Mass tree mortality leads to mangrove peat collapse at Bay Islands, Honduras after Hurricane Mitch. *Journal of Ecology* **91**:1093-1105.
- Chen, I. C., J. K. Hill, R. Ohlemuller, D. B. Roy, and C. D. Thomas. 2011. Rapid Range Shifts of Species Associated with High Levels of Climate Warming. *Science* **333**:1024-1026.
- Chmura, G. L., S. C. Anisfeld, D. R. Cahoon, and J. C. Lynch. 2003. Global carbon sequestration in tidal, saline wetland soils. *Global Biogeochemical Cycles* **17**:12.
- Deegan, L. A., D. S. Johnson, R. S. Warren, B. J. Peterson, J. W. Fleeger, S. Fagherazzi, and W. M. Wollheim. 2012. Coastal eutrophication as a driver of salt marsh loss. *Nature* **490**:388-+.
- Dessu, S. B., R. M. Price, T. G. Troller, and J. S. Kominoski. 2018. Effects of sea-level rise and freshwater management on local water levels and water quality in the Florida Coastal Everglades. *Journal of Environmental Management* **211**:164- 176.
- Doughty CL, Langley JA, Walker WS, Feller IC, Schaub R, Champan SK. 2015. Mangrove range expansion rapidly increases coastal wetland carbón storage. *Estuaries and Coasts* 39:385-396.
- D'Odorico P, He YF, Collins S, De Wekker SFJ, Engel V, and Fuentes JD. 2013. Vegetation-microclimate feedbacks in woodland-grassland ecotones. *Global Ecology and Biogeography* 22:364-379.
- Elridge DJ, Bowker MA, Maestre FT, Roger E, Reynolds JF and Whitford WG. Impacts of shrub encroachment on ecosystem structure and functioning: towards a globalsynthesis. *Ecology Letters* 14:709-722.
- Ewel KC, Twilley RR, and Ong JE. 1998. Different kinds of mangrove forests provide different goods and services. *Global Ecology and Biogeography Letters* 7:83-94.
- Fagherazzi S, Carniello L, D'Alpaos L, and Defina A. 2006. Critical bifurcation of shallow microtidal landforms in tidal flats and salt marshes. *Proceedings of the National Academy of Science* 103:8337-8341.

- Fierer N, Craine JM, McLauchlan K, and Schimel JP. 2005. Litter quality and the temperature sensitivity of decomposition. *Ecology* 86:320-326.
- Flower, H., M. Rains, and C. Fitz. 2017a. Visioning the Future: Scenarios Modeling of the Florida Coastal Everglades. *Environmental Management* **60**:989-1009.
- Flower, H., M. Rains, D. Lewis, J. Z. Zhang, and R. Price. 2017b. Saltwater intrusion as potential driver of phosphorus release from limestone bedrock in a coastal aquifer. *Estuarine Coastal and Shelf Science* **184**:166-176.
- Gill AM, and Tomlinson PB. 1977. Studies on the growth of red mangrove (*Rhizophora mangle* L.) 4. The adult root system. *Biotropica* 9:145-155.
- Guo H, Weaver C, Charles S, Whitt A, Dastidar S, D'Odorico P, Fuentes JD, Kominoski JS, Armitage AR, Pennings SC. 2017. Coastal regime shifts: Rapid responses of coastal wetlands to changes in mangrove cover. *Ecology* 98: 762-77.
- Haigh, I. D., T. Wahl, E. J. Rohling, R. M. Price, C. B. Pattiaratchi, F. M. Calafat, and S. Dangendorf. 2014. Timescales for detecting a significant acceleration in sea level rise. *Nature Communications* **5**:11.
- Herbert, E. R., P. Boon, A. J. Burgin, S. C. Neubauer, R. B. Franklin, M. Ardon, K. N. Hopfensperger, L. P. M. Lamers, and P. Gell. 2015. A global perspective on wetland salinization: ecological consequences of a growing threat to freshwater wetlands. *Ecosphere* **6**:43.
- Hurvich CM, and Tsai CL. 1989. Regression and time series model selection in small samples. *Biometrika* 76: 297-307.
- Karam A. 1993. Chemical properties of organic soils. In: Carter MR, for Canadian Society of Soil Science, Eds. *Soil sampling and methods of analysis*. London: Lewis Publishers. Pp 459-471.
- Kelleway, JJ, Saintilan N, Macreadie PI, Skilbeck CG, Zawadski A, and Ralph PJ. 2016. Seventy years of continuous encroachment substantially increases “blue carbon” capacity as mangroves replace intertidal salt marshes. *Global Change Biology* 22: 1097-1109.
- Kelleway JJ, Cavanaugh K, Rogers K, Feller IC, Ens E, Doughty C, and Saintilan N. 2017. Review of the ecosystem service implications of mangrove encroachment into salt marshes. *Global Change Biology* 23: 3967-3983.

- Kirwan, M. L., and J. P. Megonigal. 2013. Tidal wetland stability in the face of human impacts and sea-level rise. *Nature* **504**:53-60.
- Kirwan, M. L., S. Temmerman, E. E. Skeehan, G. R. Guntenspergen, and S. Fagherazzi. 2016. Overestimation of marsh vulnerability to sea level rise. *Nature Climate Change* **6**:253-260.
- Knapp AK, Briggs JM, Collins S, Archer S, Bret-Harte M, Ewers BE, Peters DP, Young DR, Shaver GR, Pendall E and Cleary MB. 2008. Shrub encroachment in North American grasslands: Shifts in growth form dominance rapidly alters control of ecosystems carbon inputs. *Global Change Biology* **14**:615-623.
- Kominoski, J. S., J. J. F. Shah, C. Canhoto, D. G. Fischer, D. P. Giling, E. Gonzalez, N. A. Griffiths, A. Larranaga, C. J. LeRoy, M. M. Mineau, Y. R. McElarney, S. M. Shirley, C. M. Swan, and S. D. Tiegs. 2013. Forecasting functional implications of global changes in riparian plant communities. *Frontiers in Ecology and the Environment* **11**:423-432.
- Krauss KW, Doyle TW, Twilley RR, Smith TJ III, Whelan KRT, and Sullivan JK. 2005. Woody debris in mangrove forests of South Florida. *Biotropica* **37**:9-15.
- Krauss K, McKee KL, Lovelock CE, Cahoon DR, Saintilan N, Reef R, and Chen L. 2013. How mangrove forests adjust to rising sea level. *New Phytologist* **202**:19-34.
- Kuzyakov Y. 2010. Priming effects: Interactions between living and dead organic matter. *Soil biology and biochemistry* **42**:1363-1371.
- Lefcheck, J. S. 2016. PIECEWISESEM: Piecewise structural equation modelling in R for ecology, evolution, and systematics. *Methods in Ecology and Evolution* **7**:573-579.
- McKee, K. L., D. R. Cahoon, and I. C. Feller. 2007. Caribbean mangroves adjust to rising sea level through biotic controls on change in soil elevation. *Global Ecology and Biogeography* **16**:545-556.
- McKee KL. 2011. Biophysical controls on accretion and elevation change in Caribbean mangrove ecosystems. *Estuarine, Coastal and Shelf Science* **91**:475-483.

- McLeod, E., G. L. Chmura, S. Bouillon, R. Salm, M. Bjork, C. M. Duarte, C. E. Lovelock, W. H. Schlesinger, and B. R. Silliman. 2011. A blueprint for blue carbon: toward an improved understanding of the role of vegetated coastal habitats in sequestering CO₂. *Frontiers in Ecology and the Environment* **9**:552-560.
- McVoy, C., P. W. Said, J. Obeysekera, J. A. VanArman, and T. W. Drescher. 2011. *Landscapes and hydrology of the predrainage Everglades*. University Press of Florida, Gainesville, Florida.
- Middleton BA, and McKee KL. 2001. Degradation of mangrove tissues and implications for peat formation in Belizean island forests. *Ecology* **89**:818-828.
- Morris JT, Sundareshwar PV, Nietch CT, Kjerfve B, and Cahoon DR. 2002. Responses of coastal wetlands to rising sea level. *Ecology* **83**:2869–2877.
- Morris JT, Barber DC, Callaway JC, Chambers R, Hagen SC, Hopkinson CS, Johnson BJ, Megonigal P, Neubauer SC, Troxler T, and Wigand C. 2016. Contributions of organic and inorganic matter to sediment volume and accretion in tidal wetlands at steady state. *Earth's Future* **4**:110-121.
- Nyman JA, Walters RJ, Delaune RD, and Patrick WH. 2006. Marsh vertical accretion via vegetative growth. *Estuarine, Coastal and Shelf Science* **69**: 370-380.
- Osland MJ, Spivak AC, Nestlerode JA, Lessmann JM, Almario AE, Heitmuller PT, Russell MJ, Krauss KW, Alvarez F, Dantin DD, Harvey JE, From AS, Cormier N, and Stagg CL. 2012. Ecosystem development after mangrove wetland creation plant-soil change across a 20-year chronosequence. *Ecosystems* **15**:848–866.
- Osland MJ, Enwright N, Day RH, and Doyle TW. 2013. Winter climate change and coastal wetland foundation species: salt marshes vs. mangrove forests in the southeastern United States. *Global Change Biology* **19**:1482-1494.
- Osland MJ, Enwright NM, Day RH, Gabler CA, Stagg CL, and Grace JB. 2016. Beyond just sea-level rise: considering macroclimatic drivers within coastal wetland vulnerability assessments to climate change. *Global Change Biology* **22**:1-11.
- Osland MJ, Feher LC, Griffith KT, Cavanaugh KC, Enwright NM, Day RH, Stagg CL, Krauss KW, Howard RJ, Grace JB, and Rogers K. 2017. Climatic controls on the global distribution, abundance and species richness of mangrove forests. *Ecological Monographs* **87**:341-359.
- Nerem, R. S., B. D. Beckley, J. T. Fasullo, B. D. Hamlington, D. Masters, and G. T. Mitchum. 2018. Climate-change-driven accelerated sea-level rise detected in the

altimeter era. Proceedings of the National Academy of Sciences of the United States of America **115**:2022-2025.

Neubauer, S. C. 2008. Contributions of mineral and organic components to tidal freshwater marsh accretion. *Estuarine Coastal and Shelf Science* **78**:78-88.

Neubauer, S. C., and J. P. Megonigal. 2015. Moving Beyond Global Warming Potentials to Quantify the Climatic Role of Ecosystems. *Ecosystems* **18**:1000-1013.

Nyman, J. A., R. D. Delaune, H. H. Roberts, and W. H. Patrick. 1993. Relationship between vegetation and soil formation in a rapidly submerging coastal marsh. *Marine Ecology Progress Series* **96**:269-279.

Nyman, J. A., R. J. Walters, R. D. Delaune, and W. H. Patrick. 2006. Marsh vertical accretion via vegetative growth. *Estuarine Coastal and Shelf Science* **69**:370-380.

Price, R. M., M. R. Savabi, J. L. Jolicoeur, and S. Roy. 2010. Adsorption and desorption of phosphate on limestone in experiments simulating seawater intrusion. *Applied Geochemistry* **25**:1085-1091.

Ross, M. S., J. F. Meeder, J. P. Sah, P. L. Ruiz, and G. J. Telesnicki. 2000. The Southeast Saline Everglades revisited: 50 years of coastal vegetation change. *Journal of Vegetation Science* **11**:101-112.

Sandoval, E., R. M. Price, D. Whitman, and A. M. Melesse. 2016. Long-term (11 years) study of water balance, flushing times and water chemistry of a coastal wetland undergoing restoration, Everglades, Florida, USA. *Catena* **144**:74-83.

Saintilan N, Wilson NC, Rogers K, Rajkaran A, and Krauss KW. 2014. Mangrove expansion and salt marsh decline at mangrove poleward limits. *Global Change Biology* **20**:147-157.

Sklar, F. H., M. J. Chimney, S. Newman, P. McCormick, D. Gawlik, S. L. Miao, C. McVoy, W. Said, J. Newman, C. Coronado, G. Crozier, M. Korvela, and K. Rutchey. 2005. The ecological-societal underpinnings of Everglades restoration. *Frontiers in Ecology and the Environment* **3**:161-169.

Smith TJ III, Foster A, Tiling-Range G, and Jones JW. 2013. Dynamics of mangrove-Marsh ecotones in subtropical coastal wetlands: fire, sea-level rise, and water

- levels. *Fire Ecology* 9:66-77.
- Titus, J. G., and C. Richman. 2001. Maps of lands vulnerable to sea level rise: modeled elevations along the US Atlantic and Gulf coasts. *Climate Research* **18**:205-228.
- Trenberth, K. E., A. G. Dai, G. van der Schrier, P. D. Jones, J. Barichivich, K. R. Briffa, and J. Sheffield. 2014. Global warming and changes in drought. *Nature Climate Change* **4**:17-22.
- Twilley RR, Lugo AE, and Patterson-Zucca C. 1986. Litter Production and Turnover in basin mangrove forests in southwest Florida. *Ecology* 67:670-683.
- Van Auken OW. 2000. Shrub invasions of North American semiarid grasslands. *Annual Review of Ecology and Systematics* 31:197-215.
- Vogt KA, Vogt DJ, and Bloomfield J. 1998. Analysis of some direct and indirect methods for estimating root biomass and production of forests at an ecosystem level. *Plant Soil* 200: 71-89.
- Wdowinski, S., R. Bray, B. P. Kirtman, and Z. H. Wu. 2016. Increasing flooding hazard in coastal communities due to rising sea level: Case study of Miami Beach, Florida. *Ocean & Coastal Management* **126**:1-8.
- White, E., and D. Kaplan. 2017a. Restore or retreat? saltwater intrusion and water management in coastal wetlands. *Ecosystem Health and Sustainability* **3**.
- Woodroffe, C. D. 1990. The impact of sea-level rise on mangrove shorelines. *Progress in Physical Geography* **14**:483-520.
- Yando ES, Osland MJ, Willis JM, Day RH, Krauss KW, and Hester MW. 2016. Salt marsh-mangrove ecotones: Using structural gradients to investigate the effects of woody plant encroachment on plant-soil interactions and ecosystem carbon pools. *Journal of Ecology* 104: 1020-1031.

Table 1. Linear mixed-effects models and model weights of fixed effects from significant relationships between distance to coast and soil nutrient characteristics (%N, %P, C:N, N:P ratios) and vegetation characteristics (mangrove cover, marsh cover and total cover). And distance to coast, soil nutrient characteristics and vegetation characteristics on soil carbon stocks and fluxes. Response variables and fixed predictors were standardized with the equation $variable = (x - mean(x))/stdev(x)$ to ensure that variables were on similar scales and to meet the assumptions of normality. Vegetation characteristics were measured in 1 m² plots, while soil characteristics were measured with one soil core in the center of each site. Carbon stocks and fluxes were measured in three plots per site. We list only the most parsimonious models for each response, as determined by lowest AICc, and any models whose AICc is within 2 points of the top model (Burnham and Anderson 2002).

Response variable	Models	Log likelihood	AICc	P - value	Conditional R ²	Equation
Influence of distance from coast						
Mangrove cover	Distance to coast	-272.91	556.89	0.049	0.19	$y = -4.3(\text{Distance}) + 35.16$
%N	Distance to coast	47.69	-79.4	0.01	0.35	$y = 0.007(\text{Distance}) + 0.02$
N:P	Distance to coast	-51.65	117.92	0.03	0.55	$y = 1.846(\text{Distance}) + 0.023$
C:N	Distance to coast	-69.71	154.03	0.01	0.34	$y = -6.55(\text{Distance}) + 64.63$
Organic Matter Fluxes						

Root productivity (g OC m ⁻² y ⁻¹)	Mangrove cover	-42.36	96.95	0.001	0.3	y = 0.55(Mangrove cover)
Root productivity (g OC m ⁻² y ⁻¹)	Mangrove cover + N:P	-41.21	97.66	Mancover = 0.0009 NP = 0.04	0.34	y = 0.53(Mangrove cover) - 0.31(N:P) - 0.004
Wood breakdown (k dd ⁻¹) 0-15 cm	C:N	-33.91	80.36	0.02	0.66	y = 0.42(C:N) - 0.1
Wood breakdown (k dd ⁻¹) 15-30 cm	C:N	-19.69	89.62	0.03	0.36	y = 0.22(C:N) - 0.25
Cellulose breakdown (k dd ⁻¹) 15-30 cm	C:N	-35.84	84.4	0.004	0.36	y = 0.54(C:N) - 0.003

Organic Carbon Stocks

Root biomass (g OC m ⁻²) 0-30 cm	Mangrove cover	-77.16	165.59	< 0.001	0.34	y = 0.58(Mangrove cover) + 0.00
Soil %OC (0-15 cm)	Distance	-63.51	138.09	< 0.001	0.63	y = 0.66(Distance) + 0.03

Figure 1. Conceptual model predicting the influence of proximity to coast on ecosystem properties and soil carbon storage. The size of plusses and minuses indicate the hypothesized magnitude of each ecosystem link. We predicted that saltwater intrusion from sea level rise and water management will drive saltwater influence further inland, thus influencing carbon stocks and fluxes on different time scales.

Figure 2. Site map. We chose 19 sites that spanned the marsh-mangrove ecotone in the Southeast Saline Everglades in Florida, USA. Sites were chosen based on location within and adjacent to the marsh-mangrove ecotone, and because previous data (Ross et al. 2000) on vegetation shows that this region has experienced large change in vegetation type and cover.

Figure 3. Proximity to the coast and vegetation and soil characteristics. We compared distance to coast (the location of each measurement to the closest open coastline) to vegetation and soil characteristics using generalized mixed effects models. For each measurement we accounted for spatial autocorrelation by creating a random effect of location (transect/region). Solid lines represent best fit from linear mixed effects models ($P < 0.05$), and dashed lines are 95 percent confidence intervals. (a) Mangrove cover measured within 1 m² vegetation plots that we utilized for root biomass and OC measurements. (b) Percent nitrogen (%N) in the surface soil (0-15 cm) taken from the center of each site (n = 19). (c) Soil molar carbon to nitrogen ratios (C:N) in the surface soil (0 -15 cm) taken from the center of each site. (d) Soil molar nitrogen to phosphorus ratios in the surface soil (0-15 cm) taken from the center of each site.

Figure 4. Soil carbon fluxes. We used generalized mixed effects models to identify the drivers of root productivity and organic matter breakdown. For each measurement we accounted for spatial autocorrelation by creating a random effect of location (transect/region). Solid lines represent best fit from linear mixed effects models ($P < 0.05$), and dashed lines are 95 percent confidence intervals. (a) The most parsimonious model to describe root ingrowth was a linear model with mangrove cover as the sole driver. Root productivity was measure as ingrowth (0-30 cm) and normalized as grams of OC per year. (b) Wood standard substrates breakdown was measured in the surface soil (10 cm) and breakdown rates were normalized per degree day to represent $k \text{ dd}^{-1}$.

Figure 5. Soil carbon stocks. We used generalized mixed effects models to identify the drivers of root productivity and organic matter breakdown. For each measurement we accounted for spatial autocorrelation by creating a random effect of location (transect/region). Solid lines represent best fit from linear mixed effects models ($P < 0.05$), and dashed lines are 95 percent confidence intervals. (a) The best model to predict root biomass solely included mangrove cover. We measured live roots from root cores (30 cm deep) taken from the center of 1 m² vegetation plots. Root biomass is expressed as OC content. (b) The model that best predicted surface soil OC (0- 15 cm) was distance from coast. Soil cores were taken adjacent to root cores and we measured distance from the location of each core location to the nearest open coastline.

Figure 6. We used a piecewise structural equation models (Lefcheck 2015) to measure linkages between proximity to the coast, vegetation and soil chemical characteristics, soil carbon fluxes (root productivity and organic matter breakdown rates) and soil carbon stocks (root biomass and soil organic carbon content). The corresponding model list is composed of linear mixed effects models (individual statistical output described in table 1), run with the R package “lme4”. We ran the model in R with the package “piecewiseSEM.” We identified the most parsimonious overall model and removed linkages to minimize AICc. We show only significant correlations ($P < 0.05$) as standardized path coefficients. We display all soil characteristics, stocks and fluxes of OC from our original conceptual figure (figure 1) despite the lack of significant linkages between them.

Figure 1.

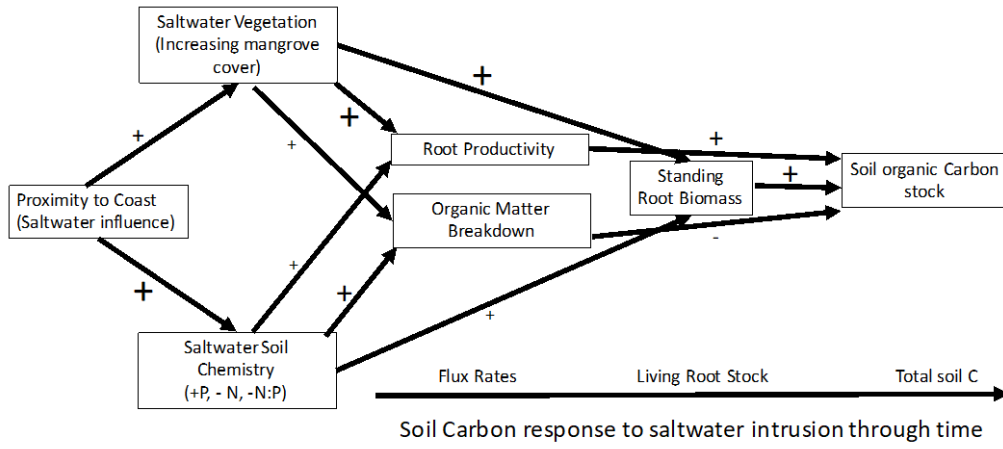


Figure 2.



Figure 3.

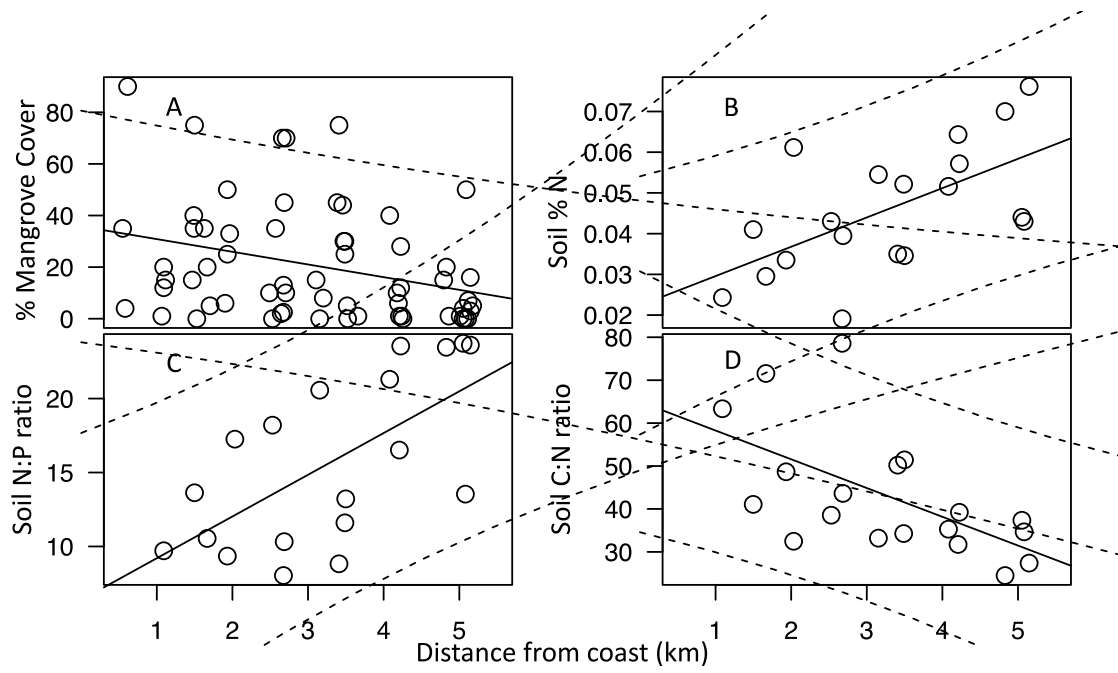


Figure 4

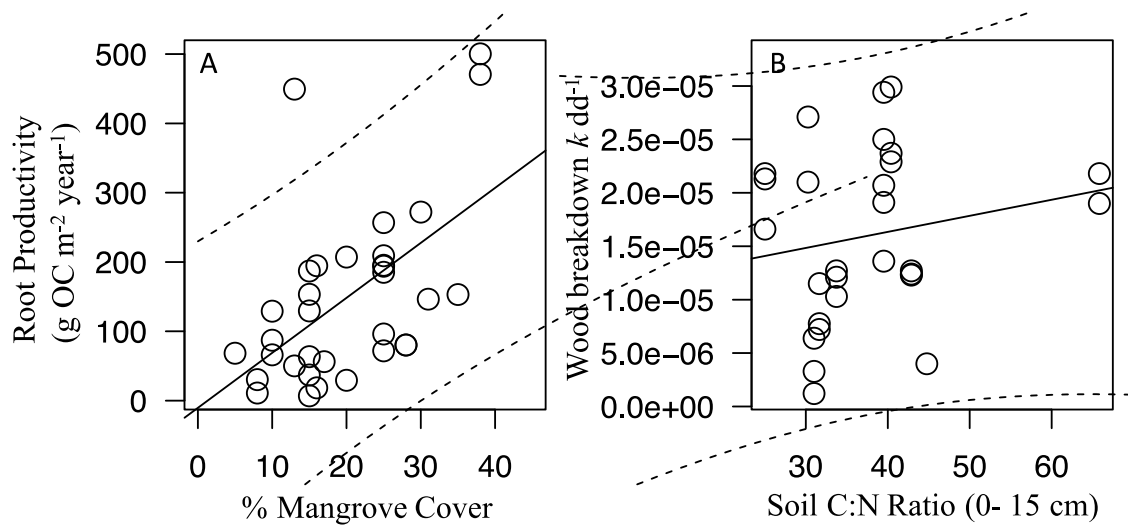


Figure 5

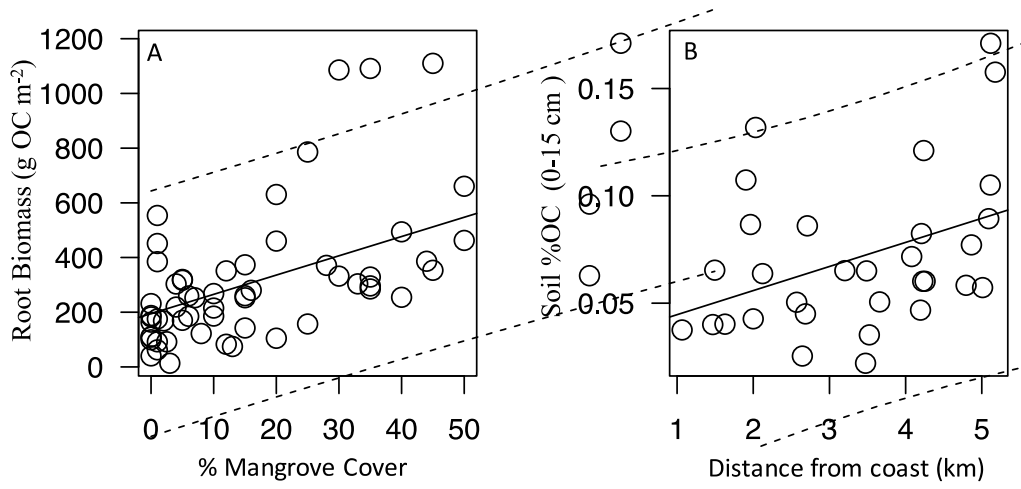


Figure 6

